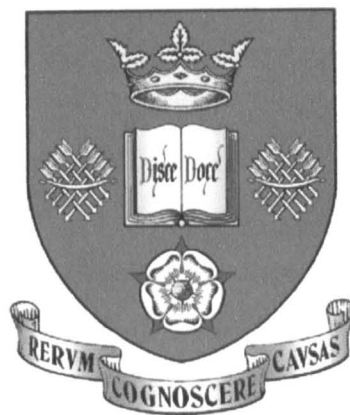


# **Fluorcanasite Glass-Ceramics for Dental Applications**

by

**Sabah Gulam Attar**



A thesis submitted for the degree of Doctor of Philosophy

Departments of Engineering Materials and Adult Dental Care  
The University of Sheffield  
March 2005

**THESIS CONTAINS**

**CD**

## Summary

### Fluorcanasite Glass-Ceramics for Dental Applications

Sabah Gulam Attar

Fluorcanasite, a chain silicate glass ceramic, displaying a combination of high flexural strength and high fracture toughness in comparison with currently available resin-bonded ceramics, is being developed as a material that should be easy to fabricate into a dental restoration. Previous work has focussed on producing a chemically durable formulation of fluorcanasite. Unfortunately, in an attempt to achieve low solubility, the mechanical properties of this material have been compromised. The aim of this study was to assess the influence of compositional changes on the crystallisation and fracture toughness of the fluorcanasite crystalline phases.

This study has focused on compositional variations to the fluorcanasite composition of  $60\text{SiO}_2\text{-}8\text{Na}_2\text{O-}7\text{K}_2\text{O-}15\text{CaO-}10\text{CaF}_2$ . Fluorite additions were attempted to ascertain the extent to which the 'known' nucleating agent influences the crystalline phase development. Zirconia and silica additions were made to the formulation to improve the mechanical properties while maintaining the chemical solubility of the material. It was found that fluorcanasite glasses of these formulations crystallize to give a combination of canasite and frankamenite phases and at higher zirconia additions, a potassium zirconium silicate phase called wadeite.

The attempted reformulations resulted in a composition ( $6.11\text{Na}_2\text{O-}5.35\text{K}_2\text{O-}11.46\text{CaO-}11.46\text{CaF}_2\text{-}64.82\text{SiO}_2\text{-}0.80\text{ZrO}_2$ ) which upon a standard two-stage heat treatment schedule crystallised to give a glass ceramic with substantially improved mechanical properties. A greater than three-fold increase was achieved in the fracture toughness in comparison to the base composition and is comparable to current commercial dental materials indicated for use as posterior restorations. This formulation has resulted in a solubility which is within the solubility limits for use as a core material (class 2, ISO 6872:1995 (E)) and the glass ceramic has been shown to have adequate machinability for development using the CAD CAM process.

## **Acknowledgements**

**In The Name of Allah, The Most Gracious, The Most Merciful.**

**I would like to express my gratitude to my supervisors: Dr. R. J. Hand, for all the guidance and for always finding the time to go through any problems that arose and Prof. R. van Noort, for providing valuable insight and advice throughout the course of this research.**

**A big thank-you to Mr. I. Watts and Mr. D. Haylock for always being able to 'squeeze a melt in' for me and to Mr. P. Staton, for all the help with the core-drilling and etching.**

**I would also like to convey my appreciation to Mr. C. Stokes for his enthusiastic advice whenever I needed it and to Miss S. Pollington, for assistance with the CAD-CAM.**

**Finally, thanks to my parents for their unwavering support through my every endeavour.**

**Funding for this project was provided by the Engineering and Physical Sciences Research Council and The University of Sheffield.**

## Table of Contents

<b>Summary</b>	<b>i</b>
<b>Acknowledgements</b>	<b>ii</b>
<b>List of Figures</b>	<b>vii</b>
<b>List of Tables</b>	<b>xii</b>
<b>Chapter 1: Introduction</b>	<b>1</b>
<b>Chapter 2: Literature Survey</b>	<b>3</b>
2.1 Introduction	3
2.2 Glass	4
2.3 Glass-ceramics	6
2.4 Canasite	8
2.4.1 Nucleation and crystallisation of canasite glass-ceramic	9
2.4.2 Other phases	9
2.5 Desired Properties in Dental Ceramics	15
2.5.1 Mechanical requirements	15
2.5.2 Aesthetic requirements	16
2.6 Current commercial dental ceramics	19
2.6.1 Ceramics bonded to ceramic-substructure	20
2.6.2 Ceramics bonded to metal-substructure	20
2.6.3 Resin-bonded ceramics	21
2.6.4 Mechanical properties	23
2.7 Development of canasite as a dental ceramic	25
2.8 Dental Material Testing	26
2.8.1 Crystallisation studies	26
2.8.2 Mechanical strength testing	26
2.8.3 Chemical durability	29
2.8.4 Dental material processing	30
2.9 Main Findings	31
<b>Chapter 3: Materials Processing and Methods</b>	<b>33</b>
3.1 Introduction	33
3.2 Experimental Procedure	33

3.2.1 Glass melting	33
3.2.2 Differential Thermal Analysis	35
3.2.3 Crystalline phase and microstructural analysis	36
3.2.4 Fracture Toughness	38
<b>3.3 Establishing the Glass Melting Protocol</b>	<b>39</b>
3.3.1 Glass making	39
3.3.2 Glass phase analysis	39
3.3.3 Heat treatment	41
3.3.4 Crystalline phase analysis	42
3.3.5 Fracture toughness tests	45
3.4 Discussion	47
3.5 Conclusions	48
<b>Chapter 4: Compositional Effects on the Fracture Toughness</b>	<b>49</b>
4.1 Introduction	49
4.2 Experimental Procedure	49
4.2.1 Glass formulation and melting	49
4.2.2 Heat treatments	50
4.2.3 Glass and crystalline phase analysis	51
4.2.4 Mechanical Testing	51
4.3 Results	51
4.3.1 Glass analysis	51
4.3.2 Phase and microstructural analysis	54
4.3.3 Fracture Indentation	56
4.4 Discussion	57
4.5 Conclusions	59
<b>Chapter 5: Effect of Fluorite Content</b>	<b>60</b>
5.1 Introduction	60
5.2 Experimental Procedure	60
5.2.1 Glass formulation	60
5.2.2 Glass melting	61
5.2.3 Differential Thermal Analysis	61
5.2.4 Heat treatment	61
5.2.5 Phase and microstructural analysis	62
5.2.6 Mechanical Testing	63

5.3 Results	63
5.3.1 Glass formulation and glass melting	63
5.3.2 Differential thermal analysis	63
5.3.3 Phase and microstructural analysis	64
5.3.4 Fracture Toughness	70
5.4 Discussion	70
5.5 Conclusions	73
<b>Chapter 6: Effect of Zirconia Additions</b>	<b>74</b>
6.1 Introduction	74
6.2 Experimental Procedure	74
6.2.1 Glass formulation	74
6.2.2 Differential Thermal Analysis	75
6.2.3 Heat treatment	75
6.2.4 Phase and microstructural analysis	76
6.2.5 Mechanical Testing	77
6.3 Results	77
6.3.1 Crystalline phase analysis	77
6.3.1 (i) Glasses with 8 mol% fluorite content	77
6.3.1 (ii) Glasses with 10 mol% fluorite content	80
6.3.1 (iii) Glasses with 15 mol% fluorite content	84
6.3.2 Fracture toughness	88
6.4 Discussion	89
6.5 Conclusions	91
<b>Chapter 7: Effect of Silica Content</b>	<b>93</b>
7.1 Introduction	93
7.2 Experimental Procedure	93
7.2.1 Glass formulation	93
7.2.2 Glass melting	94
7.2.3 Differential thermal analysis	94
7.2.4 Heat treatment	94
7.2.5 Phase and microstructural analysis	95
7.2.6 Mechanical Testing	95
7.3 Results	96
7.3.1 Crystalline phase analysis	96

7.3.2 Fracture toughness	101
7.4 Discussion	102
7.5 Conclusions	103
<b>Chapter 8: Development of Fluorcanasite as a Dental Material</b>	<b>104</b>
8.1 Introduction	104
8.2 Chemical Solubility	104
8.2.1 Experimental method	104
8.2.2 Results	106
8.3 Mechanical Properties	109
8.3.1 Experimental method	109
8.3.2 Results of mechanical testing	111
8.4 Dental Restoration Production	111
8.4.1 Experimental procedure	111
8.4.2 Results	113
8.5 Discussion	117
8.6 Conclusions	121
<b>Chapter 9: Conclusions</b>	<b>122</b>
<b>Chapter 10: Further Work</b>	<b>124</b>
<b>Chapter 11: References</b>	<b>126</b>
<b>Chapter 12: Appendix</b>	<b>138</b>
Appendix 1 Glass compositions	
Appendix 2 XRF analysis	
Appendix 3 Summary of DTA analysis	

## List of Figures

- **Figure 2.1: Simplified two-dimensional diagram of the structure of silica in the form of (a) quartz crystal, (b) glass and (c) glass with a network modifier** 5
- **Figure 2.2: Structure of frankamenite with the tetrahedron representing Si and the spheres representing O (red), Ca (blue), F (yellow) and mixed Na and K sites (green)** 10
- **Figure 2.3: Structure of canasite with the tetrahedron representing Si and the spheres representing O (red), Ca (blue) and mixed Na and K sites (green)** 11
- **Figure 2.4: Projection of the canasite structure along the elongated axis. Triclinic cell is shown by the thick line. I, II, III, IV mark the four chains forming the  $\text{Si}_{12}\text{O}_{30}$  tube. M(1) and M(2) are alternately Na and Ca octahedral, while M(3) to M(8) are mixed Ca, Na positions** 12
- **Figure 2.5: Calculated XRD trace of canasite** 13
- **Figure 2.6: Calculated XRD trace of frankamenite** 14
- **Figure 2.7: Reflection and transmission of incident light through the dentine and enamel (McLean, 1979)** 17
- **Figure 2.8: Reflection and transmission in aluminous porcelain crown (McLean, 1979)** 18
- **Figure 2.9: Light reflection and transmission in metal-ceramic crown (McLean, 1979)** 18
- **Figure 2.10: Light reflection and transmission in a resin-bonded crown (McLean, 1979)** 19
- **Figure 2.11: Fracture toughness values ( $K_{Ic}$ ) of some dental materials taken from Seghi et al, 1995; Thompson et al, 1996; Rosenstiel et al, 1989; Mueller, 1991; Höland et al, 2000; Gorman et al, 2000; Beall et al, 1986, Xu et al, 1998 and Attar, 2001** 23
- **Figure 2.12: Geometry of Palmqvist and Radial/median cracks around Vickers indentation** 28
- **Figure 3.1: Molten glass being poured onto plate** 35

• Figure 3.2: Fritting	35
• Figure 3.3: DTA trace with calculation of T <sub>g</sub> and T <sub>c</sub>	36
• Figure 3.4: DTA results of K81-K86	40
• Figure 3.5: Optical micrographs of K81 and K86	40
• Figure 3.6: Example of calibration data. The red line is the set programme and the blue dots are the recorded points from the data logger, both showing agreement within 1°C	42
• Figure 3.7: Example XRD traces from Phillips and Siemens (of FZ158 composition heat treated to 840°C and held for 2hrs, see Chapter 6)	42
• Figure 3.8: XRD results of K81 to K86.	43
• Figure 3.9: SEM of K81	43
• Figure 3.10: SEM/BEI image of K83 with EDS of the layers	44
• Figure 3.11: Simulation of inhomogeneous molten glass being poured as a plate	45
• Figure 3.12: Calculation of the fracture toughness in MNm <sup>-3/2</sup>	46
• Figure 3.13 Radial/median crack formed during Vickers indentation	46
• Figure 4.1: DTA traces for K7, C1 & C2	52
• Figure 4.2: DTA traces of K7, Z2 & T2	52
• Figure 4.3: DTA traces of K7 & B8	53
• Figure 4.4: XRD traces of glass ceramics subjected to single stage heat treatments to the given temperatures, where A: K7, B: C1, C: C2, D: T2, E: Z2, F: B8.	54
• Figure 4.5: XRD traces of glass ceramics subjected to double stage heat treatments,	55
• Figure 4.6: Scanning electron micrographs of samples etched with 1.5% HF for 1 minute.	56
• Figure 4.7: K <sub>1c</sub> values of the glass-ceramics with optical micrographs of their corresponding indents, where the scale bar represents 100µm.	57
• Figure 5.1: DTA traces of F8-F15	64
• Figure 5.2: XRD traces showing the temperature dependent phase evolution of F8 to F15 heat treated at different isotherms ranging from 600°C to 740°C	65
• Figure 5.3: XRD traces of F8-F15 heat treated to 720°C and air quenched.	66
• Figure 5.4: XRD traces of F8 to F15 after 2hr hold of 620°C and a two	67

- hour hold at 720°C.
- **Figure 5.5: SEM images of F10-F15, subjected to a two hour nucleation hold at 620°C and two hour crystallisation hold at 720°C.** 67
  - **Figure 5.6: XRD traces of F8 to F15 after 24hr hold of 620°C.** 68
  - **Figure 5.7: SEM images of F10 (left) and F15, subjected to a 24 hour hold at 620°C.** 69
  - **Figure 5.8: TEM image of FCC CaF<sub>2</sub> crystal and corresponding diffraction pattern for F10.** 69
  - **Figure 5.9: XRD traces of single stage heat treatment and two stage heat treatment.** 69
  - **Figure 5.10: K<sub>1c</sub> as a function of fluorite content where a, b and c signify the different heat treatment schedules the glasses were subjected to. a = 540°C(24 hr hold) and 720°C (2 hr hold), b = 620°C (24 hr hold) 720°C (2 hr hold) and c = 620°C (2 hr hold) 720°C (2 hr hold), lines drawn as a guide to the eye.** 70
  - **Figure 6.1: DTA traces of F8Z0 to F8Z8** 77
  - **Figure 6.2: Differences in XRD traces at x, fluorite content = 8, subjected to single stage heat treatment to peak DTA temperature.** 78
  - **Figure 6.3: Scanning electron micrographs of F8Z1 to F8Z8 subjected to two stage heat treatments, etched samples (1.5%HF for 25 seconds).** 79
  - **Figure 6.4: DTA traces of F10Z880 to F10Z8** 80
  - **Figure 6.5: XRD traces of F10Z2 89subjected to single stage heat treatments and holds at mentioned temperatures (°C).** 81
  - **Figure 6.6: Structure of wadeite with SiO<sub>4</sub> tetrahedras, ZrO<sub>6</sub> octahedra, large circles depicting K<sup>+</sup> or Na<sup>+</sup> and small circles depicting oxygen.** 81
  - **Figure 6.7: Differences in XRD traces at fluorite content = 10, subjected to single stage heat treatment to peak DTA temperature.** 82
  - **Figure 6.8: Differences in XRD traces at fluorite content = 10, subjected to a nucleation hold at 550°C for 2 hours.** 83
  - **Figure 6.9: Scanning electron micrographs of etched surfaces of F10Z4 to F10Z8 subjected to two stage heat treatments, etched samples (1.5%HF for 1 minute).** 84
  - **Figure 6.10: DTA traces of F15Z0 to F15Z8** 85
  - **Figure 6.11: Differences in XRD traces at fluorite content = 15, subjected to single stage heat treatment to peak DTA temperature.** 85

- **Figure 6.12: XRD traces of F15Z8 subjected to 2 hour holds at stated temperatures** 86
- **Figure 6.13: Scanning electron micrographs of F15Z4 to F15Z8 subjected to two stage heat treatments, etched samples (5%HF for 25 seconds).** 87
- **Figure 6.14: Transmission electron micrograph of F15Z8** 87
- **Figure 6.15:  $K_{Ic}$  as a function of  $x$ , fluorite content (red is  $x = 8$ , blue is  $x = 10$  and green is  $x = 15$ ) and  $y$  (zirconia content).** 88
- **Figure 6.16:  $B$  as a function of  $x$ , fluorite content (red is  $x = 8$ , blue is  $x = 10$  and green is  $x = 15$ ) and  $y$  (zirconia content).** 89
- **Figure 7.1: DTA traces of Silica series glasses** 96
- **Figure 7.2: XRD traces of silica series heat treated to 720°C held for 2hrs and air quenched.** 97
- **Figure 7.3: XRD traces of silica series heat treated to 760°C held for 2hrs and air quenched.** 97
- **Figure 7.4: XRD traces of silica series heat treated to 800°C held for 2hrs and air quenched.** 98
- **Figure 7.5: XRD traces of S90 and S110 heat treated to 840°C held for 2hrs and air quenched.** 99
- **Figure 7.6: Scanning electron micrographs of samples subjected to two stage heat treatments, etched at 5% HF for 25s.** 99
- **Figure 7.7: S70 subjected to two stage heat treatment, etched at 5% HF for 25s.** 100
- **Figure 7.8: S80 subjected to two stage heat treatment, etched at 5% HF for 25s.** 100
- **Figure 7.9: S90 subjected to two stage heat treatment, etched at 5% HF for 25s.** 100
- **Figure 7.10: S110 subjected to two stage heat treatment, etched at 5% HF for 25s.** 101
- **Figure 7.11:  $K_{Ic}$  as a function of silica content** 101
- **Figure 7.12:  $B$  as a function of silica where the dotted line at  $B = 4.3 \mu\text{m}^{-1/2}$  is the maximum value for the material to be machinable according to Boccaccini (1997).** 102
- **Figure 8.1: S57 glass discs within the extraction apparatus.** 106

- **Figure 8.2: Chemical solubility of S57 glass and cerammed samples. The red bar indicates standard deviation.** 107
- **Figure 8.3: Scanning electron micrograph of the surface of the S57 glass disc after 16 hours in 4 % acetic acid at ~ 80°C showing crazing on the surface.** 107
- **Figure 8.4: Scanning electron micrograph of the surface of the S57 cerrammed disc after 16 hours in 4% acetic acid at ~ 80°C showing a crazing on the surface.** 108
- **Figure 8.5: Chemical solubility of S57, S80 and B8 cerammed samples. The red bar indicates standard deviation.** 108
- **Figure 8.6: Ball on ring arrangement in a Lloyds LRX tensometer used for biaxial flexural strength test.** 110
- **Figure 8.7: Eight S80 glass-ceramic samples exhibiting a failure originating from the centre.** 110
- **Figure 8.8: Re-melting of the glass pieces and the mould it was cast in.** 112
- **Figure 8.9: (a)VITA Mark II blocks. (b) The completed fluorcanasite block prior to milling.** 112
- **Figure 8.10: The CEREC-Scan hardware with an S80 block inserted.** 113
- **Figure 8.11: The fluorcanasite block (S80) being milled.** 114
- **Figure 8.12: A direct comparison of the milled crowns on the mould, the S80 on the left and VITA Mark II crown on the right.** 114
- **Figure 8.13: Scanning electron micrographs of the occlusal (top of crown) surfaces of the S80 (above) and VITA Mark II (below)** 115
- **Figure 8.14: Scanning electron micrographs of the interproximal (sides of crown) surfaces of the S80 (above) and VITA Mark II (below)** 116
- **Figure 8.15: Scanning electron micrograph of the ridge on the occlusal surface of the S80, showing fine crystal morphology responsible for the machining crack propagation.** 117

## List of Tables

• Table 2.1: The distribution of Na and Ca atoms in the canasite and frankamenite structures	12
• Table 2.2: Intra-oral conditions	15
• Table 2.3: Physical and chemical property requirements (ISO6872:1995)	15
• Table 2.4: Reported flexural strength values of some dental materials	24
• Table 3.1: Melting Schedules	34
• Table 3.2: Heat treatment schedules used, where AQ is air quenched	41
• Table 4.1: Batched glass compositions in molar percent	49
• Table 4.2: Heat treatment schedules for fracture toughness testing	50
• Table 5.1: Glass compositions (as-batched) in molar percent	60
• Table 5.2 Annealing schedules used	61
• Table 5.3 Two-stage heat treatment schedules used; all samples were furnace cooled	62
• Table 6.1: Glass compositions (as-batched) in mol %	75
• Table 6.2: Two-stage heat treatment schedules used to produce samples for $K_{Ic}$ measurements	76
• Table 6.3: Crystalline phase analysis after two-stage heat treatment	79
• Table 6.4: Crystalline phase analysis after two-stage heat treatment	83
• Table 6.5: Crystalline phase analysis after two-stage heat treatment	86

• <b>Table 7.1: Glass compositions (as-batched) in mol%</b>	<b>93</b>
• <b>Table 7.2 Annealing schedules used</b>	<b>94</b>
• <b>Table 7.3 Two-stage heat treatment schedules used</b>	<b>95</b>
• <b>Table 8.1: Heat treatment schedules glass ceramics were subjected to</b>	<b>105</b>
• <b>Table 8.2: Summary of the mechanical testing results</b>	<b>111</b>

## Chapter 1: Introduction

Ceramic materials have been considered for dental restorations for over two hundred years. Despite their hard and brittle nature, they are seen as the future of dental restorations because of their unsurpassed aesthetic qualities and their biocompatibility. Unfortunately their use has been handicapped due to fracture toughness and strength limitations and thus all-ceramic materials have mostly been restricted to the anterior of the mouth. Therefore strong, tough, aesthetic ceramic restorations that are cheap to manufacture should be attractive to the market.

Dental porcelains have historically evolved in such a way that the material was essentially a feldspathic glass by the mid 20<sup>th</sup> century. Improvements in strength accompanied the development of alumina-reinforced feldspathic porcelain (McLean and Hughes, 1965). Enhanced fracture toughness was also achieved by the addition of approximately 50 per cent by weight of alumina crystals (Morena *et al*, 1986). However, the presence of a second phase in the glassy matrix substantially reduced the translucency of the porcelain and the material was still highly susceptible to brittle fracture (McLean and Hughes, 1965), limiting its usefulness to providing a refractory framework capable of supporting weaker, more translucent dentine and enamel porcelains. Recent developments have seen the increase in the use of glass-ceramic systems as they allow forming by casting or pressing or machining, which are time and cost-effective techniques compared to the sintering of built up slurry previously employed.

Despite the advantages of using glass-ceramics, problems remain when compared to metallic restorations. Ceramic restorations often fail catastrophically whereas metal restorations often only deform. The development of ceramics bonded onto the 'tooth-substructure' accompanied the discovery that many dental porcelains and glass ceramics can be etched with hydrofluoric acid or other acids to create retentive channels similar to those in acid etched enamel. Termed resin-bonded, acid-etched ceramic restorations or RBC's, these ceramics present a more conservative approach than the use of full crowns. It has been shown that by resin-bonding a weaker, but etchable crown to the underlying dentine, the crown will exhibit superior fracture resistance to that of conventional alumina

or metal reinforced luted crown.

Fracture toughness is an important criterion in ceramics that are intended for use as dental restorations, and is intrinsically linked to the microstructure of the material. Canasite ( $\text{Ca}_5\text{Na}_4\text{K}_2\text{Si}_{12}\text{O}_{30}(\text{OH},\text{F})_4$ , a quadruple chain silicate, for which high flexural strengths of  $>200$  MPa and high fracture toughnesses of  $> 5 \text{ MNm}^{-3/2}$  have been reported (Beall, 1991), is being considered as a castable glass-ceramic, that should be easy to fabricate into a dental restoration. Previous researchers have reformulated fluorcanasite (synthetic form of the mineral canasite) to optimise its properties for dental restorations, but have not managed to produce an acceptable material (Anusavice and Zhang, 1998 and Stokes, 2003).  $\text{CaF}_2$ , which acts as a heterogeneously nucleating agent in this system (Beall, 1983) is also associated with loss in chemical durability of the glass ceramic. Anusavice and Zhang made some modifications to the formulation, but did not sufficiently increase the durability of fluorcanasite without compromising other properties. Similarly Stokes (2003) showed that the composition of  $60\text{SiO}_2\text{-}8\text{Na}_2\text{O}\text{-}7\text{K}_2\text{O}\text{-}15\text{CaO}\text{-}10\text{CaF}_2$  had an increased chemical durability over the original formulations of fluorcanasite, but this increase in durability came at the expense of fracture toughness. The aim of the current work was therefore to try and identify canasite compositions for which both high fracture toughness and chemical durability could be obtained. Thus through the course of these studies reformulations of Stokes' more durable  $60\text{SiO}_2\text{-}8\text{Na}_2\text{O}\text{-}7\text{K}_2\text{O}\text{-}15\text{CaO}\text{-}10\text{CaF}_2$  composition have been attempted in order to increase the fracture toughness of the material.

## Chapter 2: Literature Review

### 2.1 Introduction

In the year of the battle of Waterloo, the basis of artificial restoration was that the restorative dental material should replace its predecessor exactly. The obvious replacement of one tooth would, therefore be another of the same size and colour. The crowns of teeth removed from the victims of battle were subsequently fixed on to ivory bases by pinning, to make dentures for those wealthy enough to afford them. Although the dentures were superior in appearance to those, carved entirely from ivory or tusk, the teeth were far from permanent. They darkened and stained and frequently succumbed to dental decay. Alternative materials were sought to counteract this problem of putrefaction of ivory, bone, tusk or shell and it was Duchateau, a French chemist, who in 1776, first had the idea of using porcelain to replace both tooth and denture base. He made one denture successfully for himself. In 1788, Dubois de Chemant, a Parisian dentist, pursued and perfected the manufacture of mineral teeth (MacCulloch, 1968).

By the middle of the 20<sup>th</sup> century dental porcelains had evolved in such a way that the material was essentially a feldspathic glass, i.e. a potassium and sodium alumino-silicate glass, as distinct from porcelain which is a mixture of kaolin, feldspar and silica. In 1968, MacCulloch suggested that glass-ceramics, offering a combination of superior strength and translucency, might provide an alternative to dental porcelains. Industrial development of glass-ceramics was aimed at producing refractory crystalline or partially crystalline bodies at relatively low temperatures. The ceramic material, initially cast as a glass, is subsequently converted to a mechanically stronger, crystalline body.

This chapter initially reviews the literature on glass ceramics; specifically the quadruple chain silicate canasite and then covers the properties required by a dental glass ceramic, re-evaluates the current commercial glass ceramics and finally concentrates on how canasite can be developed as a dental restorative material.

## 2.2 Glass

A glass is considered amorphous like a liquid, with no long-range order (no regularity in the arrangement of its molecules beyond a few linked molecular units). However, the glass structure is of a more solid nature consisting of three-dimensional networks of covalent and ionic bonds giving rise to a reduced freedom of movement. For a melt to form a glass or for 'vitrification' to take place the melt should be very viscous at temperatures close to its freezing point, generally in the region of  $10^4 - 10^6$  Pa.s. For a melt that has been undercooled very quickly to a highly viscous state, it becomes energetically more favourable to form the solid bonds that result in the reduction of free energy to form a glass. The high viscosity of the molten glass limits the molecular mobility to the extent that perfect crystals do not form upon solidification.

Common commercial glasses are non-crystalline silicates containing other oxides, notably CaO, Na<sub>2</sub>O, K<sub>2</sub>O and Al<sub>2</sub>O<sub>3</sub>. A typical soda-lime-silica glass composition is approximately 70 wt% SiO<sub>2</sub>, which the remainder being made up of Na<sub>2</sub>O (soda) and CaO (lime). Pure silica (SiO<sub>2</sub>) in crystalline form is a quartz mineral, the crystal structure of which is illustrated in Figure 2.1(a). Glass formed from molten silica has a network structure that is similar but highly imperfect as in (b), which is adapted from 'The Atomic Arrangement in Glass' (Zachariasen, 1932). The random network theory that was proposed by Zachariasen in 1932 suggested that the bonds remained in place but the angles and lengths may vary due to the random network. The basic idea was derived from the observation that mechanical properties of glasses are similar to those of crystals of the same composition. Hence Zachariasen concluded that the atoms in a glass are linked together by the same forces as in crystals. This led Zachariasen to propose a structure consisting of an extended three-dimensional network made up of well defined small structural units which are linked together in a random way. Zachariasen suggested a set of four rules for glass formation in an oxide A<sub>m</sub>O<sub>n</sub>, in order to obtain a random network:

- Oxygen atoms are linked to no more than two atoms A
- The oxygen co-ordination number is small (i.e., 2 or 3)
- Oxygen polyhedra do share corners but not edges or faces
- At least three corners are shared.

Based on which, Zachariasen developed the following criteria for oxide glass formers (where A represents the cation and O, the anion):

- $A_2O$  and  $AO$  do not meet the rules
- $A_2O_3$ , if oxygen atoms form triangles around each A atom
- $AO_2$ ,  $A_2O_5$  if oxygen atoms form tetrahedra around each A atom
- $AO_3$ ,  $A_2O_7$  if oxygen atoms form octahedra around each A atom
- $AO_4$  if oxygen atoms form cubes around each A atom

$SiO_2$ ,  $GeO_2$ ,  $P_2O_5$ ,  $As_2O_5$  and  $B_2O_3$  are examples of such glass forming oxides. The temperature for glass forming can be lowered by adding  $Na_2O$ ,  $K_2O$  or  $CaO$ . These oxides are called ‘network modifiers’ because the metal ions involved tend to form non-directional ionic bonds with oxygen atoms, resulting in the creation of non-bridging oxygens (NBO’s) in the structure as illustrated by Figure 2.1(c).

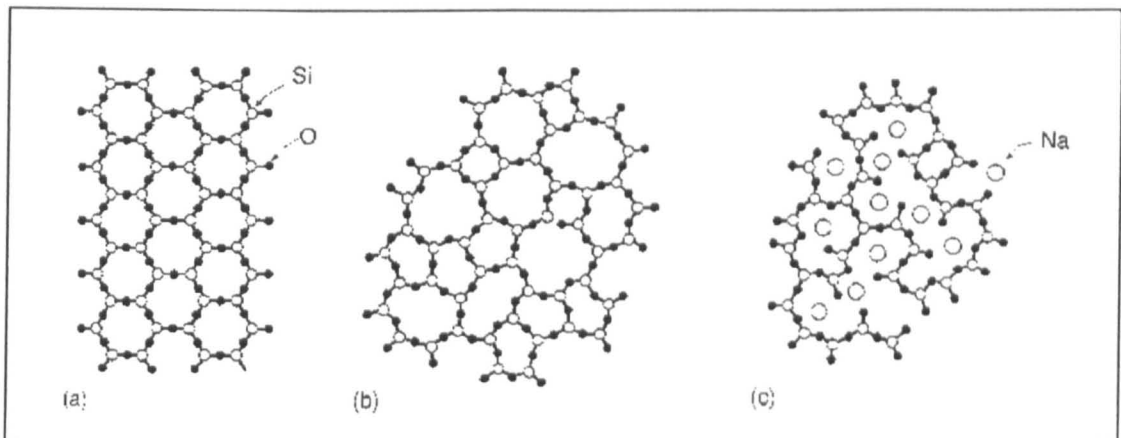


Figure 2.1: Simplified two-dimensional diagram of the structure of silica in the form of (a) quartz crystal, (b) glass and (c) glass with a network modifier.

Every alkali ion creates one NBO. However, modifiers are not always oxides; they may be cations that are oxidised by fluorine. The resulting network gets loose and by decreasing the connectivity a larger flexibility of the structure is obtained and hence the thermal expansion coefficient, the fluidity (inverse of viscosity), diffusion, electrical conduction and chemical corrosion all increase with increasing modifier content. ‘Intermediate oxides’ are a third type of oxide that can take part in the glass-network. Their behaviour is in-between that of a network-former and a network modifier, which do not form glasses themselves but act like glass formers when combined with others. An example is  $Al_2O_3$ , which directly substitutes for silica in the network as long as the extra negative charge can be balanced by a cation.

## 2.3 Glass-ceramics

Glass ceramics are polycrystalline materials formed through the controlled crystallisation of glass. The first practical glass ceramics, materials prepared by the controlled crystallisation of special glasses, were developed nearly forty years ago. Since that time, a wide variety of applications of these versatile materials have developed as a result of their many outstanding properties and the distinct advantages of the glass ceramic method, in certain circumstances, over conventional ceramic processing routes.

Of particular importance in many applications is the high uniformity of the microstructures of glass ceramics, the absence of porosity and the minor changes in volume during the conversion of glass into glass ceramic (usually only a few percent) (James *et al*, 1997). Hot-glass-forming techniques such as pressing, blowing, spinning, rolling, and casting are used to rapidly produce a variety of articles, that are heat treated to give a glass ceramic.

Crystallisation is the process by which the regular lattice of the crystal is generated from the less well-ordered glass structure. The two parts of the crystallisation process are nucleation and crystal growth. Nucleation may be homogeneous or heterogeneous. In homogeneous nucleation the first nuclei are of the same constitution as the crystals which grow on them, but in heterogeneous nucleation, the nuclei can be quite different from the crystals which are deposited.

Inducing volume nucleation in melt-derived bulk silicate glasses, usually by the addition of nucleating agents, produced the original glass ceramics. A nucleating agent can be defined as a constituent added, typically in amounts of a few percent, which promotes volume nucleation and the production of a glass ceramic. Metallic oxides such as  $\text{TiO}_2$ ,  $\text{ZrO}_2$  and  $\text{P}_2\text{O}_5$  are commonly used in silicate systems (James *et al*, 1997).

More recently, glass ceramic processing has been greatly extended to include non-silicates and even non-oxide compositions, and to include the preparation of the precursor glasses by sol-gel techniques. Also the powder-processing route has developed in importance. In this method, fine glass powders (melt- or sol-gel-derived) are formed into bodies of desired shapes, densified and crystallised. Densification may be achieved by cold-pressing and sintering or by hot-pressing and must be largely complete prior to crystallisation if low porosity is required. In this case nucleation probably takes place at the surfaces of the glass particles during sintering but the major part of the crystal growth occurs at a later stage to produce a 'bulk' crystallised product.

Glass ceramic microstructures are characterised by fine-grained, randomly oriented crystals with some residual glass but no voids, micro-cracks, or other porosity. Eight main glass-ceramic microstructures have been identified by Beall (1992):

- **Dendritic** – Dendrites form when growth is accelerated in certain lattice directions or planes within a glassy medium. The dendrites form a three dimensional continuous path through the residual glassy matrix.
- **Ultra fine-grained** – Tiny crystals of  $<100\text{\AA}$  are precipitated, usually achieved through the addition of nucleating agents. Crystal growth is slow, resulting in small grains and a translucent material.
- **Cellular membrane** – When the developing crystal phase is slightly lower in silica than the bulk composition, a stable film of siliceous glass envelopes the impinging grains during crystallisation.
- **Relic** – Heat-treating some phase-separated glasses above the annealing temperature causes droplets to become more fluid than the matrix. These droplets immediately crystallise but reflect the original droplet form. Hence the term relic, as the microstructure inherits and mirrors the original morphology of the parent glass.
- **Coast and Island** – This microstructure is produced when an equilibrium crystal phase forms at the expense of a metastable assemblage of phases.
- **House of cards** – A microstructure with randomly orientated flakes result in high fracture toughness and machinability, as fractures are either stopped or deflected by the flakes.
- **Acicular interlocking** – A microstructure with interlocking rod or blade-like crystals generally results in high strength and toughness. Energy absorption occurs through crack branching and deflection due to the high aspect ratio and cleavage splintering.
- **Lamellar twinned** – Lamellar or polysynthetic twinning is developed during growth or on cooling of certain silicate crystals.

As a result of these unique microstructures, properties such as translucency, high strength, and very low and uniform thermal expansion can be routinely produced. Since the advent of these higher strength glass-ceramic materials, the use of glass-ceramics as a dental restorative material has become widespread. Although they are bio-compatible and offer excellent aesthetics, ceramics are mostly characterised by their refractory nature,

hardness, susceptibility to brittle fracture and chemical inertness. Thus the development of glass-ceramics for dental applications has been geared towards exploring stronger and tougher materials with hardness similar to that of enamel, to minimise the wear of resulting restorations and also wear of the opposing dentition.

## 2.4 Canasite

Canasite and its close relatives, frankamenite and f-canasite (see below) are chain silicates. Chain silicates are polymeric crystals in which single or higher order multiple chains of silica tetrahedra form the structural backbone. Natural jade provides an example of such a tough material, the interlocking and often acicular microstructure of which can be simulated in glass-ceramics.

Three chain silicates, displaying a combination of high flexural strength (>200 MPa) and high fracture toughness (>3 MNm<sup>-3/2</sup>), have been identified as forming the basis of potentially useful and novel glass-ceramic systems. The first, enstatite (MgSiO<sub>3</sub>), is a single chain silicate and a representative of the pyroxene mineral group. The second, potassium fluorrichterite (KNaCaMg<sub>5</sub>Si<sub>8</sub>O<sub>22</sub>F<sub>2</sub>), is a double chain silicate and a member of the amphibole mineral group (Beall, 1991). The third is canasite (K<sub>3</sub>Na<sub>3</sub>Ca<sub>5</sub>Si<sub>12</sub>O<sub>30</sub>(OH)<sub>2.5</sub>F<sub>1.5</sub>), a quadruple chain silicate (Rozhdestvenskaya *et al*, 1996).

Being potentially very strong, tough, and potentially inexpensive, canasite is being investigated for potential applications such as memory disc substrates, architectural cladding and thin translucent panels. Studies have shown that heating rates and times for the casting and ceramming process can be undertaken in existing dental laboratory furnaces within a working day (Shareef *et al*, 1998). The material is the subject of a number of studies as a promising all-ceramic restoration (Shareef *et al*, 1998; Zhang and Anusavice, 1999 and Stokes, 2003)

Canasite is a rare mineral found in the Khibini mountains of the Kola Peninsula, Russia (Beall, 1991). It is described as monoclinic and translucent with two perfect cleavage directions at a 118° angle, a splintery fracture, and a density of 2.71 g/cm<sup>3</sup>. The crystal structure has been determined in detail by Rozhdestvenskaya and Nikishova, (1996) and consists of four silicate chains running parallel to the b-axis cross-linked to form a tubular unit. These quadruple chains give the basic structural unit Si<sub>12</sub>O<sub>30</sub>, a high Si/O ratio for a chain silicate, and suggest glass-forming behaviour (Beall, 1991).

Thermal processing of glass-ceramic materials is based on a conventional two-stage heat treatment involving an isothermal nucleation stage followed by an isothermal growth stage. The magnitude of the crystal population density, for a given material and processing time, is dependent upon the efficiency of the heat treatment schedule. Beall (1991) claims that the canasite stoichiometry forms a stable glass requiring only a few per cent of excess fluoride to achieve efficient nucleation and that it is easy to produce an essentially monophasic glass-ceramic. Internal nucleation is achieved through precipitation of  $\text{CaF}_2$  crystallites and spherulitic growth of canasite upon these nuclei to give a fine-grained glass-ceramic (Beall *et al*, 1986). A highly acicular crystalline microstructure of interpenetrating blades produces strong and tough material. This material can be diamond-machined or ground and polished to extremely fine tolerances despite crystal lengths of several microns (Beall, 1991). This is currently being investigated as both a replacement for aluminium as a substrate for hard disk drives (Poon & Bhushan, 1995) and also with some phosphate based additions as a bioactive bone replacement material (Miller *et al*, 2000) and a dental glass-ceramic.

#### 2.4.1 Nucleation and crystallisation of canasite glass-ceramic

As noted above it is believed that nucleation of canasite occurs through the precipitation of  $\text{CaF}_2$  crystallites, with the subsequent growth of canasite on these nuclei. Omar (1994) has suggested that an alkali silicate phase, devitrite ( $\text{Na}_2\text{Ca}_3\text{Si}_6\text{O}_{16}$ ) forms at the same time as the  $\text{CaF}_2$ , and these two phases then react together and with the residual glass lead to the formation of fluorcanasite. The growth of the canasite crystals is spherulitic. In a glass ceramic, these crystals do not precipitate in the entire glass mass simultaneously; at certain points nuclei first appear which then grow into the ambient melt (Hlavác, 1983).

As noted above the nucleation of the  $\text{CaF}_2$  also determines the final microstructure of the glass-ceramic. Likitvanichkul and Lacourse (1995) showed that the F content of the parent glass is critical for the formation of canasite glass-ceramics. Fluorine is required for both nucleation by  $\text{CaF}_2$  and, since it is a constituent of canasite, it must also be available during the growth stage.

#### 2.4.2 Other phases

Recently Miller *et al* (2004) have reported that, in most cases a mixture of canasite (JCPDS 13-0553) and canasite-A (JCPDS 45-1398) is present in canasite compositions

derived from the stoichiometric glass formulation. It has been found that canasite-A is in fact a different mineral to canasite, which although closely related, has been given its own mineral designation, frankamenite (Rozhdestvenskaya *et al*, 1996), although the aforementioned JCPDS card still refers to the mineral as canasite-A. This high F-content canasite-like mineral was first reported from the pegmatites in South Yakutia, Russia (Lazebnik and Lazebnik, 1981). In a later paper (1996), Rozhdestvenskaya and Nikishova have compared the mineralogical and structural characteristics of frankamenite with canasite. The Yakutian mineral frankamenite ( $K_3Na_3Ca_5Si_{12}O_{30}(OH)F_3H_2O$ ) occurs as semi-transparent, prismatic crystals of gray, lilac, blue or green colour. The mineral frankamenite differs from canasite by having a higher fluorine content. Rozhdestvenskaya and Nikishova (1996) believed that the high fluorine content is responsible for the orderly filling of the octahedra in the walls, which results in the lowering of the symmetry to triclinic. The 3D structures of both frankamenite and canasite can be seen in Figures 2.2 and 2.23.

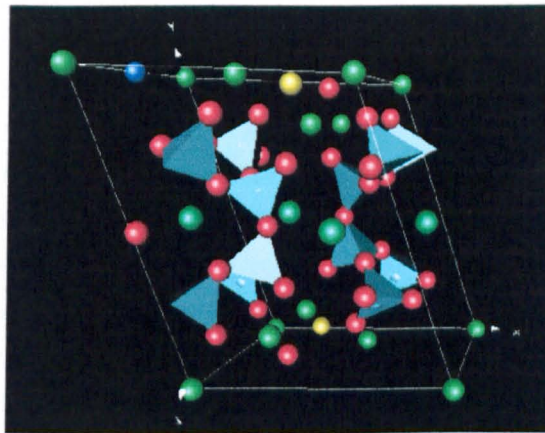


Figure 2.2: Structure of frankamenite with the tetrahedron representing Si and the spheres representing O (red), Ca (blue), F (yellow) and mixed Na and K sites (green).

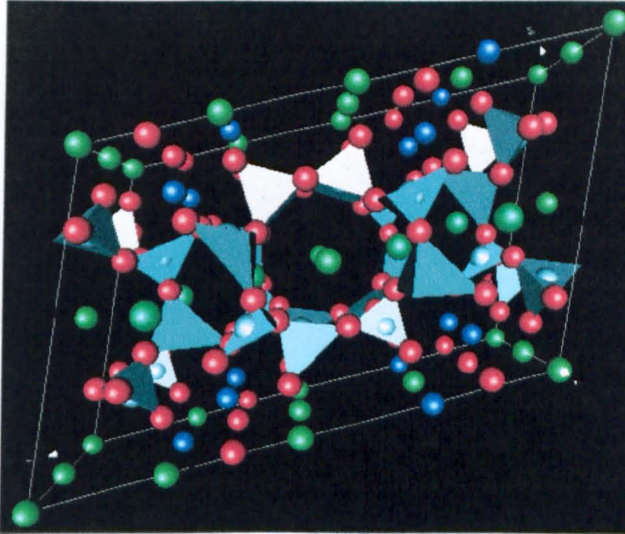


Figure 2.3: Structure of canasite with the tetrahedron representing Si and the spheres representing O (red), Ca (blue) and mixed Na and K sites (green).

The crystal structure of frankamenite is composed of zigzag walls of Ca-Na octahedra joined together by infinite octagonal cross-section tubes of Si-O tetrahedra with the composition ( $S_{12}O_{30}$ ) and are topologically similar to the canasite structure. The distribution of Na and Ca atoms in the canasite and frankamenite structures has been given in Table 2.1 and Figure 2.4, which is a projection of the canasite structure along the elongated axis (Rozhdestvenskaya *et al*, 1996).

In the monoclinic structure of canasite the Na and Ca cations are ordered over the various octahedral sites. Two octahedral sites, M(1) and M(6) are occupied by  $Na^+$ , M(4) and M(7) by  $Na^+$  and  $Ca^{2+}$  cations and the rest by  $Ca^{2+}$  cations. Whereas in the triclinic structure of frankamenite, of the eight octahedral positions, M(1) is completely occupied by  $Na^+$  and M(2) completely by  $Ca^{2+}$  cations. M(3) and M(4) octahedral are isomorphically occupied by almost equal  $Na^+$  and  $Ca^{2+}$ . The rest (M(5) to M(8)) can be occupied by Ca and Na cations approximately in the ratio 1:2. The overall octahedral atomic composition was calculated to be  $Na_{3.14}Ca_{4.86}$ , which although slightly different from the average chemical composition, was found to fall within the range of compositions found by microprobe analysis.

Table 2.1: The distribution of Na and Ca atoms in the canasite and frankamenite structures

Octahedral positions	Frankamenite	Canasite
M(1)	Na	Na
M(2)	Ca	Ca
M(3)	Na, Ca	Ca
M(4)	Na, Ca	Na, Ca
M(5)	Na, Ca	Ca
M(6)	Na, Ca	Na
M(7)	Na, Ca	Na, Ca
M(8)	Na, Ca	Ca

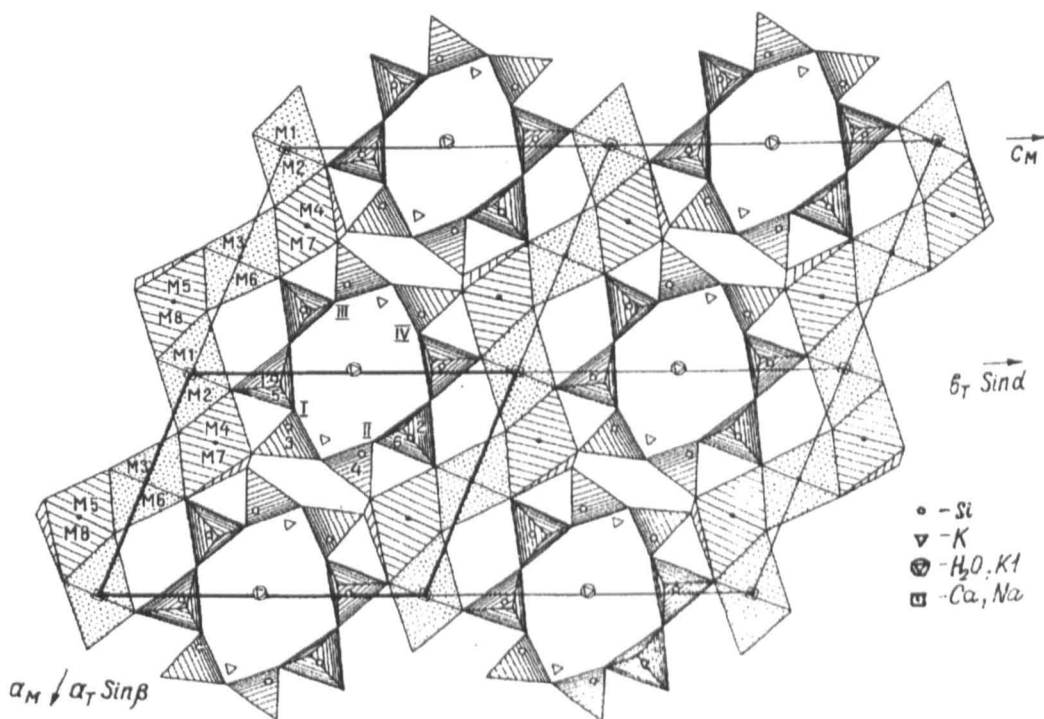


Figure 2.4: Projection of the canasite structure along the elongated axis. Triclinic cell is shown by the thick line. I, II, III, IV mark the four chains forming the  $Si_{12}O_{30}$  tube. M(1) and M(2) are alternately Na and Ca octahedral, while M(3) to M(8) are mixed Ca, Na positions.

X-ray powder patterns of the two minerals are similar, except that there are twelve weak reflections in the high  $2\theta$  region for frankamenite (Rozhdestvenskaya and Nikishova, 1996). Previous work on the differentiation of these two phases (Miller, 2004; Stokes,

2003) has referenced these cards and found specific peaks for canasite to exist at 25.3, 32.2, 33.3, 37.8 and 43.4  $^{\circ}2\theta$  and for frankamenite to exist at 10.1, 21.1 and 29.5  $^{\circ}2\theta$ . However the calculated XRD traces derived from the Inorganic Crystal Diffraction Database for both canasite and frankamenite (Figs. 2.5 and 2.6) indicate the opposite, for example, the greater intensity peak at 10.1  $^{\circ}2\theta$  is for canasite not frankamenite.

Having noted this discrepancy, it is necessary to establish at the outset that the notation followed by this study will be that already established in the literature. The presence of peaks at 10.1, 21.1 and 29.5  $^{\circ}2\theta$  shall be taken as evidence for the presence of the phase frankamenite.

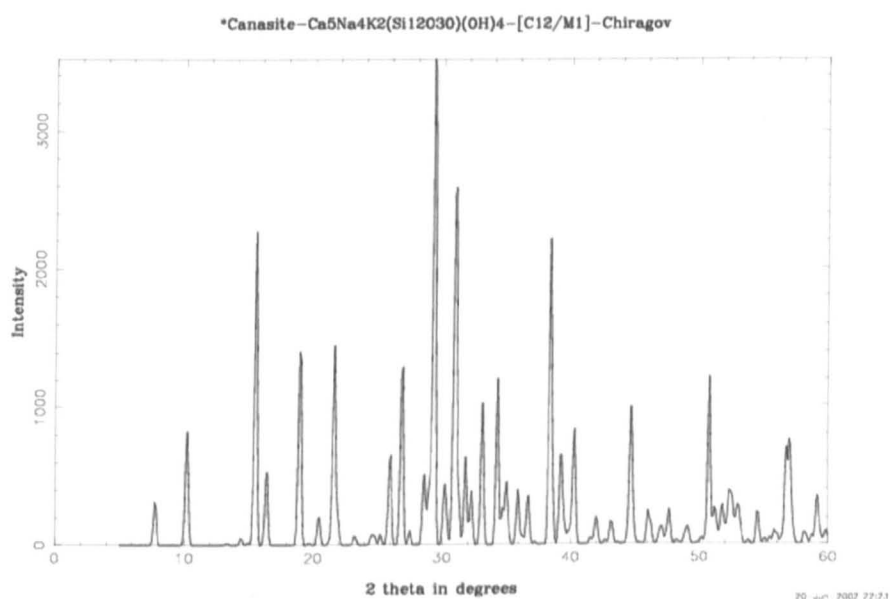


Figure 2.5: Calculated XRD trace of canasite.

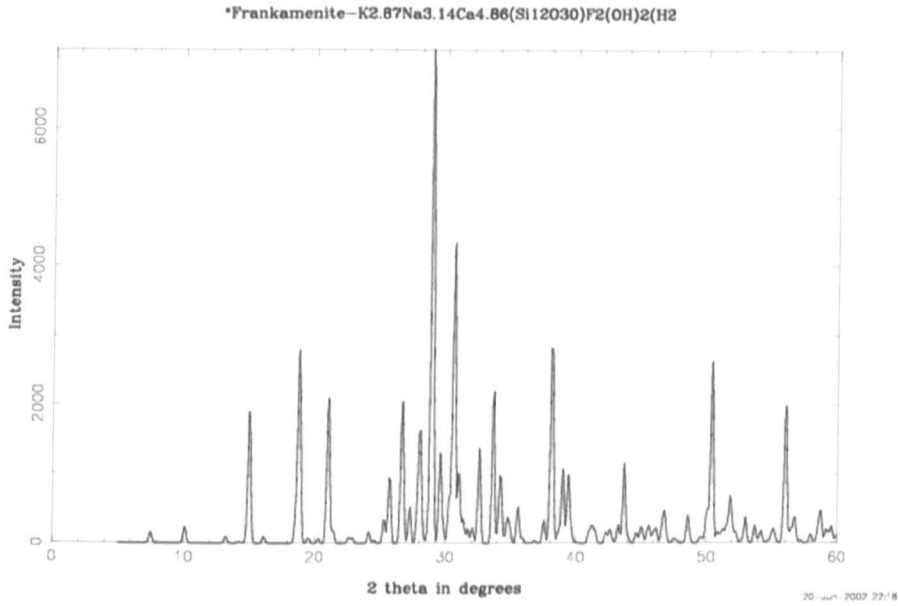


Figure 2.6: Calculated XRD trace of frankamenite.

Unfortunately, the majority of the work prior to Miller *et al* (2004) published on canasite does not distinguish between the two types. Beall (1983) concluded that the predominant crystal phase developed in the stoichiometric compositions, through heterogeneous nucleation, was canasite as the X-ray powder diffraction patterns obtained were comparable to those from the naturally occurring minerals. Miller suggested that two individual sequences of nucleation and growth govern the formation of the two phases, with canasite heterogeneously nucleating in the presence of CaF<sub>2</sub> nuclei and frankamenite homogeneously nucleating in its absence.

Rastsvetaeva *et al* (2003) have further identified a high fluorine analogue of canasite which retains the monoclinic structure. The mineral called F-canaseite, found to have the empirical formula of (Ca<sub>4.5</sub>Mn<sub>0.45</sub>Fe<sup>2+</sup><sub>0.05</sub>)K<sub>3</sub>Na<sub>3</sub>Si<sub>120</sub>O<sub>30</sub>(OH)<sub>1.2</sub>F<sub>2.8</sub>.*n*H<sub>2</sub>O by microprobe analysis, can also be claimed to be a monoclinic analogue of frankamenite. Jambor and Roberts (2004) have identified the F-dominant analogue of canasite as a new mineral awaiting approval by the Commission on New Minerals and Mineral Names, International Mineralogical Association.

## 2.5 Desired Properties in Dental Ceramics

### 2.5.1 Mechanical requirements

Some aspects of the intra-oral environment are listed in Table 2.2 (Kelly, 1997). The wide temperature range and pH shifts are of only secondary concern with respect to clinical survival of ceramic restorations. Any material replacing teeth should be able to withstand the maximum biting forces sustained during activities like clenching and grinding as well as chewing cycles.

Table 2.2: Intra-oral conditions

Forces measured during mastication	6-130N
Maximum average biting forces sustained	200-800N
Chewing cycles/day	1000-1400
Temperature range	5-65°C
pH range	0.5-8.0

The International Standard ISO6872:1995(E) for dental ceramics defines minimum values of flexural strength and maximum values of chemical solubility that potential dental ceramics must obtain. The values are dependent on the intended use of the dental ceramic within the mouth. Table 2.3 summarises these requirements where class 1 is a core ceramic which would be used for the fabrication of supporting structure for crowns, veneers, inlays and onlays, referring to materials which are intended to be layered and class 2 are those materials which are used for the fabrication of veneers, inlays and onlays without layering.

Table 2.3: Physical and chemical property requirements (ISO6872:1995)

Property	Requirement	
	Class 1	Class 2
Flexural Strength , MPa (minimum)	100	30
Chemical solubility, $\mu\text{gcm}^{-2}$ (maximum)	2000	100

The use of porcelain and glass-ceramics in restorative dentistry is increasing due to improved and new formulations and processing techniques, improvements in mechanical performance, and because of their abilities to mimic the appearance of natural teeth and maintain favourable aesthetics. However, their main shortcoming remains the low fracture toughness values associated with these materials. An exacerbating factor is the tendency to absorb only low quantities of strain energy, prior to brittle fracture, at a critical strain of about 0.1 % (Anusavice, 1996). This is brought about by the growth of subcritical size flaws to critical dimensions by the interaction of the oral fluids with residual or biting stresses. As a result they are relatively easily broken. Incisal and gingival (body) porcelains and glass-ceramics transmit biting forces directly from the contacting areas, while the opaque and aluminous core porcelains, being part of the substructure, transmit them indirectly. The development of the canasite is geared towards the production of a stronger dental ceramic, which will maintain the aesthetic standards of ceramics used anteriorly, as well as combine the strength required for posterior use.

The strength of a material is the stress that is required to break that material. Brittle materials have low tensile & flexural strength because of their inability to plastically deform and reduce the tensile stress at flaw tips. This is true of all brittle dental materials, such as composites, cements, and ceramics. Fracture begins from a single location called the fracture origin, which is a discontinuity such as a flaw or a defect that has developed from mechanical, chemical or thermal processes that will act as a localised stress concentrator. Under a specific critical applied stress, the crack will initiate from these defect-sites and propagate catastrophically, leaving characteristic markings on the fracture surfaces. Crack growth may also occur subcritically. In brittle materials this usually occurs via chemical interactions. The time taken for subcritical crack extension governs the 'fatigue' behaviour of the material.

### 2.5.2 Aesthetic requirements

The two main requirements for ceramic restorations are appropriate aesthetics and mechanical properties. The structure and how closely a restoration can match the translucent properties of a human tooth influence the aesthetics of a restoration. Dentin is more opaque than enamel and reflects light. Enamel is a composite layer over the dentin and is composed of tiny interlocking crystalline prisms or rods of hydroxyapatite cemented together by an organic matrix.

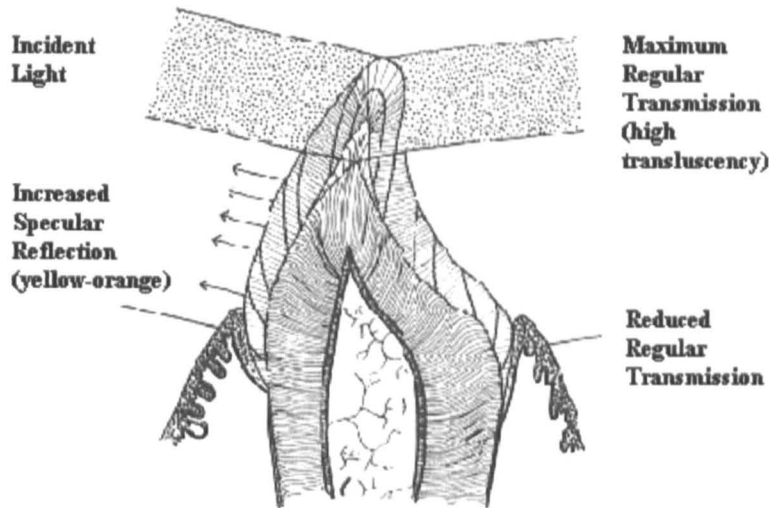


Figure 2.7: Reflection and transmission of incident light through the dentine and enamel (McLean, 1979).

The indices of refraction of the rods and the cementing substance are different. As a result, a light ray is scattered by reflection and refraction to produce a translucent effect and a sensation of depth as the scattered light ray reaches the eye. As the light ray strikes the tooth surface, part of it is reflected, and the remainder penetrates the enamel and is scattered. Any light reaching the dentin is either absorbed or reflected, to be again scattered within the enamel (Figure 2.7). Gingival colour would also be influenced by the gum and root dentine.

In ceramic restorations bonded onto a ceramic-substructure, there is a reduced reflection from the alumina core, especially in the gingival areas thus giving a duller appearance in comparison to the natural tooth (Figure 2.8).

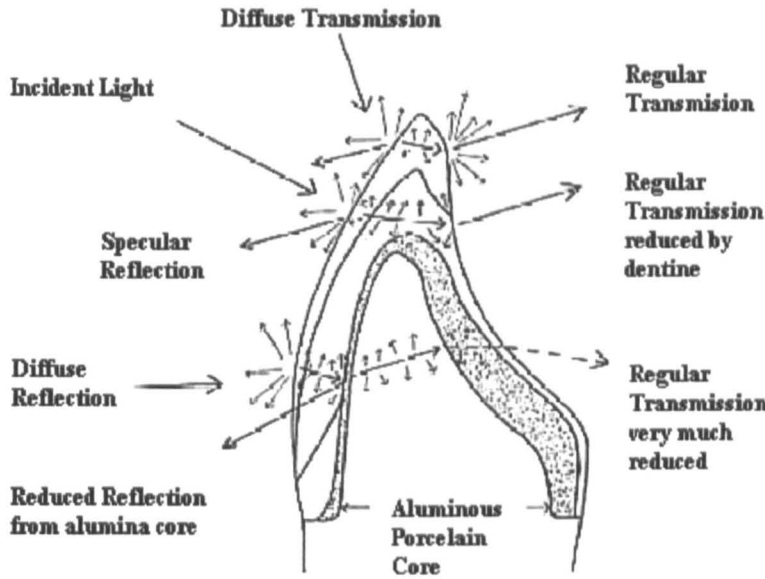


Figure 2.8: Reflection and transmission in aluminous porcelain crown (McLean, 1979)

High spots are produced on ceramics bonded to metal-substructure, due to high reflection from the porcelain-metal boundary (Figure 2.9). High reflection is undesirable since natural teeth seldom produce areas of high reflectivity. Translucent enamel reduces reflection but increases light transmission.

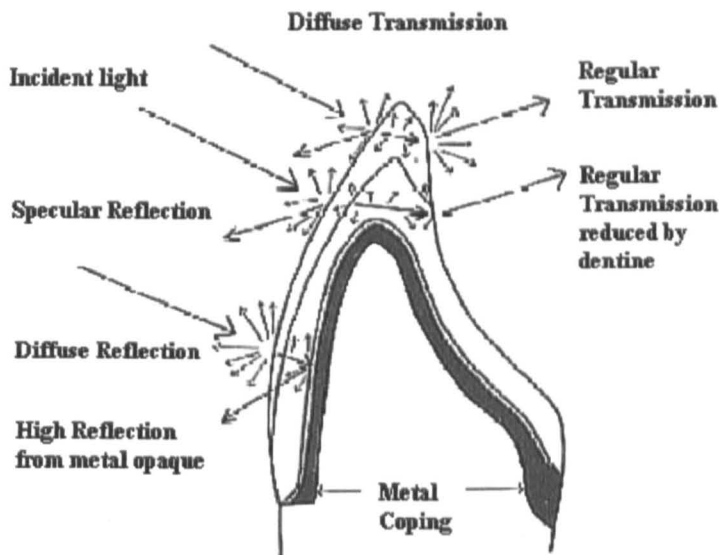


Figure 2.9: Light reflection and transmission in metal-ceramic crown (McLean, 1979).

Resin bonded ceramics (RBCs) consist of a thin shell of feldspathic porcelain or glass-ceramic, bonded to tooth enamel using an acid etch technique. The approach focuses on conserving the tooth substructure, and hence, the reflection and transmission of incident light through the dentine and in some cases, the enamel, is unaffected giving a better aesthetic appearance than either the PJs or the PFMs (Figure 2.10).

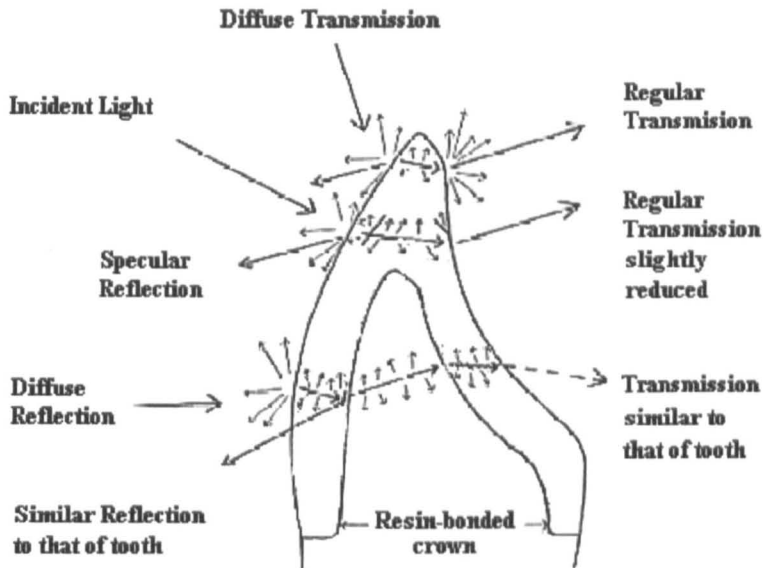


Figure 2.10: Light reflection and transmission in a resin-bonded crown (McLean, 1979).

## 2.6 Current commercial dental ceramics

Conventional dental ceramics can be classified by type (feldspathic porcelain, leucite-reinforced porcelain, aluminous porcelain, glass-infiltrated alumina, glass-infiltrated spinel and glass-ceramic), by use (denture teeth, veneers, inlays, crowns and anterior bridges), by processing method (sintering, casting, or machining and CAD-CAM), or by the substructure material. A broad categorisation can be achieved by considering the last of these, the substructure used to support the ceramic; (1) a ceramic substructure as in the case of the core-reinforced ceramics, (2) a metal substructure or (3) the 'tooth substructure', as in the case of the resin-bonded systems. Within this classification, various types of ceramic materials can be identified.

### 2.6.1 Ceramics bonded to ceramic-substructure

Since the Porcelain Jacket Crown (PJC) introduced by Land in 1903, essentially a coloured feldspathic glass, various systems have been developed with higher percentage inclusions of alumina in the porcelain in an attempt to increase the strength. The alumina crystal size in the PJC (25 - 37  $\mu\text{m}$  or 400 mesh) was selected for its economical and commercial reasons. However, PJCs are only suited for anterior teeth because their strength is insufficient for posterior use (McLean, 1979). Typical fracture toughness values associated with these dental ceramics are up to  $2\text{MPam}^{-3/2}$  (Bieniek and Marx, 1994). Development to improve conventional all-ceramic restorations has concentrated mainly on improving the crown's fracture resistance by producing a stronger core material. The *Inceram Porcelain Core* (Inceram, Vita Zahnfabrik, Bad Sackingen, Germany; Vident Balden Park, CA, USA) permits the inclusion of a high proportion (85%) of crystalline material with reported strengths as high as 446 MPa (Seghi and Sorensen, 1995) and the *Ceramic Jacket Crown (CJC)* commercially called Techceram System, produced by (Techceram Ltd, Shipley, UK), in which a thin layer, 0.1mm to 1.0mm, of alumina core is produced using a thermal gun-spray technique that results in a density of 80~90 % (Qualtrough, 1996). Alison (1999) indicates CJs for the construction of single crowns and a three-unit bridge, but no data has been reported on their longevity.

In addition to alumina, other reinforcement phases developed include magnesia. O'Brien in 1985 suggested that materials which contain 40-60% magnesia would react with silica on heating to form forsterite ( $\text{Mg}_2\text{SiO}_4$ ). Zirconia has been added to feldspathic material in the past as a reinforcing phase in Mirage II (Myron Int. Inc., Kansas City) as short tetragonal whiskers in the same way that alumina had, resulting in flexural strengths of 70 MPa (Seghi *et al*, 1990). InCeram Zirconia (Vita Zahnfabrik), a material with two crystal phases (67% alumina and 33% zirconia), has been developed with reported flexural strength values of 603 MPa (Seghi *et al*, 1995).

### 2.6.2 Ceramics bonded to metal-substructure

Porcelain-fused-to-metal substructure (PFM) restorations were developed to overcome the problems of brittle fracture associated with all-ceramic crowns. In 1956, Brecker described the manufacture of crowns and bridges by fusing dental porcelains to gold alloys. Later, Weinstein *et al* (1962) tried to address the problem of thermal expansion coefficient

mismatch between porcelain and metal substrate, which continues to be a matter of concern; precious metals and nickel alloys have a higher coefficient of thermal expansion ( $14-15.7 \times 10^{-6}/^{\circ}\text{C}$ ) (McLean and Hughes, 1965) than porcelain. This was overcome to a certain extent by mixing tetragonal leucite into the feldspar. It was shown that the expansion coefficient of dental porcelains is altered by multiple firings (Fairhurst *et al*, 1980), which can raise the crystalline leucite content of the ceramic, which in turn produces an increase in the thermal expansion of the porcelain. However, the leucite phase itself undergoes a displacive transformation reaction on heating above  $400^{\circ}\text{C}$  from a tetragonal to a cubic form with a resultant 1.2% volumetric expansion and a change in expansion coefficient (Mackert *et al*, 1986).

To prevent debonding of the ceramic layer, a strong bond should exist between porcelain and metal (Pidcock and Qualtrough, 1990). This bond must be capable of withstanding the interfacial shear forces generated during fabrication due to the differences in expansion coefficient and to the sintering shrinkage of the porcelain. A range of test methods has been utilised to determine the magnitude of the bond between porcelain and metal. Jones (1988) has correlated results from a number of studies and has highlighted the wide variation in bond strength data that exists, depending on the test procedures adopted. In fact there still remains the need for an appropriate standard test method for assessing porcelain-alloy compatibility.

A further disadvantage of metal-based restorations is that, they are increasingly being shown to be a health risk, or are being perceived as unsafe (Dobson, 1999). A number of studies have looked at the factors affecting biocompatibility of the alloys used. Nickel-containing alloys such as nickel-chromium, used for porcelain bonded to metal restorations, are seen as dangerous due to allergic reactions and gold alloys because of their copper content.

### 2.6.3 Resin-bonded ceramics

The development of ceramics directly bonded onto the 'tooth-substructure' accompanied the discovery that many dental porcelains and glass ceramics can be etched with hydrofluoric acid or other acids to create retentive channels similar to those in acid etched enamel. Termed resin-bonded, acid-etched ceramic restorations or RBCs, these ceramics present a more conservative approach than the use of full crowns. It has been shown that by resin-bonding a weaker, but etchable crown to the underlying dentine, the crown will exhibit superior fracture resistance to that of conventional alumina or metal reinforced luted

crown (Potiket *et al*, 2004). These RBC's, as stated before, provide considerably better aesthetics than the PJs or PFMs.

*Leucite-reinforced porcelains* are feldspathic porcelains reinforced with leucite crystals, which have been developed for use as resin bonded restorations. Optec HSP (Jeneric/Pentron, Wallingford, CT USA) is an all ceramic restoration based on this system. The tetragonal leucite ( $\text{KAlSi}_2\text{O}_6$ ) in the glass matrix is as high as 45% leading to a high coefficient of thermal expansion of  $18 \times 10^{-6}/^\circ\text{C}$  (McLean and Hughes, 1965). The opacity present in the body and incisal eliminates the need for the core layer. Due to shrinkage, the fit is not as good as that of the PFM crowns. The material has a moderate flexural strength, but has the potential to break when used in the posterior region (Denry *et al*, 1998).

IPS Empress (Ivoclar / Vivadent, Amherst, NY, USA. or Schaan, Liechtenstein), a pre-cerammed glass-ceramic, is similar to the Optec HSP system, but with a much higher content of leucite crystals (Denry *et al*, 1998), that increases the resistance to crack propagation or fracture. This is a hot pressed or injection moulded glass-ceramic. The leucite undergoes a crystallographic transformation from tetragonal to cubic, with a high coefficient of thermal expansion ( $\approx 25 \times 10^{-6}/^\circ\text{C}$  from room temperature to  $625^\circ\text{C}$ ). However, the high-temperature cubic form exhibits a low coefficient of thermal expansion ( $\approx 3 \times 10^{-6}/^\circ\text{C}$  from  $625^\circ\text{C}$  to  $900^\circ\text{C}$ ). The final crown is then stained and glazed. These hot-pressed ceramics have a good fit and adequate aesthetics, but also have the potential to fracture in the posterior region (Höland *et al*, 2000).

*Lithium disilicate* and *apatite* have been used as reinforcement in a new composition, IPS Empress II (Ivoclar Vivadent, Schaan, Liechtenstein). Höland *et al* (2000) suggest the application of Empress II for areas where high stresses are induced (e.g. for posterior crowns and for three unit bridges) but have conducted no fatigue tests to prove their claim. More recently the *Procera ALL-Ceram* system (Nobel Biocare, Gotenborg, Sweden) (Alison, 1999) has been introduced which consists of 99.9% high-alumina. Clinical evaluation of this material shows a very favourable outcome of 4.5% cumulative failure rate, suggesting all-ceramic restorations can compete with ceramometal restorations, even in posterior tooth replacement (Naert *et al*, 2005). The most recent core materials for all ceramic restorations are the yttrium tetragonal zirconia polycrystals (Y-TZP) based materials like *Cercon* (Dentsply Ceramco, Burlington, NJ), *DCS-Precident DC-Zirkon* (Dentsply Austenal, York) and *Lava* (3M ESPE, St. Paul, Minn) with flexural strength values of 900-1200 MPa and associated fracture toughness of 9-10  $\text{MNm}^{-3/2}$  (Raigrodski, 2004; Tinschert *et al*, 2001 and Christel *et al*, 1989). The resin bond to silica is well documented, however, the few available studies on resin-bonding to zirconium oxide

ceramics suggest the use of resin cements that contain special adhesive monomers (Blatz *et al*, 2003). Compared with silica based ceramics, the number of in-vitro studies on the resin bond to high strength ceramics is small.

Although resin-bonded ceramics have performed better than many materials scientists had predicted, their use in the posterior region has been limited due to fracture toughness and strength constraints. RBCs that have been indicated for posterior use, like the IPC Empress II, require specialist techniques and equipment, leading to higher costs, whereas the methods of fabrication of high strength Y-TZP ceramics still need to be optimised (Luthardt *et al*, 2003). Bearing in mind the excellent aesthetics, and the lack of a cost effective, metal-free restoration, experimental glass-ceramics that are easy to fabricate, specifically the chain-silicates considered here, have great potential in restorative dentistry.

#### 2.6.4 Mechanical properties

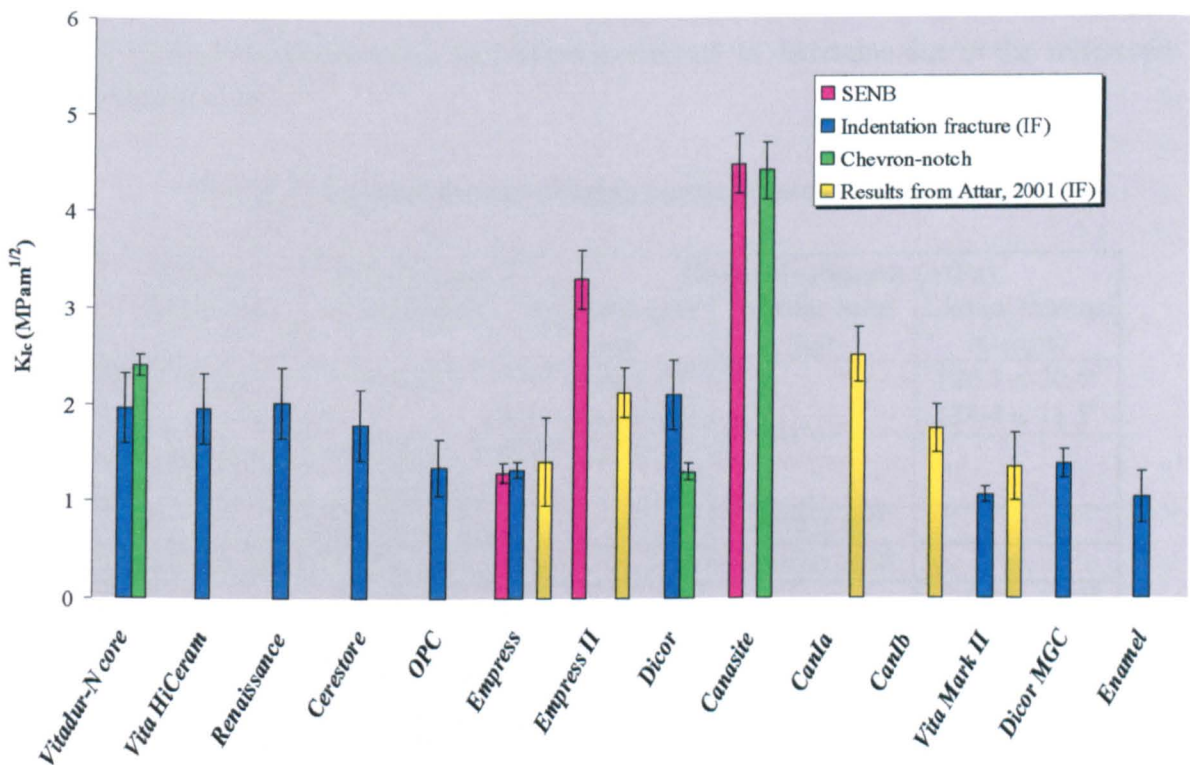


Figure 2.11: Fracture toughness values ( $K_{Ic}$ ) of some dental materials taken from Seghi *et al*, 1995; Thompson *et al*, 1996; Rosenstiel *et al*, 1989; Mueller, 1991; Höland *et al*, 2000; Gorman *et al*, 2000; Beall *et al*, 1986, Xu *et al*, 1998 and Attar, 2001.

The development of dental ceramics over the past two decades has been geared towards manipulative tailoring of the microstructure. All new dental ceramics that have microstructures that include a crystalline phase in a glassy matrix inhibit crack propagation by: (1) pinning the crack between the particle and glassy matrix, as in the alumina reinforced porcelains (Kelly, 1997), (2) residual stress fields caused by the difference in thermal expansion of glass and crystalline phase (Morena *et al*, 1986), (3) residual stress fields caused by phase transformations, as in the case of leucite (Seghi *et al*, 1995) and (4) the refinement of the crystal sizes in the glassy matrix, as seen with lithium disilicate in Empress II (Höland *et al*, 2000). Mechanical properties of dental ceramics tested conventionally are flexural strength, fracture toughness and fatigue strength.

Figure 2.11 compares the values of the fracture toughness,  $K_{Ic}$  obtained for current ceramic systems as well as the experimental material, canasite. The figures, although dependent on the test method, show higher fracture toughness values for Empress II, the lithium disilicate heat pressed ceramic ( $> 3 \text{ MNm}^{-3/2}$ ) and very promising results for canasite ( $> 4 \text{ MNm}^{-3/2}$ ). A value for enamel has been included for comparison, however a single fracture toughness value for enamel is difficult to determine due to the anisotropic nature of the rods.

Table 2.4: Reported flexural strength values of some dental materials.

Dental Material	Reinforcing Component	Flexural strength (MPa)		
		3-point flexure test	4-point bend test	Biaxial flexural strength
<i>IPS Empress</i>	Leucite	$126 \pm 15^b$		$120.1 \pm 20.5^c$
		$112 \pm 10^f$		$134.4 \pm 11.5^d$
<i>IPS Empress 2</i>	Lithium disilicate	$400 \pm 40^i$		
<i>Dicor</i>	Fluormica		$107.8 \pm 8.5^e$	
<i>Vita InCeram</i>	Alumina		$236.2 \pm 21.9^e$	
<i>OPC</i>	Leucite			$139.1 \pm 14.3^c$
				$153.6 \pm 17.8^d$
<i>Vita Mark II</i>	Sanidine & nepheline			$84 \pm 6^g$
<i>Canasite</i>	Canasite			$261.4 \pm 21.1^a$

<sup>a</sup> Johnson *et al*, 1998b

<sup>d</sup> Gorman *et al*, 2000

<sup>g</sup> Thompson *et al*, 1996

<sup>b</sup> Dong *et al*, 1992

<sup>f</sup> Giordano *et al*, 1995

<sup>e</sup> Cattell *et al*, 1999

<sup>c</sup> Höland *et al*, 2000

Table 2.4 compares results of flexural strength quoted in studies carried out in some commercial systems over the past 10 years. The spread in the results obtained from different studies, on the leucite reinforced materials, IPS Empress I and OPC, demonstrates the effect of test operator variance.

## 2.7 Development of canasite as a dental ceramic

The stoichiometric canasite glass composition as stated by Beall, 1983 (ie.  $60\text{SiO}_2\text{-}10\text{Na}_2\text{O-}5\text{K}_2\text{O-}15\text{CaO-}10\text{CaF}_2$ ) was said to result in a  $K_{Ic}$  of  $5 \text{ MNm}^{-3/2}$  (see Figure 2.10). However in the patent of 1983, Beall lists various compositional variations to the above stated and it is unclear as to which one is associated with the high  $K_{Ic}$  value. Fluorcanasites have been synthesised from glasses with general formula  $\text{Ca}_5\text{Na}_{4-x}\text{K}_{2+x}\text{Si}_{12}\text{O}_{30}\text{F}_4$ , where  $1 \geq x \geq 0$ . Van Noort *et al* (1997) have shown that these glass-ceramics have potential as a restorative material for crowns and inlays. Anusavice and Zhang (1998) used a base glass composition of  $58.36\text{SiO}_2\text{-}8.26\text{Na}_2\text{O-}9.19\text{K}_2\text{O-}16.83\text{CaO-}7.36\text{CaF}_2$  which gave them a  $K_{Ic}$  value of  $2.7 \pm 0.1 \text{ MNm}^{-3/2}$ . They investigated the addition of alumina to the batch in an effort to increase chemical durability but found additions of  $\geq 2 \text{ wt}\%$  reduced the mechanical properties. Stokes *et al* (2001) have suggested that the ISO test for solubility gave large variances in the result. Stokes (2001) suggests that the residual glass within the glass-ceramic may be the cause of the high chemical solubility of fluorcanasite and thus the ways of reducing solubility in conventional glass systems could be considered. These include raising the Si or Ca content of the glass to inhibit alkali diffusion. Systematic additions of  $\text{SiO}_2$  and  $\text{AlPO}_4$  have been noted as reducing the solubility of fluorcanasite from 2359 to  $624 \mu\text{gcm}^{-2}$  (Bubb *et al*, 2004). Beall (1983) reports that the addition of zirconia decreases solubility but increases opacity, which may be acceptable if fluorcanasite is to be used as a high strength core material. Alternative nucleating agents to  $\text{CaF}_2$  may also exist, although the formation of canasite seems to be dependent on fluorite being present within the glass. A low solubility glass composition, suitable for dental applications, has been identified by Stokes *et al* (2001). They examined a series of glasses,  $60\text{SiO}_2\text{-(y-15)Na}_2\text{O-yK}_2\text{O-}15\text{CaO-}10\text{CaF}_2$  where  $0 \leq y \leq 15$ , and found that the solubility varied with the alkali content, exhibiting a minimum value at a  $[\text{K}]/[\text{K}+\text{Na}]$  molar ratio of 7/15. The mechanism for the dissolution of the fluorcanasite was thought to be based upon a  $\text{Na}^+$  and  $\text{H}^+/\text{H}_3\text{O}^+$  exchange on the surface, followed by the formation of a silica gel layer that then sloughs away.

Unfortunately, this increase in chemical durability was associated with inferior mechanical properties than those previously reported for canasite based glass-ceramics. Any future development of this glass-ceramic would have to start with the low solubility composition with the aim of improving the mechanical strength.

## **2.8 Dental Material Testing**

### **2.8.1 Crystallisation studies**

The properties of glass ceramics depend on the types and amounts of crystal phase formed and on the composition of the residual glass. Thus the determination of the degree of crystallisation and the investigation of the transformation of the parent glass in glass-ceramics is very important.

A number of techniques have been employed for the determination of the crystal content of the glass-ceramics. The most common and well established technique is X-ray diffraction. XRD has been combined with electron microscopy in several studies to determine the phases present in crystalline material (Kim *et al*, 1989; Strnad, 1986; James *et al*, 1997). However, these techniques are accompanied by experimental difficulties and can be time consuming when carrying out quantitative studies. In addition to this, Karamanov and Pelino, 1998, have suggested that the associated experimental error is up to 10%. In some cases, the result of the crystallisation process may result in modification of properties, which lends itself to indicate the transformation or degree of crystallisation affects these. The properties that have been measured to assess the extent of crystallisation include changes in viscosity and electrical resistivity, thermal expansion coefficient and density (Karamanov and Pelino, 1999).

### **2.8.2 Mechanical strength testing**

Flexural strength, transverse strength, or modulus of rupture, as this property is variously called, is essentially a strength test of a bar supported at each end, or a thin disk supported along a lower support circle, under a static load. The strength testing of brittle materials is complicated by the flaw sensitivity of the materials leading to a statistical distribution of strengths. In addition the tests that can be conducted relatively simply usually have a more

complicated stress distribution. Thus for example, the flexural test is a collective measurement of tensile, compressive, and shear stresses simultaneously; however, for sufficiently thin specimens, failure is usually dominated by the tensile stress that develops along the lower surface. For brittle materials such as ceramics, flexure tests are preferred to the diametral compressive test because they more closely simulate the stress distributions in dental prostheses such as cantilevered bridges and multiple-unit bridges (Anusavice, 1996) and there is widespread use of flexure tests for current commercial and experimental systems.

Fracture toughness is a mechanical property that describes the resistance of materials to the catastrophic propagation of the flaws under an applied stress. Strength is related to toughness via the flaw size and the higher the ductility (total plastic strain), the greater the toughness. For brittle materials such as dental ceramics, strength values are of limited value in the design of ceramic prostheses. Small defects (porosity and micro-cracks) are randomly distributed in location and in size throughout a ceramic, causing large strength variations in otherwise identical ceramic specimens. Furthermore, surface flaws caused by grinding, such as from coarse-grit, medium-grit, or fine-grit diamond particles, can greatly weaken a ceramic, especially in the presence of tensile stress in the area of these flaws. The strength is inversely proportional to the square root of the depth of the flaw into the surface. A better design criteria is the fracture toughness which is a material constant and thus independent of crack size (Mecholsky, 1995).

A number of techniques have been developed which all aim at determining the fracture toughness of ceramics. One group of techniques is based on conventional fracture mechanics using notches and secondarily induced pre-cracks (compact tension, CT; double cantilever beam, DCB; single-edge-notched-beam, SENB; single-edge pre-cracked-beam, SEPB and chevron notch, CN) (Scherrer *et al*, 1998). A second group of techniques is based on the sharp-indenter approach, introducing diagnostic micro-cracks by Vickers or Knoop indentation [indentation fracture (IF), (Evans and Charles, 1976) indentation strength (IS) (Chantikul *et al*, 1981) surface crack in flexure (SCF) (Quinn *et al*, 1996)].

Conventional fracture mechanics procedures are afflicted with a number of inherent difficulties such as (1) minimising the notch tip width (SENB), (2) detecting stable (i.e. self limiting) crack-growth (CN, CT), (3) keeping control and measuring the length of the pre-crack (SEPB), (4) mastering specimen preparation (CT), and (5) controlling the environment (temperature; humidity). As an alternative to conventional fracture toughness tests, the indentation fracture technique has been established as a procedure suitable for approximate determinations of  $K_{Ic}$  for brittle materials. An accuracy of 10% can be

obtained when Young's modulus ( $E$ ) is known, or 30% when  $E$  is unknown (Evans and Charles, 1976). The indentation strength technique (IS) as described by Chantikul *et al* (1981) is a two step technique that requires (1) the introduction of a flaw by micro-hardness indentation and (2) controlled fracture in either a bend test (bars) or a biaxial flexure test (disks). There is no need to determine the initial size of the flaw. The crack will extend in a stable manner during the subsequent fracture test until it reaches a critical size at which point catastrophic failure will occur (Chantikul *et al*, 1981). The addition of a specific residual stress intensity factor term into the strength/ toughness formulation overcomes the systematic error inherent to all indentation techniques which do not adequately account for residual stress fields. Reportedly, the IS method is insensitive to post-indentation radial crack extension (Chantikul *et al.*, 1981). In most studies on dental ceramics reported in the literature,  $K_{Ic}$  was determined using the IF technique. This method requires only small specimens and is fairly simple to apply (Morena *et al.*, 1986; Rosenstiel and Porter, 1989, Anusavice and Lee, 1989; Seghi *et al.*, 1995; Denry and Rosenstiel, 1993). A comparison between the indentation fracture (IF), indentation strength (IS) and the single-edge V-notched beam test (SEVNB) was conducted by Scherrer *et al*, 1998, in which was concluded that all three methods agreed within 10%. In a paper evaluating the effect of test method on the fracture toughness of canasite glass-ceramic, Beall (1986) found that IF method gave significantly lower  $K_{Ic}$  values of approximately  $1.5 \text{ MPam}^{1/2}$  compared with  $4.48 \pm 0.31 \text{ MPam}^{1/2}$  from SENB method.

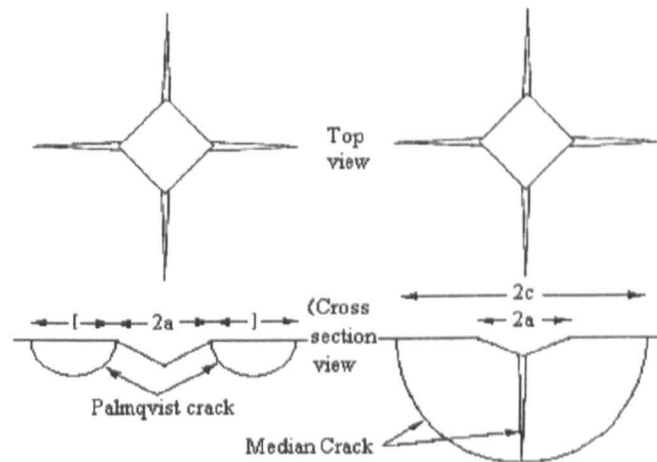


Figure 2.12: Geometry of Palmqvist and Radial/median cracks around Vickers indentation.

In an evaluation of various indentation toughness equations for glass ceramics, Ponton & Rawlings (1989) suggest  $K_{Ic} = 0.0824 P/c^{3/2}$  gives results that are most in line with other materials, assuming the cracks are of the radial/median type. Although they found that this equation has given values of  $K_{Ic}$  lower than 25% compared with other equations, it was found to be most reliable when correlating and ranking results obtained on different materials

### 2.8.3 Chemical Durability

The reactions which occur during glass-ceramic dissolution have been likened to those which occur in glasses (Stokes, 2003). When a glass is immersed in an aqueous solution, reactions which occur commonly are known to be uniform dissolution, ion exchange and hydration (Koenderink *et al*, 2000). Glass composition, temperature and solution pH determine the relative rates of these reactions (El-Shamy *et al*, 1972). At a high pH (>9), uniform dissolution of the glass is favoured, whilst ion exchange is suppressed. At low pH (<9), ion exchange prevails over uniform dissolution. El-Shamy *et al* found that the reaction rate of ion exchange was proportional to the square root of time, which they suggested implied that the reaction was controlled by diffusion of the exchanging cations. Leaching is usually described in terms of the exchange of  $H^+$  or  $H_3O^+$  and alkali cations.

Sinton and Lacourse (2001) have described the two stages generally thought to occur during the dissolution of glass. The first stage is an exchange at the glass surface of an alkali (or possibly alkaline earth) atom in the glass with a hydrogen atom in the water through the reaction:



The surface of the glass becomes depleted in alkali, and a silica-rich layer may form. The changes in the solution depend on: (1) whether or not the aqueous system is closed or open; and (2) the surface area of glass exposed to the solution. In a closed system, the solution pH increases with the addition of  $OH^-$ , which can then attack the  $Si-O-Si$  bonds to dissolve the silica in the glass through a second reaction:



The rate of the dissolution increases with increasing pH, so dissolution accelerates with time in a closed system. In an open system, the solution pH does not increase and dissolution of silica dissolution may not occur. Lanford et al proposed the idea that the  $\text{H}_3\text{O}^+$  ions are the exchanging species.

As previously stated ISO states that ceramics for use in the mouth that have exposed surfaces (i.e. class 1, Table 1.3) should have a chemical solubility of less than  $100 \mu\text{g}/\text{cm}^2$ , and materials which are not in direct contact with oral tissue (class 2, Table 1.3) should have a solubility of less than  $2000 \mu\text{g}/\text{cm}^2$ . These figures are obtained by means of an accelerated solubility test, which immerses samples of specific geometry in 4% HAc solution at  $80^\circ\text{C}$  for 16 hours.

Various research to date has focussed on improving the solubility of fluorcanasite. As previously mentioned, Anusavice and Zhang (1998) tested the effect of adding alumina to the frit before casting and results of  $2170\mu\text{g}/\text{cm}^2$  (2% alumina) and  $790\mu\text{g}/\text{cm}^2$  (5% alumina) after 16 hours in 4% acetic acid were reported. The addition of more alumina (up to 10%) significantly reduced the chemical durability of the material. Anusavice and Zhang attributed this to phase separation during heat treatment of the glass. Stokes (2003) varied the alkali content and found a minimum solubility of  $650\mu\text{g}/\text{cm}^2$  with variability between the discs of  $\pm 198 \mu\text{g}/\text{cm}^2$  (using the ISO 6872 test) for canasite glass-ceramic. This was achieved with a glass composition of  $60\text{SiO}_2\text{-}8\text{Na}_2\text{O-}7\text{K}_2\text{O-}15\text{CaO-}10\text{CaF}_2$ . Although there was a decrease of 73% over the original formulation (Stokes 2003), it was still not acceptable as a dentine replacement material. It was suggested during this research that the existing ISO standard chemical solubility test for dental ceramics, did not produce very reproducible results and a new bead test was proposed which offered reduced variability.

#### 2.8.4 Dental Material Processing

Glass ceramic restorations can be processed by casting as in the case of Dicor ( $\text{K}_2\text{Mg}_25\text{Si}_4\text{O}_{10}\text{F}_2$ ), by hot pressing like the Empress systems (leucite or lithium disilicate) or by machining of porcelains or pre-crystallised glasses. Johnson *et al* (1998b) have shown canasite glasses to have good castability at  $1200^\circ\text{C}$ . However the composition has been varied considerably and Stokes, 2001 found that casting might not remain a viable processing route for compositions examined more recently.

With the advent of computers and increased understanding of ceramics in dentistry, computer aided design and manufacture (CAD-CAM) has found its way into dental

processing. Calamia (1994) claims that the chair-side Cerec system is the most successful of the CAD-CAM systems. Most CAD-CAM systems in the dental field use diamond tipped tooling and dental porcelains based on leucite ( $K_2Al_2Si_4O_{12}$ ) as the ceramic material. The leucite phase is hard and has been associated with wear of the tool as well as of the opposing teeth during clinical use (Henry and Hill, 2003). Dental porcelains and Dicor MGC intended for CAD-CAM are prone to edge chipping during machining (Sindel *et al*, 1998). In addition to this, the dental porcelains and Dicor MGC lack sufficient fracture toughness for many applications, with values in the range of 1.0 – 1.4  $MNm^{-3/2}$  (Graf *et al*, 1996). Luthardt *et al* (2002) have found that the grinding associated with CAD-CAM significantly reduces the strength and fracture toughness (a 50% reduction) of yttria-stabilized tetragonal zirconia polycrystals (Y-TZP). Therefore, there is a need for a material that can be CAD-CAM machined and have high fracture toughness, which canasite could fill. It would also be beneficial if the material could be resin-bonded to the underlying tooth structure.

Various parameters have been suggested to 'measure' machinability, such as tool wear, surface roughness, cutting force, cutting energy, drilling rates etc (Baik *et al*, 1995). These parameters depend on the microstructure and properties of the glass ceramic. Boccaccini (1997) has suggested that there is a relationship between the machinability and the brittleness of glass ceramic materials. He showed that machinability parameters such as the slope of the log-log plot of the specific cutting energy versus the cutting rate, or the specific cutting energy at low cutting rates, are in good agreement with the brittleness indices for seven different glass ceramics. It was found that in order to be machinable, the brittleness index of a material (given by the ratio of the hardness to the fracture toughness) should be lower than  $4.3 \mu m^{-1/4}$ .

## 2.9 Main Findings

Canasite glass-ceramics have significant potential to be developed as a dental restorative material. Canasite has considerably higher reported values of fracture toughness and flexural strength compared with other resin-bonded ceramics. Thus if developed as a dental restoration using accepted dental laboratory practice, would fulfil the demand for a tougher, tooth-coloured, inexpensive dental material, which is biocompatible.

A low solubility fluorcanasite composition has been identified, but this has resulted in a compromise in the mechanical properties. There is a need to modify fluorcanasite to

increase its strength whilst retaining its durability, by refinement of the microstructure. This may be undertaken by assessing the mechanisms involved during crystallisation, the effect of varying compositions, melt durations and heat-treatment schedules on the phases present. Fracture toughness has been shown to be a good initial parameter to test the mechanical properties of glass ceramics intended for use as a restorative material.

## Chapter 3: Materials Processing and Methods

### 3.1 Introduction

In previous studies at the University of Sheffield on fluorocanasite forming glasses derived from the stoichiometric composition  $10\text{Na}_2\text{O}-5\text{K}_2\text{O}-15\text{CaO}-10\text{CaF}_2-60\text{SiO}_2$  work has concentrated on producing a more chemically durable fluorocanasite composition (Stokes et al, 2000). It was initially decided to base the glasses studied in this work on these low solubility compositions identified by Stokes *et al.* In these compositions  $0.45 \leq [\text{K}]/[\text{Na}+\text{K}] \leq 48$ .

It was important to establish, at this initial stage, the experimental protocol- melting procedure, the phase analysis and the mechanical tests that could be used for these starting compositions and repeated for any future studies. Reproducibility was most important when it came to the melting schedule. Fluorine loss as NaF and SiF<sub>4</sub> is a known problem during melting of these glasses (Likitvanichkul and LaCourse, 1995) thus a suitable schedule, which minimised fluorine loss while producing a homogenised clear glass had to be identified.

In dealing with these preliminary issues, this chapter first tries to establish the glass melting procedure and then will discuss initial compositional variations.

### 3.2 Experimental Procedure

#### 3.2.1 Glass melting

The glass melt procedural studies were carried out using the low solubility composition of  $7\text{Na}_2\text{O}-8\text{K}_2\text{O}-15\text{CaO}-10\text{CaF}_2-60\text{SiO}_2$  referred to as K8. Batch composition was calculated to produce approximately 200g of glass, assuming complete decomposition and no losses. The source ingredients, Loch Aline Sand (high purity silica) and Fisher Scientific Reagent Grades of sodium carbonate; potassium carbonate; fluorite and calcium carbonate (all 99%+ pure), were hand mixed to break up agglomerated clumps and to produce a homogenised powder.

The batch was melted in a zirconia grain-stabilised platinum crucible at 1350°C in a SiC element electric furnace. The batch was filled up to 4 cm from the crucible lip to prevent overspill into the furnace. Any remaining batch was added to the crucible after 10min, but in most cases one charge was sufficient. The first 10 minutes of the melt were monitored to check for excessive bubbling which could lead to any spills. Previous studies had proved that the temperature of 1350°C had produced clear glasses that were suitable for pouring.

To assess the effect of melt duration on the crystallisation of canasite, the melt duration was varied from 1½ hrs to 6hrs (Table 3.1). The first hour of the melt was static to allow initial batch reactions to occur. After this the melts were stirred for the subsequent duration at approximately 60 r.p.m. using a platinum paddle attached to a mullite rod which in turn was attached to a motor. Occasionally, either during the stirring process, or when removing the rod, the edge of the paddle would catch the side of the crucible and the assembly would fail. This led to the paddle dropping into the crucible and the glass being contaminated by the cement that was used to attach the paddle to the mullite rod. These melts were abandoned.

Table 3.1: Melting Schedules.

Glass	Melt Duration (min)			
	Static	Stirred	Re-melt	Total
K81	60	30	-	90
K82	60	105	-	165
K83	60	180	-	240
K84	60	240	-	300
K85	60	300	-	360
K86	60	30	60	150

The final melt was poured onto a pre-heated steel plate to produce a glass plate, approximately 150 mm by 70 mm and 8 mm thick (Figure 3.1). The glass was then annealed 550°C for 1 hour with a cooling rate of 1°C per minute in a muffle furnace. T<sub>g</sub> (glass transition temperature) was determined using differential thermal analysis (see below).

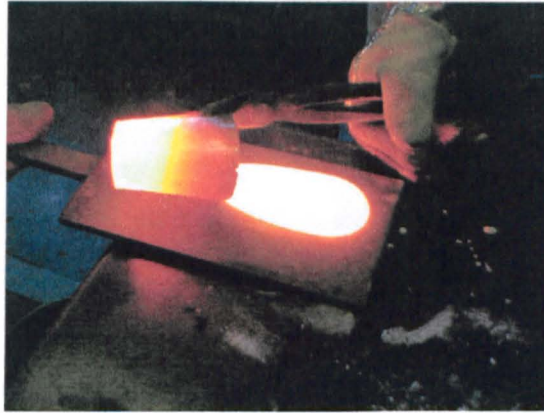


Figure 3.1: Molten glass being poured onto plate.

A separate run of the batch was poured into water (temperature 21°C) to form frit after 1hr static and ½ hr stirred (Figure 3.2). The glass was captured in a nickel-chromium wire basket and the frit was re-melted in the zirconia grain-stabilised platinum crucible at 1350°C for an hour and recast onto a steel plate to judge whether this affected the homogeneity of the glass. This glass was called K86. Through previous attempts it was found that the glass required an hour long re-melt to rid it of any trapped air bubbles.



Figure 3.2: Fritting

### 3.2.2 Differential Thermal Analysis

Differential thermal analysis (DTA) was used to determine the glass transition temperature,  $T_g$  and crystallisation temperature,  $T_c$  (Figure 3.3). If a glass melt is cooled so fast that the solidification reaction was not to occur, the melt would contract at the same rate but

continue under the freezing point. At a degree of undercooling, the rate of volume changes to a rate very similar to that of a crystalline solid. This point is said to be the glass transition temperature 'T<sub>g</sub>'. This is a second order reaction indicated on the DTA by a change in differential, probably brought about by a rate of change of energy related to temperature change as opposed to the large volume change of crystallisation indicates a state of much greater order being realised, thus leading to an exothermic peak in the trace.

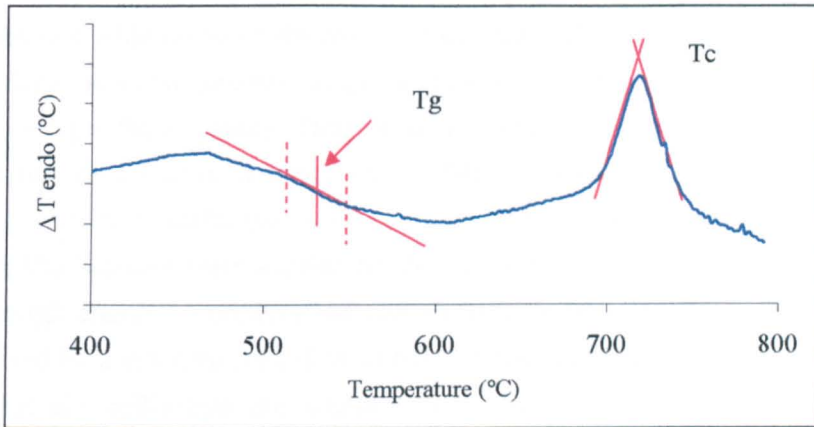


Figure 3.3: DTA trace with calculation of T<sub>g</sub> and T<sub>c</sub>

The samples were crushed using a percussion mortar, ground and then passed through a 45 $\mu\text{m}$  sieve. The process was repeated until all the powder passed through the sieve. DTA measurements were carried out on a PerkinElmer PYRIS Diamond analyser. Fired Al<sub>2</sub>O<sub>3</sub> powder was used as a reference phase. 0.1g of sample and of the reference powder was used. The samples were heated in covered platinum crucibles at 5 $^{\circ}\text{C}/\text{min}$  to 820 $^{\circ}\text{C}$  in air.

### 3.2.3 Crystalline Phase and Microstructural Analysis

Scanning electron microscopy (SEM) was carried out on both the glasses and glass ceramics, using either CamScan or Jeol 6400 scanning electron microscopes to analyse the microstructure. The samples (10 x 10mm) were resin mounted and prepared by sequentially grinding with 120, 400, 800 and 1200 grit SiC grinding papers, and then sequentially polishing with 6, 3 and 1  $\mu\text{m}$  diamond paste, giving an optical finish. The samples were etched using 5% HF in water for 25 seconds. All the specimens were either carbon-coated using an Edward's evaporation unit or gold-coated to prevent charging. Energy dispersive X-ray analysis was carried out on some of the samples using the CamScan, in order to

obtain an elemental analysis of the different phases. Optical microscopy was undertaken on the ground and polished samples, etched using 5% HF in water for 25 seconds.

Crystalline phase analysis was undertaken using powder X-ray diffraction. Diffractometers used were Philips PW1050 and Siemens D500 with  $\text{CuK}\alpha$  radiation ( $\lambda = 1.5406\text{\AA}$ ) and an accelerating voltage of 50 kV between  $2\theta$  values of  $10\text{--}60^\circ$ , using a step-scanning technique with a fixed step size of  $0.02^\circ$  and a rate of  $2^\circ/\text{min}$ .

X-ray diffraction takes advantages of the coherent scattering of x-rays by polycrystalline materials to obtain a wide range of structural information. The X-rays are scattered by each set of lattice planes at a characteristic angle, and the scattered intensity is a function of the atoms which occupy those planes. Only a small range of x-rays are widely used for diffraction. In this case  $\text{CuK}\alpha$  radiation ( $\lambda = 1.5406\text{\AA}$ ) was used. Inside the X-ray tube, there was a 50,000 volt difference between a tungsten filament and a copper target. Electrons from the filament were accelerated by this voltage difference and hit the copper target with enough energy to produce the characteristic x-rays of copper. The radiation is monochromatised by a graphite crystal mounted just ahead of the scintillation counter. The  $\theta$  compensating slit collimates the x-rays before they reach the sample. The sample chamber is where the sample is held.

The ceramics were crushed and ground using a percussion mortar, then ground to powder using a silica pestle and mortar and passed through a  $100\mu\text{m}$  sieve. These were then mounted on sample holders and placed in the sample chamber. The collimated x-rays enter the chamber and hit and scatter from the sample. When certain geometric requirements are met, x-rays scattered from a crystalline solid can constructively interfere producing a diffracted beam. In 1912, W.L. Bragg recognised a predictable relationship among several factors:

$$n\lambda = 2d\sin\theta.$$

where  $\lambda$  is the wavelength of the x-rays,  $d$  is the d-spacing or the distance between similar atomic planes in a mineral and  $\theta$  is the angle of diffraction. This is known as Bragg's Law and forms the basis of X-ray diffraction.

The diffracted beams were detected by the scintillation counter which was mounted on the goniometer. The goniometer is motorised and moves through a range of  $2\theta$  angles. For practical reasons the diffractometers measure the angle twice that of the  $\theta$  angle. Hence the measured angle is called  $2\theta$ . Characteristic X-rays were acquired using a pentafet detector and a beryllium window to give results.

A diffraction pattern records the x-ray intensity as a function of  $2\theta$  angle. All the diffraction patterns produced in this research were prepared as step scans. To run a step-scan, once the tube voltage and current are specified, the parameters entered include a starting  $2\theta$  angle, a step size, a count time per step and an ending  $2\theta$  angle (as stated above). The resulting diffraction patterns were analysed using JCPDS cards and the STOE WinXPOW programme (version 2.0 © STOE & CieGmbH, Hilpertstr.10, D 64295, Darmstadt).

### 3.2.4 Fracture Toughness

In light of the spread of data and the variety of tests used to assess the fracture toughness of dental ceramics; the accuracy, scatter and inter-examiner reproducibility of results depend strongly on the procedural approach, the test parameters used and the conditioning of the specimen.

Fracture toughness was measured using Vickers indentation because (i) Previous work using the same method has been carried out on some commercial systems and could be used for comparative purposes (Attar, 2001); (ii) it can be used on small samples of material, (iii) specimen preparation is relatively simple requiring only the provision of a polished, reflective plane surface, (iv) the Vickers diamond indenter used to produce the hardness indentations is a standard item used on a dedicated hardness tester or on a universal-testing machine, (v) it is both quick and cost effective.

After annealing, all samples (40mm diameter or 30x30mm squares) were sequentially ground with 120, 400, 800 and 1200 grit SiC grinding papers, and then sequentially polished with 6, 3 and 1  $\mu\text{m}$  diamond paste to remove any prior surface damage. Vernier callipers were used to ensure samples were parallel to within 0.01mm. Using the Vickers diamond indenter, the samples were indented at varying loads ranging between 24 to 200N, until 3 acceptable crack patterns were obtained at each load (with the total number of acceptable patterns per sample  $\geq 15$ ). Assuming that radial crack systems are formed during a Vickers indentation test, the criteria for acceptability were: (i) all cracks originated at the corners of the indent, (ii) presence of only 4 radial cracks, (iii) no chipping from the cracks and (iv) no crack branching.

The radial cracks were optically examined and measured. The fracture toughness was calculated using the formula:

$$K_{Ic} = \chi P/c^{3/2}, \quad (3.1)$$

where  $\chi = 0.0824$ ,  $P$  the load in Newtons and  $c$  the radial crack length in metres, as suggested by Ponton and Rawlings, 1989b for use when correlating or ranking different materials in order of toughness.

The Vickers hardness was calculated by measuring the indent diagonal ( $2a$ ) and using the formula (Lawn, 1993):

$$H_v = 0.47P/a^2, \quad (3.2)$$

where  $2a$  is the length of the indent diagonal in metres.

The brittleness index, ratio of the hardness to the fracture toughness was suggested by Lawn and Marshall in 1979 (Boccaccini, 1997):

$$B = H_v / K_{Ic} \quad (3.3)$$

### **3.3 Establishing the glass melting protocol**

#### **3.3.1 Glass making**

All glass batches formulated, formed glasses upon cooling from the melt. X-ray diffraction showed no signs of residual batch within any of the glass.

#### **3.3.2 Glass phase analysis**

DTA of the glasses made during the melt duration study (Figure 3.4) showed a decrease in the temperature needed to crystallise the glass as the melt duration increased. This decrease was approximately  $30^\circ\text{C}$  in going from a  $1\frac{1}{2}$  hr melt to a 6 hr melt.

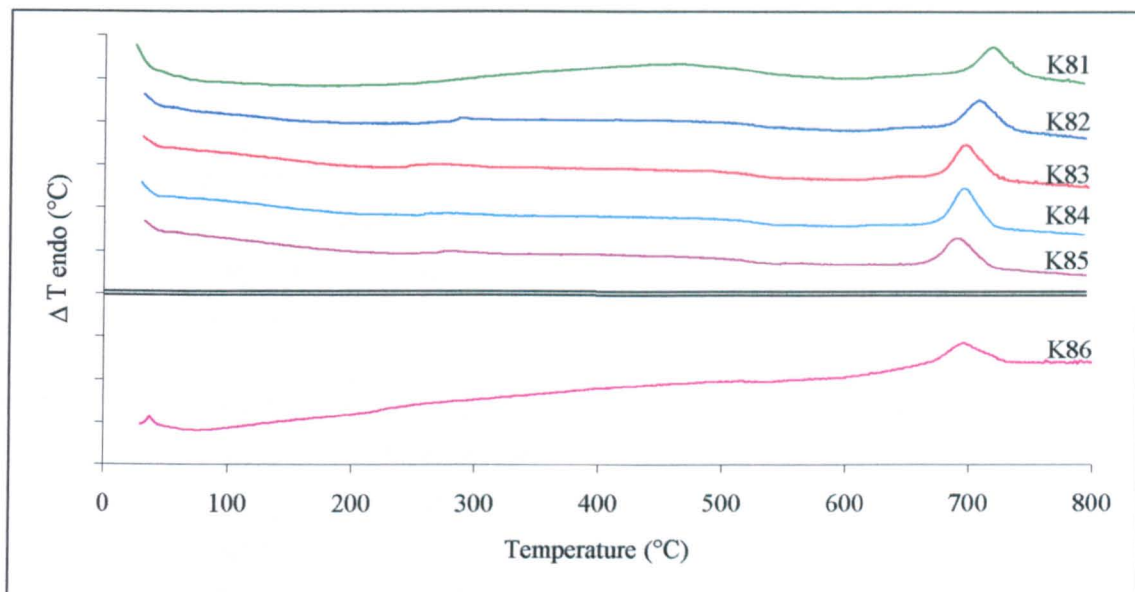


Figure 3.4: DTA results of K81-K86

Optical microscopy of the glass undergoing the melting schedule K81 revealed the presence of banding due to differences in the refractive indices of the different layers, thus indicating inhomogeneity in the poured glass (Figure 3.5a). These layers were present despite extended stirring times of the melt. This seemed to be resolved by re-melting the frit as in the case of K86 (Figure 3.5b).

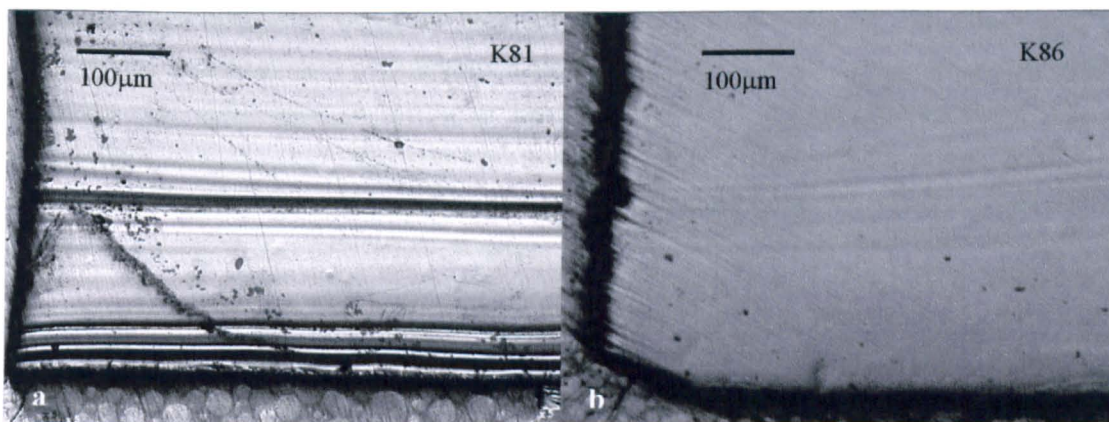


Figure 3.5: Optical micrographs of K81 and K86

### 3.3.3 Heat Treatment

To assess the effect of melt duration on crystallisation a simple one-stage heat treatment schedule was used thereby avoiding complications with varying temperatures of maximum nucleation and crystallisation. Samples were heated at a rate of 5°C/min to the peak crystallisation temperature  $T_c$ , determined from the DTA (Figure 3.3) results, held for an hour and air quenched (AQ).

Table 3.2: Heat treatment schedules used, where AQ is air quenched.

Glass	Heating rate (/min)	Hold temp (°C)	Cooling rate
K81	5	720	AQ
K82	5	710	AQ
K83	5	700	AQ
K84	5	700	AQ
K85	5	695	AQ
K86	5	700	AQ

For all heat-treatments, the furnaces used were Lenton Thermal Design chamber furnaces, heated on two sides by canthal resistance wire in a castable alumina block. The furnaces were calibrated using an independent Pt/Rh thermocouple and data-logger and found to be calibrated to  $\pm 1^\circ\text{C}$  (Figure 3.6). Samples of glass cut to approximately 10mm<sup>2</sup> from the cast slabs were heated in an alumina boat lined with powdered alumina to the appropriate temperatures, and then air quenched. The samples were dried, ground and polished for optical and electron microscopy or crushed (using a percussion mortar) and ground for X-ray diffraction phase analysis.

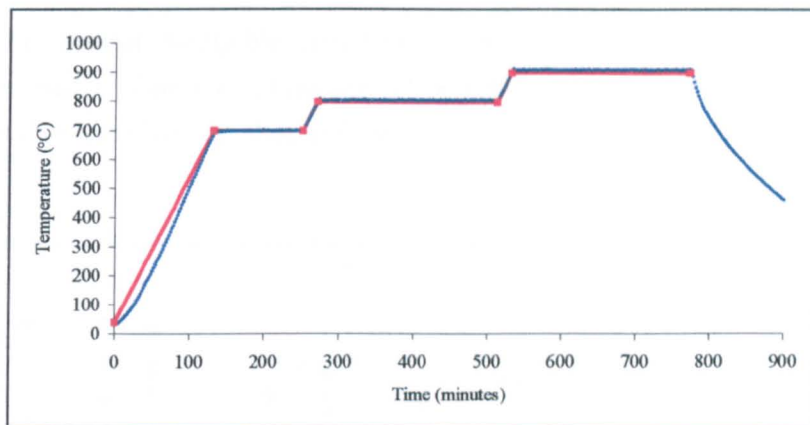


Figure 3.6: Example of calibration data. The red line is the set programme and the blue dots are the recorded points from the data logger, both showing agreement within 1°C.

### 3.3.4 Crystalline phase analysis

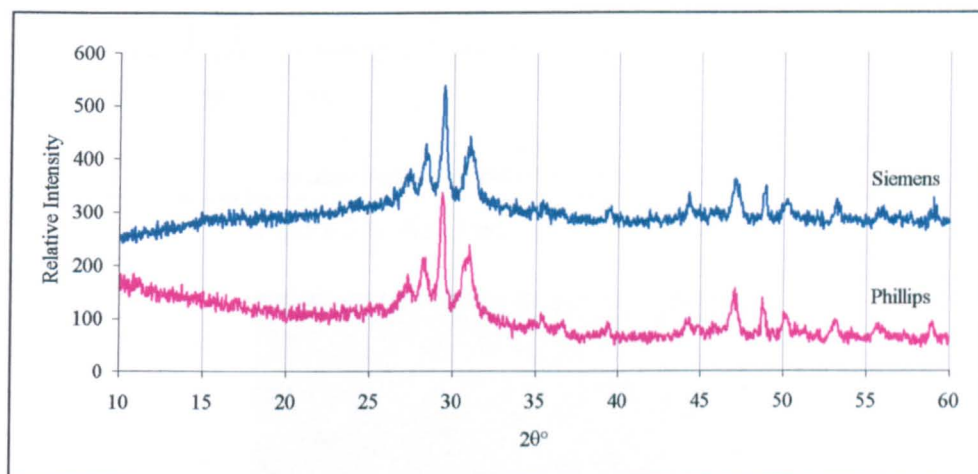


Figure 3.7: Example XRD traces from Phillips and Siemens (of FZ158 composition heat treated to 840°C and held for 2hrs, see Chapter 6)

Ideally the XRD equipment should have been kept constant, but this was not possible due to equipment failure and time restrictions. Figure 3.7, however, shows that the traces obtained from both the Phillips and the Siemens do not differ in intensity of peaks or  $2\theta^\circ$  values. The same was true of numerous repeats.

The XRD traces of the series (Figure 3.8) showed that only K81, K82 and K86 crystallised to form canasite glass-ceramic (JCPDS 13-0553). These traces can also be indexed to frankamenite (JCPDS 45-1398). The K83 – K85 traces have a very large amorphous hump

and very little, almost negligible crystalline content, despite the DTA traces showing crystallisation peaks. This was attributed to possible surface nucleation occurring in the bulk samples that were later crushed and sieved for XRD as opposed to the powder used for DTA.

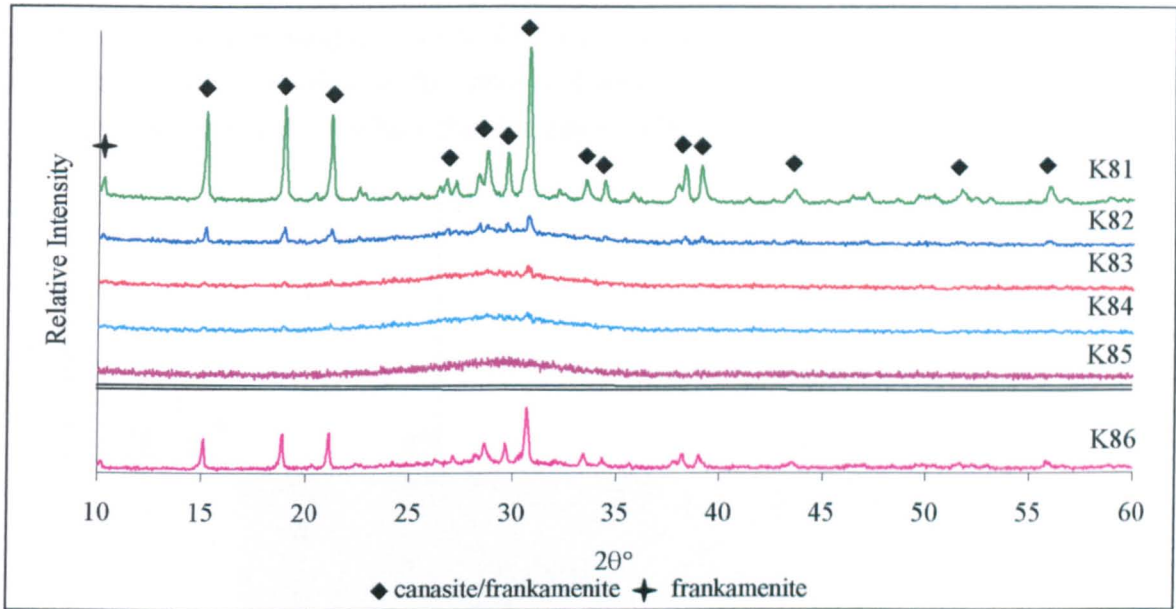


Figure 3.8: XRD results of K81 to K86.

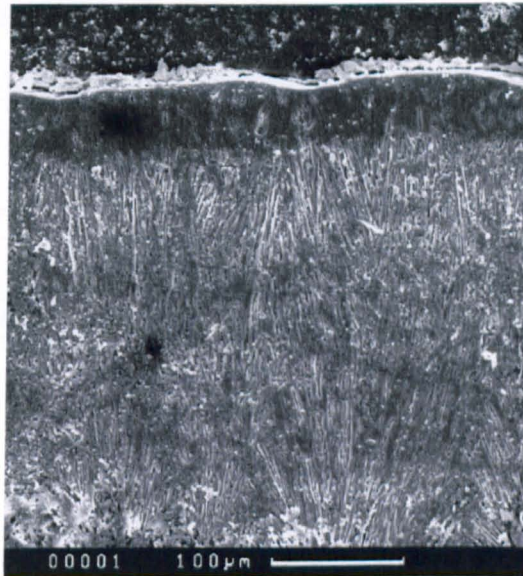


Figure 3.9: SEM of K81

Evidence of this surface nucleation was noticed in the heat treated K81 under SEM (Figure 3.9), where crystal growth is perpendicular to the edge of the sample. The samples also had very large crystals, in the order of 100 $\mu\text{m}$ . Figure 3.10, K81 at a lower magnification, showed the presence of different layers. EDS from these layers confirms elemental inhomogeneity. These results indicate that the stirring process alone does not result in homogeneous glass. A possible reason could be that the platinum paddle stirs in the horizontal plane, whereas the uncovered lid allows fluorine loss from the top and thus the glass when poured may have fluorine depleted layers.

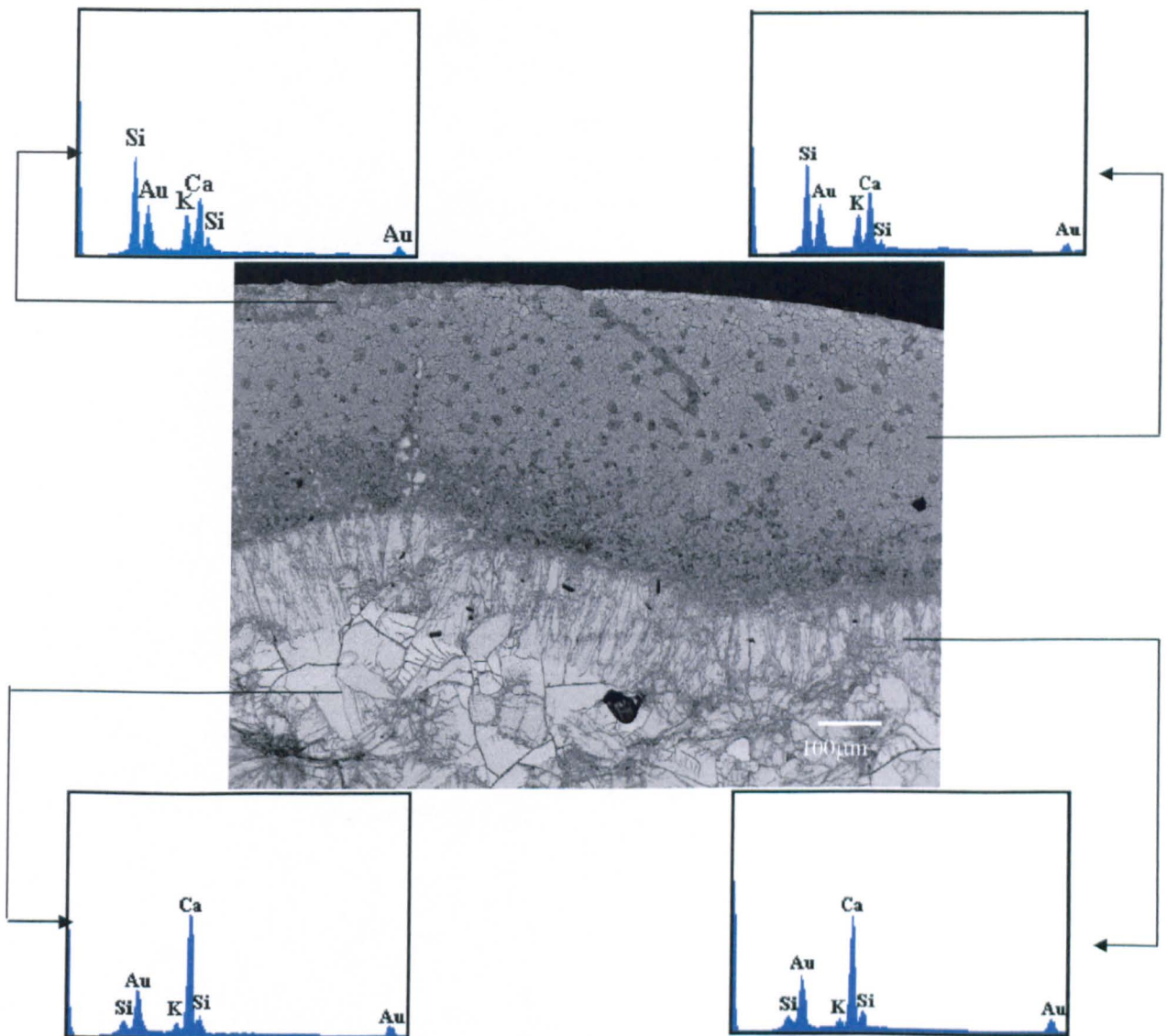


Figure 3.10: SEM/BEI image of K83 with EDS of the layers

However, Figure 3.10 (a cross section of the top mm of the glass) indicates a crystallised region above a glassy region. Thus a very basic simulation was carried out to assess molten glass being poured as a plate (Figure 3.11). The liquid used was honey on account of its viscosity being similar to the molten glass. If the fluorine depleted top layer can be envisaged as the red coloured honey, it can be noted that once poured the top layer does not remain as the top layer in the plate. It merely results in inhomogeneous layering in the plate which if crystallised could result in a similarly crystallised glass ceramic as K83.

Unfortunately EDS in the Camscan does not detect fluorine, and this initial assumption needs to be further verified. If fluorine loss from the melt is the cause, these findings would be consistent with the results of Beall (1983), in that the nucleating phase for canasite is  $\text{CaF}_2$ . The extra fritting process, as in the case of K86, produced a homogeneous glass (Figure 3.5). The hour long re-melt was necessary to produce a bubble free glass plate when poured. Based on these findings it was decided to use this melting schedule for any further glasses that were studied.

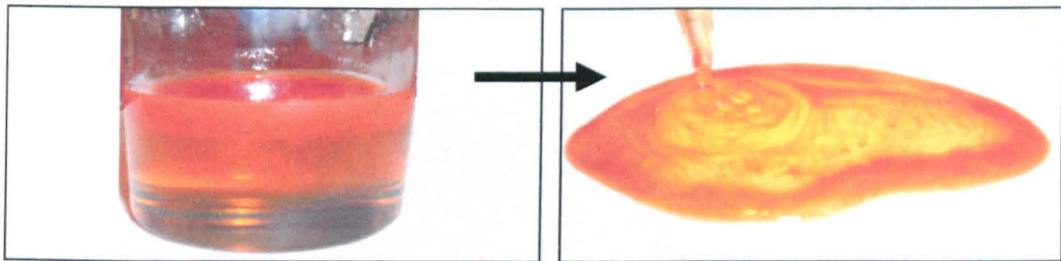


Figure 3.11: Simulation of inhomogeneous molten glass being poured as a plate

### 3.3.5 Fracture toughness tests

Figure 3.12 shows the method used to calculate the toughness values from the Vickers indentation tests carried out on the samples. The equations of the trendlines, with an intercept of 0, were used for the calculations.

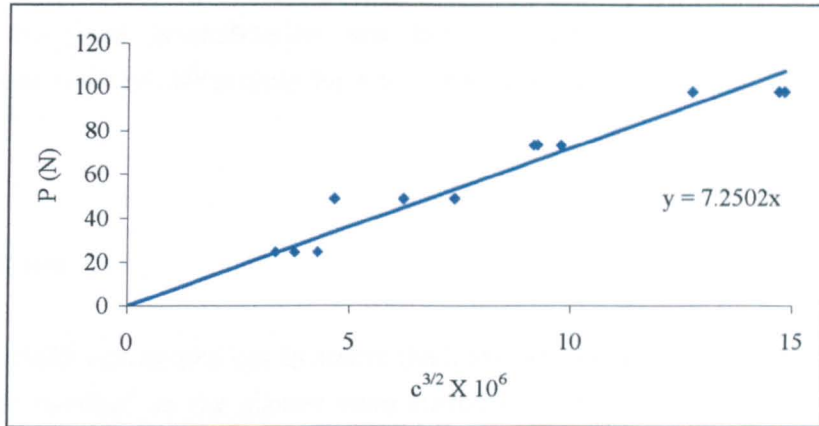


Figure 3.12: Calculation of the fracture toughness in  $\text{MNm}^{-3/2}$

The slope is  $P/(c^{3/2} \times 10^6)$ , which if multiplied by the constant 0.0824, gives the  $K_{Ic}$  in  $\text{MNm}^{-3/2}$ . Plotting the load, which is the variable on the y-axis and the measured value of crack length on the x-axis, although opposite to conventional practice, relates the increasing gradient with increasing toughness. Figure 3.13, cross section of the indents observed under SEM, verifies that the crack system formed during Vickers indentation is of the radial/median type.



Figure 3.13 Radial/median crack formed during Vickers indentation

Due to the poor crystallisation and inhomogeneities useful indentation fracture toughness data were not obtainable for K81 - K85 glass ceramics.  $K_{Ic}$  of K86 was  $1.13 \pm 0.20 \text{ MNm}^{-3/2}$ .

### 3.4 Discussion

The melt study was carried out to assure the homogeneity of the glasses. After the initial hour of static melting, all the glasses were stirred for the remaining duration of the melt (usually 30 minutes). However the rotational stirring movement seems to be inadequate to produce homogeneous glass, as the glasses demonstrate a distinct layering effect, despite the longer melt durations. The problem seems to have been substantially reduced by re-melting the frit. This agrees with other studies (see for example Tian *et al*, 2002) where a fritting process was added to the melting schedule to increase homogeneity.

Increasing the melt duration resulted in a glass that produced a less cerammed product. The poor ceramming might be due to the loss of fluorine from the melt. Likitvanichkul and Lacourse (1995) found the longer melt durations increased the volatilisation of F as either  $\text{SiF}_4$  or NaF during melting. They have suggested that this loss substantially inhibits the formation of canasite crystals as F is required for the formation of  $\text{CaF}_2$  nuclei and is a constituent of canasite.

Further to the glass analysis mentioned previously in section 3.2, XRF analysis was undertaken by Glass Technology Services Ltd. on some of the glasses in subsequent chapters, to ascertain loss of any components during the glass melting procedure. Discs of 40mm diameter were core-drilled from the glass plate, and prepared by sequentially grinding with 120, 400, 800 and 1200 grit SiC grinding papers, and then sequentially polishing with 6, 3 and 1  $\mu\text{m}$  diamond paste, giving an optical finish. This was then analysed using a semi-quantitative XRF programme. The compositions did not record any significant loss in fluorine (see Appendix).

$K_{Ic}$  of K86 was  $1.13 \pm 0.20 \text{ MNm}^{-3/2}$  which on first inspection seems very low compared to the values reported by Beall, of  $5 \text{ MNm}^{-3/2}$ . However, these are just initial tests without optimisation of either the composition or of the heat treatment schedule. Moreover, IF test method is known to give significantly lower  $K_{Ic}$  values for canasite glass ceramics (Beall, 1986)

### 3.5 Conclusions

- A glass manufacturing procedure has been developed that will ensure a homogeneous glass where the first hour of the melt is static after which the melt is stirred at approximately 60 r.p.m. for half an hour using a platinum paddle. The glass is then fritted and the glass frit re-melted under static conditions for 1hr at 1350°C. The final melts are cast onto a hot steel plate to produce plates, approximately 15cm by 7cm and 8mm thick and annealed at approximately 500°C for 1 hour with a cooling rate of 1°C per minute.
  
- The glass composition used has been shown to readily nucleate canasite and/or frankamenite.
  
- The  $K_{Ic}$  value of K86 was  $1.13 \pm 0.20 \text{ MNm}^{-3/2}$ , which needs to be improved upon if the material is to be developed as a 'high toughness' dental ceramic.

## Chapter 4: Compositional Effects on the Fracture Toughness

### 4.1 Introduction

Noting the lower fracture toughness values of this composition as compared to the previously reported high values for canasite, it was deemed necessary to determine which compositional variations would result in a more suitable fracture toughness for dental applications, without compromising the chemical durability. From the literature review, it was noted that the canasite composition (58.36SiO<sub>2</sub>-8.26Na<sub>2</sub>O-9.19K<sub>2</sub>O-16.83CaO-7.36CaF<sub>2</sub>) reported by Anusavice and Zhang (1998) to have fracture toughness values of  $2.7 \pm 0.1 \text{ MNm}^{-3/2}$  differed from the base composition by essentially CaO and CaF<sub>2</sub> content. Thus the glasses in this chapter include two compositions with increased CaO content in the composition. This was compensated by a decrease in the CaF<sub>2</sub>. It was also important to assess the addition of metal oxides as nucleating agents as this is known to produce a finer dispersion of crystals in the glass-ceramic and thus a tougher microstructure (McMillan, 1979). Specifically ZrO<sub>2</sub> has been suggested to produce a finer canasite glass ceramic (Beall, 1983).

### 4.2 Experimental procedure

#### 4.2.1 Glass formulation and melting

Table 4.1: Batched glass compositions in molar percent

	K <sub>2</sub> O	CaO	Na <sub>2</sub> O	SiO <sub>2</sub>	CaF <sub>2</sub>	TiO <sub>2</sub>	ZrO <sub>2</sub>
<b>B8</b>	7.0	11.8	9.3	54.2	17.9	-	-
<b>K7</b>	7.0	15.0	8.0	60.0	10.0	-	-
<b>C1</b>	6.8	17.1	7.8	58.5	9.8	0	0
<b>C2</b>	6.8	19.4	7.8	58.3	7.8	0	0
<b>T2</b>	6.9	14.7	7.8	58.8	9.8	1.9	0
<b>Z2</b>	6.9	14.7	7.8	58.8	9.8	0	1.4

As before (see section 3.1) glasses were based on a known low solubility composition. This time the composition with  $[K]/[Na+K] = 0.47$  (Stokes et al, 2000) called K7 ( $8Na_2O-7K_2O-15CaO-10CaF_2-60SiO_2$ ) was used. Variations to this composition used were the two higher CaO content glasses, C1 & C2 (based on the work by Anusavice and Zhang, 1998); a glass with titania addition, T2; and with zirconia addition, Z2 (Table 4.1). B8, the composition reported by Beall (1988) to have the highest strength was used as a control.

Glass melting was carried out according to the procedure previously developed (see chapter 3) to result in the production of a homogeneous glass. The first hour of the melt was static after which the melt was stirred at approximately 60 r.p.m. using a platinum paddle for 30 minutes. The glass was then fritted and the glass frit was re-melted under static conditions for 1hr at 1350°C. The final melts were cast onto a hot steel plate to produce plates, approximately 15cm by 7cm and 8mm thick. The glass was then annealed at approximately 500°C for 1 hour with a cooling rate of 1°C per minute.

#### 4.2.2 Heat treatments

To carry out phase analysis the glasses were heated at 5°C/min up to a range of temperatures between 560°C and 720°C, held for 2hrs at each temperature and air quenched, to retain the crystalline content at these temperatures.

Table 4.2: Heat treatment schedules for fracture toughness testing

Glass	Nucleation		Crystallisation 1		Crystallisation 2	
	Temp. (°C)	Time (min)	Temp. (°C)	Time (min)	Temp. (°C)	Time (min)
K7	550	120	700	120	-	-
C1	550	120	705	120	-	-
C2	550	120	710	120	-	-
T2	550	120	720	120	-	-
Z2	550	120	710	120	-	-
B8	700	120	800	240	900	240

Glass-ceramics that were to undergo fracture toughness tests underwent a two-stage heat treatment. In the case of B8, a three stage heat treatment was chosen according to the one defined in the patent for this particular composition (Beall, 1983). For the rest of the

glasses, in light of the DTA results not indicating a  $\text{CaF}_2$  crystallisation peak, the temperature dependent phase evolution results from the XRD were used to design 2-stage heat treatment schedules for each of the glasses, incorporating the optimum nucleation and crystallisation temperatures (Table 4.2). The samples were furnace cooled at  $10^\circ\text{C}/\text{min}$  to room temperature.

#### 4.2.3 Glass and crystalline phase analysis

X-Ray diffraction was carried out using both the Phillips and the Siemens diffractometers. Fracture surfaces and etched surfaces were examined under the Jeol and the Camscam electron microscopes. Detailed description of the methodology used was given above (section 3.2.3).

#### 4.2.4 Mechanical Testing

Fracture toughness was measured using Vickers indentation as described in section 3.3.3. The radial cracks were optically examined and measured. The fracture toughness ( $K_{Ic}$ ) Vickers hardness ( $H_V$ ) and brittleness (B) were calculated using equations 3.1, 3.2 and 3.3.

### 4.3 Results

#### 4.3.1 Glass Analysis

All glass batches formulated formed glasses upon cooling from the melt. X-ray diffraction showed no signs of residual batch within the glass. There was no clear  $\text{CaF}_2$  crystallisation peak in the DTA results of any of the glasses.

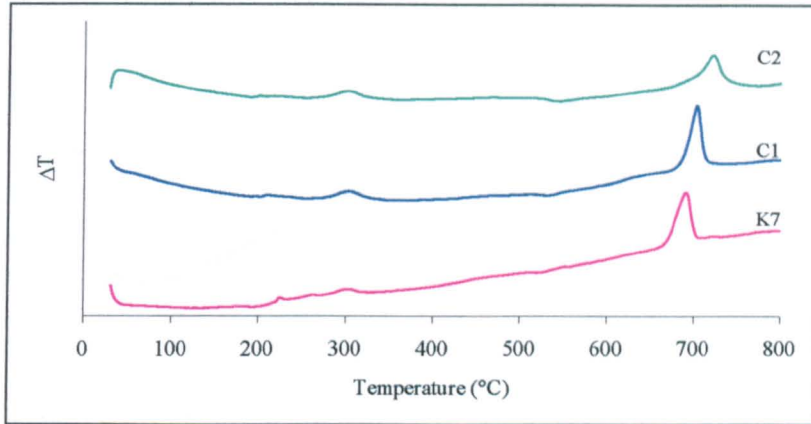


Figure 4.1: DTA traces for K7, C1 &amp; C2

DTA traces of C1 and C2 compared to K7 show an increase in the onset of crystallisation as CaO increases in the glass.  $\text{Ca}^{2+}$  occupies the interstitial positions in the glass network while the O ions link to network forming ions (Si), thus making the glass structure more stable and increasing the crystallisation temperature.

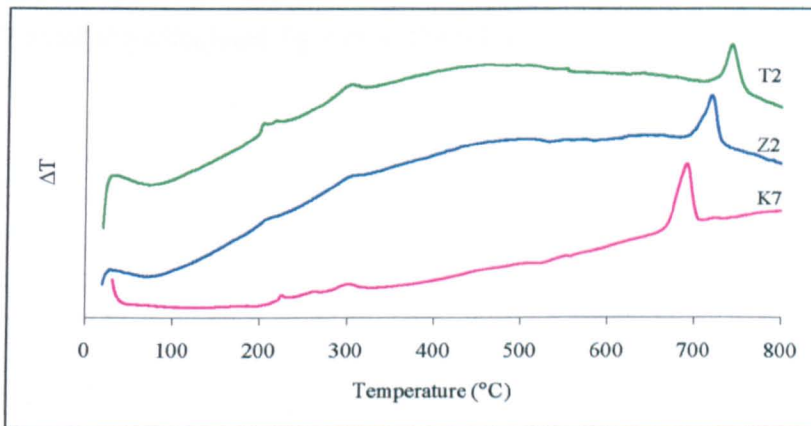


Figure 4.2: DTA traces of K7, Z2 &amp; T2

Inclusion of Ti and Zr ions in the glass results in an increase in the crystallisation temperature, indicating that the intermediate ions help to stabilise the glass structure.  $\text{Ti}^{4+}$  being the larger ion, has a greater field strength than  $\text{Zr}^{4+}$ . This explains the later onset of crystallisation.

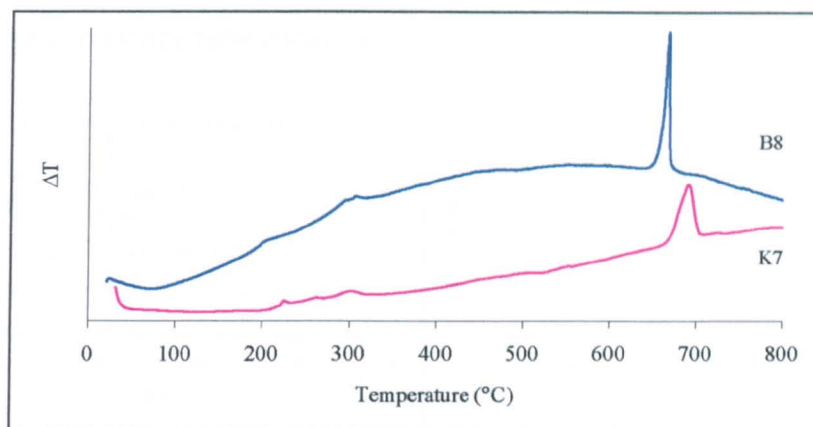


Figure 4.3: DTA traces of K7 &amp; B8

All the crystallisation traces have been similar so far, in that there has been a single peak of roughly of the same shape. The crystallisation event in B8 however has been characterised in DTA by a sharper, taller peak. B8 has 17.9 mol%  $\text{CaF}_2$  compared to 10mol% in the composition of K7. Fluorine is known to be a powerful network disrupter, replacing bridging oxygens by non bridging fluorine, and aids crystallisation. Thus the temperature required for crystallisation has decreased as has the  $T_g$  from 530°C in K7 to 500°C in B8. Appendix 3 lists all the calculated  $T_g$ 's from the DTA traces.

## 4.3.2 Phase and Microstructural Analysis

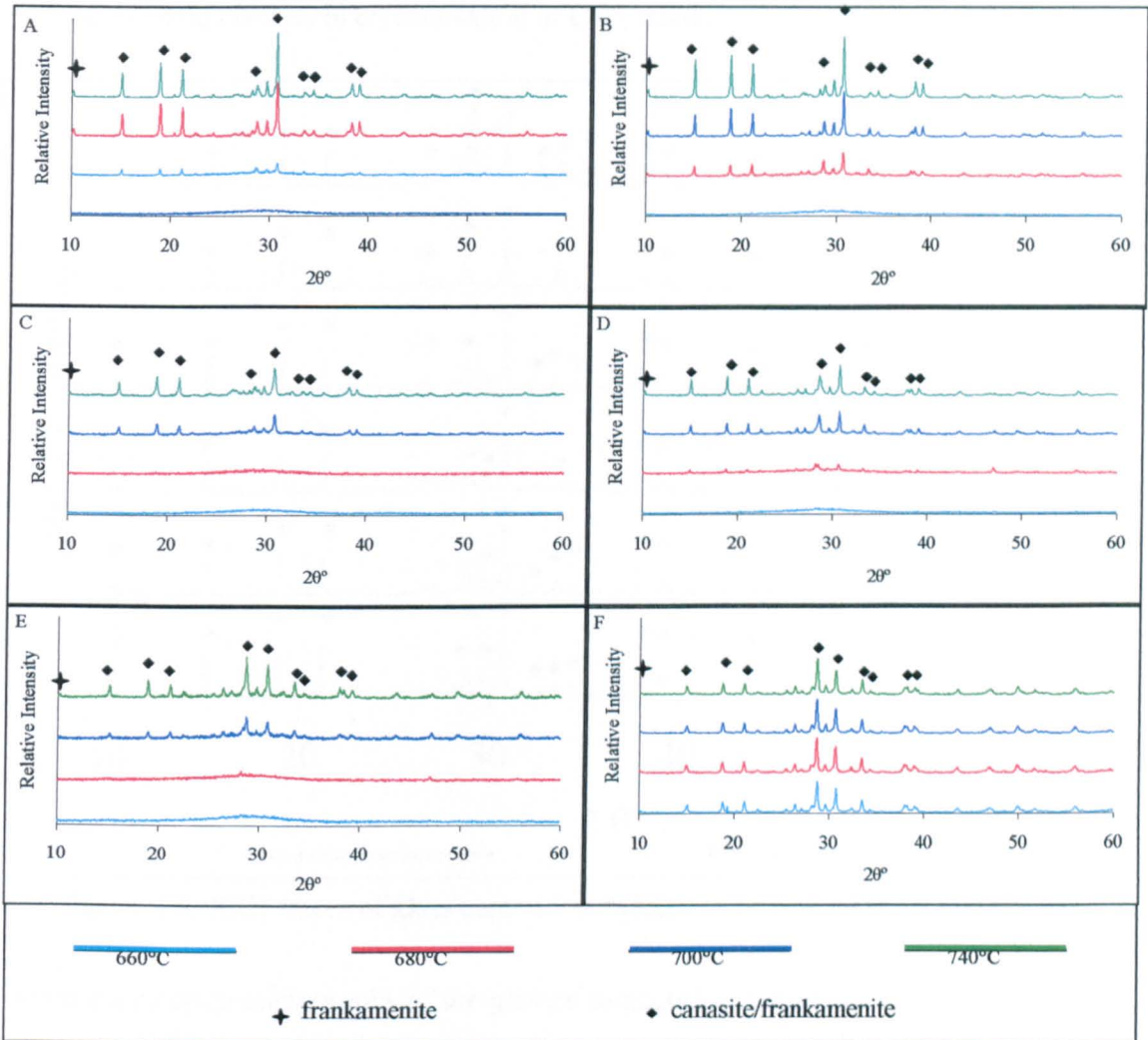


Figure 4.4: XRD traces of glass ceramics subjected to single stage heat treatments to the given temperatures, where A: K7, B: C1, C: C2, D: T2, E: Z2, F: B8.

Figure 4.4 summarises the XRD results. All glasses crystallised to give canasite glass ceramic. The peaks in the XRD traces also closely correspond with frankamenite, which can be distinguished by the presence of peaks at 10.1, 21.1 and 29.5  $^{\circ}2\theta$ . Associated with these peaks was a significantly smaller peak at 28.6 $^{\circ}2\theta$  compared to that of canasite. Z2 and B8 appeared to contain a greater amount of canasite and were the only two glass ceramics in which the 2 hour holds at 620 $^{\circ}\text{C}$  nucleated  $\text{CaF}_2$ . The relative intensity scales

of all 6 graphs have been kept equal in Figure 4.4. Similar results were found in the glass ceramics subjected to a two stage schedule (Figure 4.5). In the case of B8 and Z2, the nucleation hold resulted in crystallisation of  $\text{CaF}_2$  nuclei.

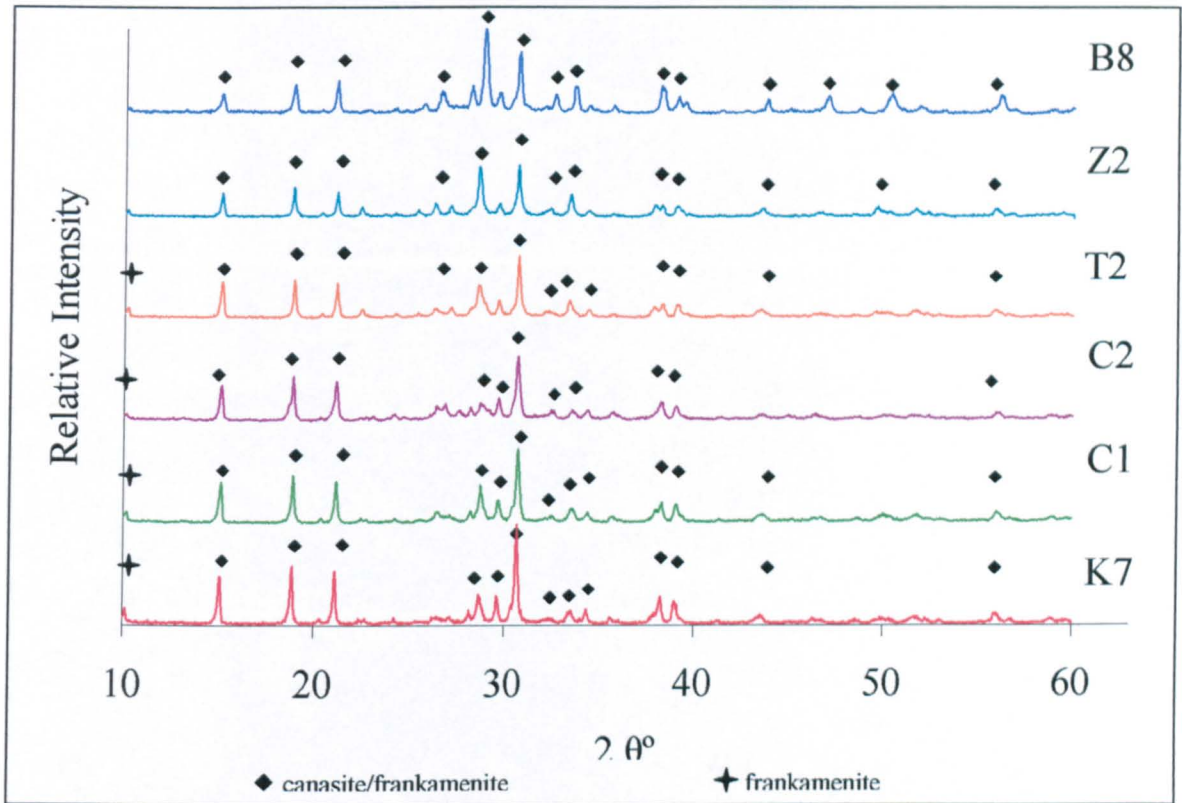


Figure 4.5: XRD traces of glass ceramics subjected to double stage heat treatments,

Scanning electron micrographs of the glasses subjected to two stage heat treatment and in the case of B8 three stage heat treatments are shown in Figure 4.6. As the shift from a predominantly frankamenite structure to a predominantly canasite structure occurred (K7 compared with Z2 and B8), it was accompanied by a refinement in the microstructures. The microstructures of K7, C1 and C2 demonstrated uncontrolled spherulitic growth with spherulites of lath sizes in the order of  $100\mu\text{m}$ . But the titania and zirconia additions resulted in a finer glass ceramic with laths of the order of  $30\mu\text{m}$  and  $<5\mu\text{m}$  respectively and a move away from the spherulitic to a more desirable interlocked structure. The crystal morphology of B8 seems less like the 'house of cards' morphology of T2, where there appear to be randomly orientated flakes, and more like a needle shaped droplet structure.

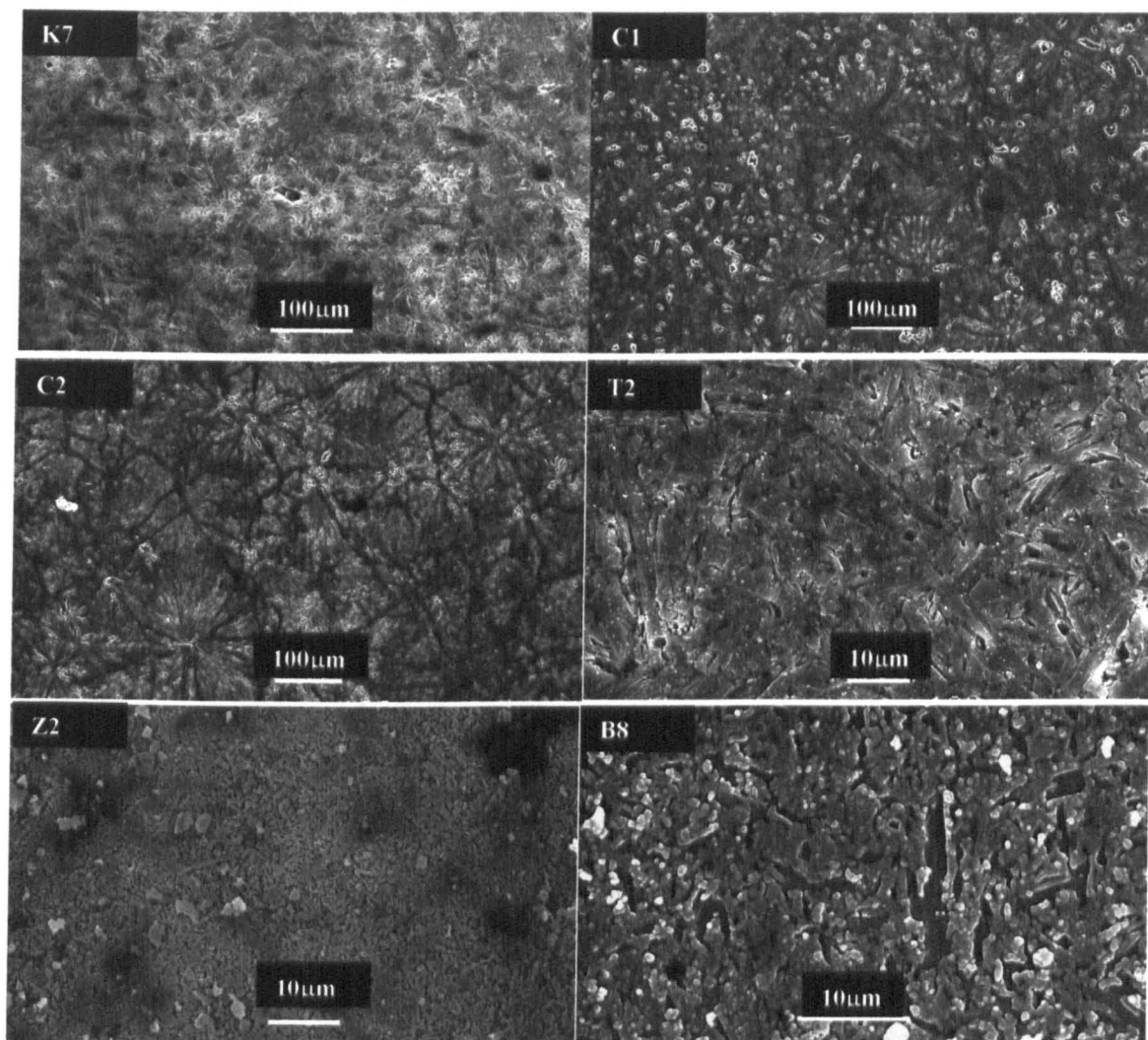


Figure 4.6: Scanning electron micrographs of samples etched with 1.5% HF for 1 minute.

#### 4.3.3 Fracture Indentation

The toughness values with their standard deviations, calculated using ‘descriptive statistics’ in Microsoft Excel spreadsheets, are given in Figure 3.14. It was not possible to get fracture toughness values for the higher CaO glass-ceramics or the titania addition, by the indentation fracture method, as there was too much chipping and none of the cracks met the criteria for acceptability. This can be seen in the examples of the corresponding indents that were obtained during the toughness tests (Figure 4.7).

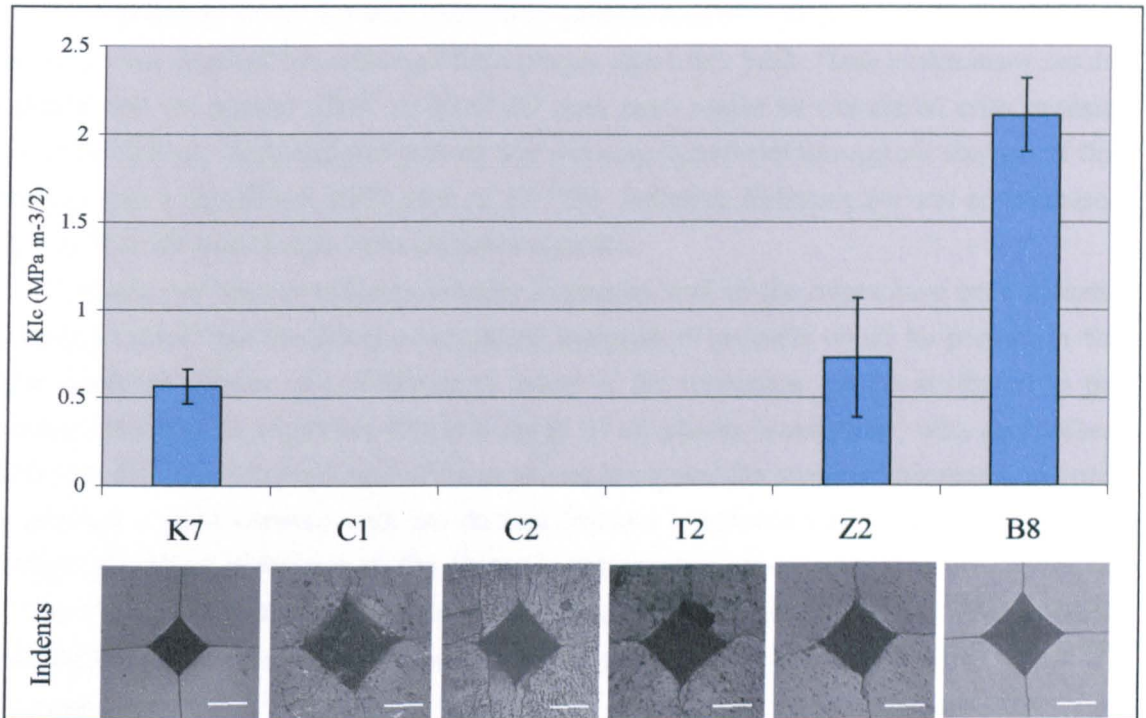


Figure 4.7:  $K_{Ic}$  values of the glass-ceramics with optical micrographs of their corresponding indents, where the scale bar represents  $100\mu\text{m}$ .

B8 had the highest fracture toughness value, of  $2.01 \pm 0.21 \text{ MNm}^{-3/2}$ , more than twice the values obtained for addition of 2 mol% zirconia and the base composition K7. Unfortunately the corresponding fracture toughness values for this particular composition have not been cited by Beall.

#### 4.4 Discussion

All the glass ceramics crystallised to both canasite and frankamenite phases. The results of the compositional variations study indicate agreement with the results of Beall (1983), in that the nucleating phase for canasite is  $\text{CaF}_2$ . This is substantiated by the increased presence of canasite in the B8, which had 17.9 mol%  $\text{CaF}_2$  in its batch composition. XRD results indicate that K7, C1, C2 and T2 contain frankamenite (Figures 4.4 and 4.5 show peaks at  $10.1^\circ 2\theta$ ) whereas in B8 and Z2, this peak is either much smaller or not present at

all. An associated trend is the significantly greater intensity peak at  $28.6^\circ 2\theta$  and lower intensity peak at  $30.6^\circ 2\theta$ . Although both phases share this peak, these preliminary results indicate that the greater  $28.6^\circ$  to  $30.6^\circ 2\theta$  peak ratio might be associated with canasite phase dominance. Although not proven, the working hypothesis throughout the rest of this thesis is that a significant XRD peak at  $10.1^\circ 2\theta$  indicates frankamenite and an increased  $28.6$  to  $30.6^\circ 2\theta$  peak height ratio indicates canasite.

It has also not been possible to identify f-canasite, and all the traces have been indexed bearing in mind that the fluorine dominant analogue of canasite could be present in the glass ceramics. Hence, it is difficult to assess if the toughness can be attributed to the canasite phase or to a product that is a result of all phases 'competing' with each other. Although detailed differentiation of these phases is beyond the scope of this study, in order to produce a glass ceramic with the desired fracture toughness values, it is important to evaluate the effect of fluorine on the crystallisation mechanisms.

The Ca content was varied based on the formulation of Anusavice and Zhang which produced canasite glass ceramics with fracture toughness values of  $2.7 \pm 0.1 \text{ MNm}^{-3/2}$ . However, C1 and C2 produced very brittle and porous glass ceramics. The poor crystallisation characterised by uncontrolled spherulitic growth of the crystals is indicative of too few nucleation sites in the glass. Bearing in mind that frankamenite is thought to be the dominant phase in these glass ceramics, the absence of sufficient  $\text{CaF}_2$  in the compositions could be contributing to the lack of canasite phase presence. Miller (2004) suggests that frankamenite may have a crystallising mechanism distinct to that of canasite, and that its nucleation does not require a precursor. The current results apparently agree with this observation.

The addition of 2 mol% titania resulted in a finer glass ceramic (Figure 4.6), but under optical microscopy of  $K_{Ic}$  specimens there was a lot of cracking and chipping evident around the indents. Thus the crystalline phases present in T2 themselves appear to be 'less tough' XRD indicates a frankamenite phase dominance in T2 similar to K7, C1 and C2. Zirconia was successful as an additive, in that it produced a glass ceramic with canasite as a dominant phase, for which the  $K_{Ic}$  was measurable, without the need for excess fluorite. The very fine microstructure achieved by the 1.5 mol% addition of  $\text{ZrO}_2$  is very promising (Figure 4.6). Zirconia has been known to 'aid'  $\text{CaF}_2$  in the crystallisation of canasite (Beall, 1983), although the exact method by which it assists in the production of canasite has not been discussed. The  $K_{Ic}$  increase associated with a  $>10x$  reduction in crystallite size from the base composition, K7, to Z2, was only  $\sim 0.2 \text{ MNm}^{-3/2}$  which could be due to the crystal morphology, which (very different to that of B8) might not be interlocked enough to deflect

the crack path. Further work is required to assess the role of zirconia in the crystallisation process and refinement of the microstructure.

It was not clear from the DTA trace as to why the specific three stage heat treatment schedule was used by Beall for B8, however for the sake of reproducibility, as many variables as possible were kept constant in relation to this particular formulation in an effort to reproduce the 'high' toughness values. As mentioned previously, in the absence of an exact composition associated with a fracture toughness of  $5\text{MNm}^{-3/2}$ , the composition used was the 'high strength' composition quoted in the patent (Beall, 1983). As the indentation method has been known to give lower  $K_{Ic}$  values for glass ceramics, the lower  $K_{Ic}$  values of B8 than what has been quoted from previous canasite formulations can be explained. It has to be borne in mind that as this was an assessment of the result of varying compositions on the fracture toughness these glass ceramics, the heat treatment schedules have not been optimised. The  $K_{Ic}$  of K7 was  $0.60 \pm 0.17 \text{MNm}^{-3/2}$  which although a reduction from the value of K86 ( $1.13 \text{MNm}^{-3/2}$ ) found in the previous chapter, was not a significant difference. This difference was attributed to the variation of alkali contents in these glass-ceramics, as there was no discernable variation in the microstructures of the two. A  $K_{Ic}$  of  $0.6 \text{MNm}^{-3/2}$  would preclude the material for restorative dental use. Formulations tested in this chapter indicate that this fracture toughness can be improved upon. Hence these findings would be used as a basis for future studies in the subsequent chapters.

## 4.5 Conclusions

- All compositions crystallised to give a mixture of canasite and frankamenite crystalline phases.
- Canasite seemed to nucleate and crystallise more readily in B8, resulting in higher fracture toughness values for this glass ceramics.
- $\text{ZrO}_2$  addition was successful in producing a canasite glass-ceramic, which shows promise for development for use as a dental glass-ceramic, and further work is required to assess its role in the crystallisation process and its microstructure refinement.

## Chapter 5: Effect of Fluorite Content

### 5.1 Introduction

The study on compositional variations indicated that the amount of fluorite content in the composition affected the crystallisation of canasite and/or frankamenite. This in turn affected the microstructure and fracture toughness of the glass ceramics. It was decided to investigate the effect of fluorite on crystallisation of these phases and thus the resulting effect on the fracture toughness.

### 5.2 Experimental Procedures

#### 5.2.1 Glass Formulation

The glasses, were based on the known low solubility composition where  $[K]/[Na+K] = 0.47$  (Stokes, 2003). Only the  $CaF_2$  content was varied in the base glass composition and the ratios were re-normalised to 100:

$$\frac{100}{90+x} (60SiO_2-8Na_2O-7K_2O-15CaO-xCaF_2) \text{ where } 8 \leq x \leq 15.$$

The glass compositions used in this study are given in table 5.1, where F10 is the base glass composition.

Table 5.1: Glass compositions (as-batched) in molar percent.

Composition	K <sub>2</sub> O	CaO	Na <sub>2</sub> O	SiO <sub>2</sub>	CaF <sub>2</sub>
<b>F8</b>	7.14	15.31	8.16	61.22	8.16
<b>F10</b>	7.00	15.00	8.00	60.00	10.0
<b>F13</b>	6.80	14.56	7.77	58.25	12.62
<b>F15</b>	6.67	14.29	7.62	57.14	14.29

### 5.2.2 Glass Melting

Glass melting followed the protocol outlined in section 3.5. As the fluorine content was increased in the composition, the  $\text{CaF}_2$  nucleation temperature coincided with the annealing temperature, thus to produce clear glasses, the annealing schedule needed to be varied according to the fluorine content in the composition (Table 5.2).

Table 5.2 Annealing schedules used

<b>Glass</b>	<b>Temperature (°C)</b>	<b>Hold duration (min)</b>	<b>Cooling Rate (°C/min)</b>
<b>F8</b>	500	60	1
<b>F10</b>	500	60	1
<b>F13</b>	490	120	1
<b>F15</b>	480	240	1

### 5.2.3 Differential Thermal Analysis

Differential thermal analysis (DTA) was used to determine crystallisation temperatures. The samples were crushed using a percussion mortar, and then passed through a  $45\mu\text{m}$  sieve. DTA measurements were carried out on a PerkinElmer PYRIS Diamond analyser as described in section 3.2.1

### 5.2.4 Heat Treatment

All series of glasses were subjected to single stage heat treatments at  $5^\circ\text{C}/\text{min}$  up to temperatures increased in  $20^\circ\text{C}$  intervals between  $600$  and  $740^\circ\text{C}$ , for phase analysis. The samples were held for two hours at the temperatures and air quenched to retain the phases present at those temperatures. Both XRD and DTA results were used to determine the nucleation and crystallisation temperatures. Two stage heat treatments were used for fracture toughness tests. These included longer nucleation holds that were used to see if this had any effect on the crystalline structure and hence the fracture toughness of the glass-ceramic. The samples were heated at a rate of  $5^\circ\text{C}$  upto the nucleation and growth temperatures and furnace cooled at an approximate rate of  $10^\circ\text{C}/\text{min}$ . Table 5.3 shows the two stage heat treatment schedules that the glasses were subjected to.

The furnaces used were Lenton Thermal Design chamber furnaces (calibrated using an independent thermocouple and data-logger), heated on two sides by canthal resistance wire in a castable alumina block. Samples of glass were heated in an alumina boat to the appropriate temperatures, and then air or furnace cooled. The samples could then be ground and polished for fracture toughness tests or dried, crushed (using a percussion mortar) and ground for X-ray diffraction phase analysis.

Table 5.3 Two-stage heat treatment schedules used; all samples were furnace cooled.

Glass	Heating rate (°C /min)	Nucleation temp. (°C)	Hold duration (min)	Heating rate (°C /min)	Crystallisation temp. (°C)	Hold duration (min)
F8	5	540	1440	5	720	1440
	5	620	1440	5	720	1440
	5	620	120	5	720	120
F10	5	540	1440	5	720	1440
	5	620	1440	5	720	1440
	5	620	120	5	720	120
F13	5	540	1440	5	720	1440
	5	620	1440	5	720	1440
	5	620	120	5	720	120
F15	5	540	1440	5	720	1440
	5	620	1440	5	720	1440
	5	620	120	5	720	120

### 5.2.5 Phase and Microstructural Analysis

X-Ray diffraction was carried out using both the Phillips and the Siemens diffractometers. Fracture surfaces and etched surfaces were examined under the Jeol and the Camscam electron microscopes. Detailed description of these techniques was given in section 3.2.3. In addition transmission electron microscopy (TEM) was carried out. Samples were prepared by sequentially grinding a small piece of the glass ceramic on either side, mounted onto the metal stub of a Gatan disc grinder with a heat sensitive thermoplastic resin, using 400, 800 and 1200 grit SiC grinding papers down to a thickness <30µm. A 3mm outer-diameter copper ring was glued onto the sample using epoxy resin prior to the

sample being removed from the stub (by melting the thermoplastic resin). Precaution was taken to remove excess material around the ring with a razor; and any excess resin with acetone, so as not to contaminate the microscope.

Ion beam milling as carried out at a 15° angle of incidence on a Gatan dual mill under operating conditions of 6kV with a beam current of 0.6 $\mu$ A. Samples were carbon coated using an Edward's evaporation unit. A Phillips EM 420 transmission electron microscope was used to analyse the samples.

### 5.2.6 Mechanical Testing

Fracture toughness was measured using Vickers indentation as described in section 3.3.3. The radial cracks were optically examined and measured. As before the fracture toughness ( $K_{Ic}$ ) Vickers hardness ( $H_V$ ) and brittleness (B) were calculated using equations 3.1, 3.2 and 3.3.

## 5.3. Results

### 5.3.1 Glass Formulation & Glass Melting

All glass batches formulated formed glasses upon cooling from the melt. X-ray diffraction showed no signs of phase separation or residual batch within the glass.

### 5.3.2 Differential Thermal Analysis

There was no evidence of CaF<sub>2</sub> crystallisation peak in the DTA results of any of the glasses, although the crystallisation peak becomes sharper with increasing CaF<sub>2</sub> (Figure 5.1). There was an associated decrease in the T<sub>g</sub> from 538°C in F8 to 511°C in F15 as the CaF<sub>2</sub> content in the composition was increased (Figure 5.1 and refer to Appendix 3). This is consistent with the previously found results in Chapter 4.

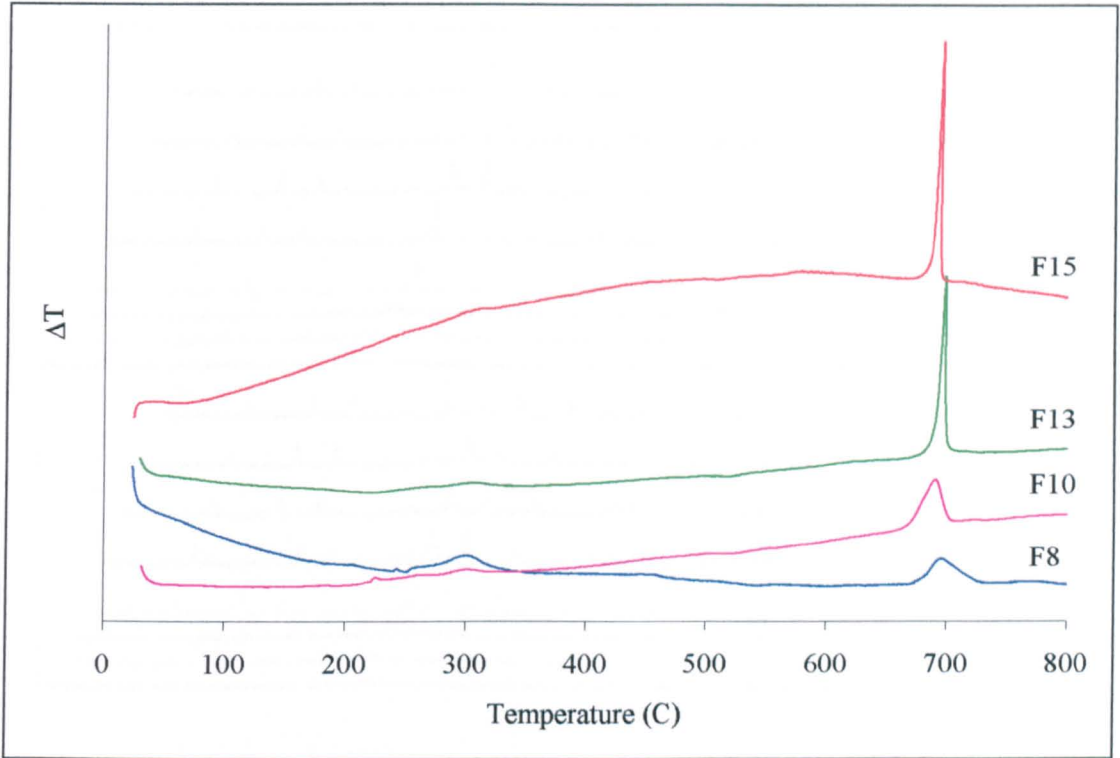


Figure 5.1: DTA traces of F8-F15

### 5.3.3 Phase and Microstructural Analysis

All glasses subjected to single stage heat treatments crystallised to give canasite and/or frankamenite glass ceramic.

Figure 5.2 shows the temperature dependent phase evolution of these glass ceramics. For the sake of clarity, indexing of the phases has been carried out in Figure 5.3.

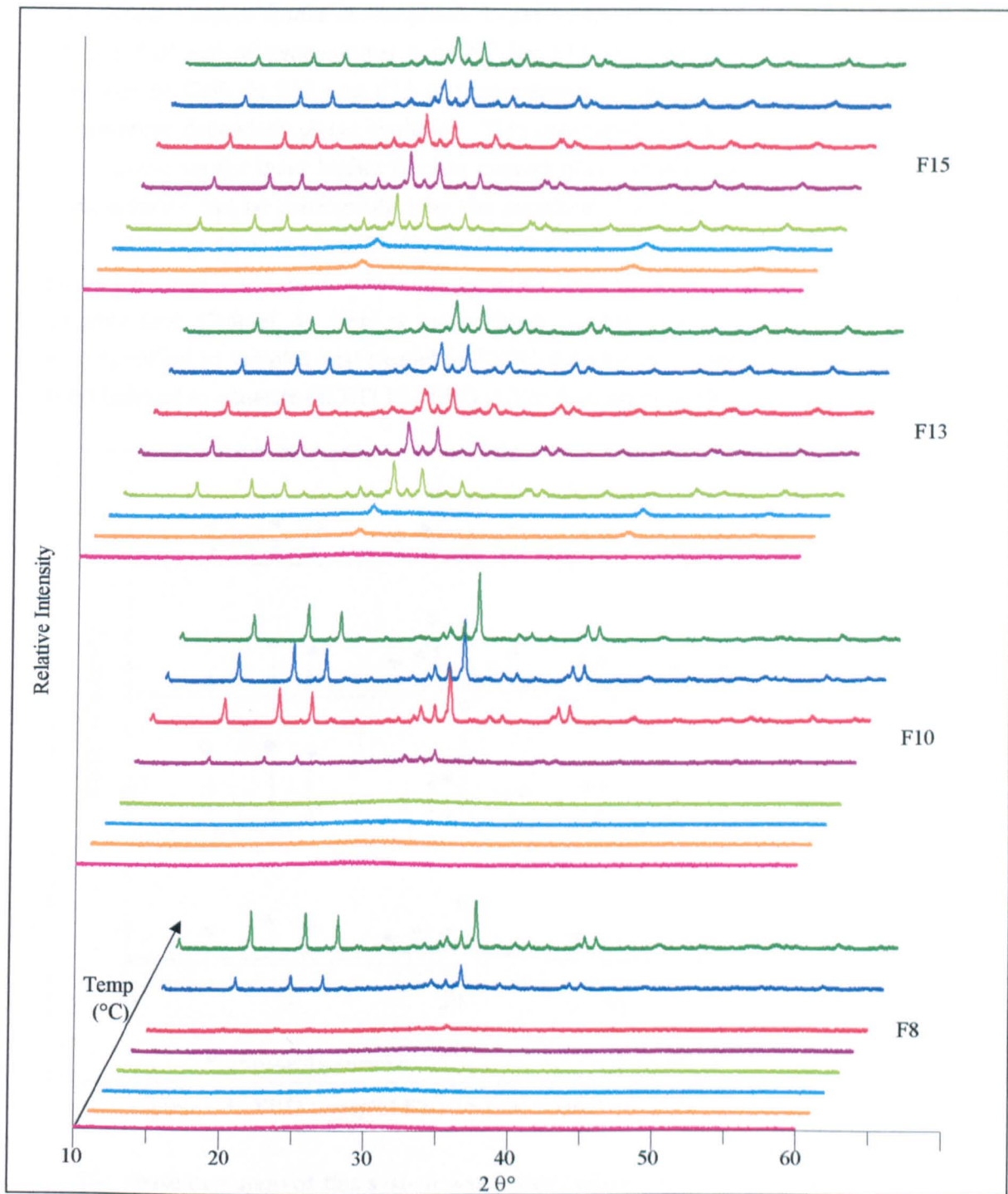


Figure 5.2: XRD traces showing the temperature dependent phase evolution of F8 to F15 heat treated at different isotherms ranging from 600°C to 740°C

The canasite and/or frankamenite phases began to crystallise at temperatures  $\geq 680^\circ\text{C}$  for F8 and F10 and at temperatures  $\geq 660^\circ\text{C}$  for F13 and F15. There was evidence of the presence of  $\text{CaF}_2$  in F13 and F15 at temperatures  $\geq 600^\circ\text{C}$  during the XRD studies of temperature dependent phase evolution. This correlated with an increase in the canasite phase presence for these higher fluorite content glass ceramic compositions (Figure 5.2). Frankamenite can be distinguished by the presence of a peak at  $10.1^\circ 2\theta$  and there is a lower intensity peak ratio of  $28.6^\circ 2\theta$  to  $30.6^\circ 2\theta$  associated with the presence of the aforementioned  $10.1^\circ$  peak when compared to the  $28.6^\circ 2\theta$  to  $30.6^\circ 2\theta$  peak ratio of canasite (see Chapter 4). This is more clearly visible in Figure 5.3, where the traces corresponding to samples heat treated to  $720^\circ\text{C}$ , held for two hours and air-quenched, have been indexed as canasite (ICDD 13-0553) and/or frankamenite (ICDD 45-1398).

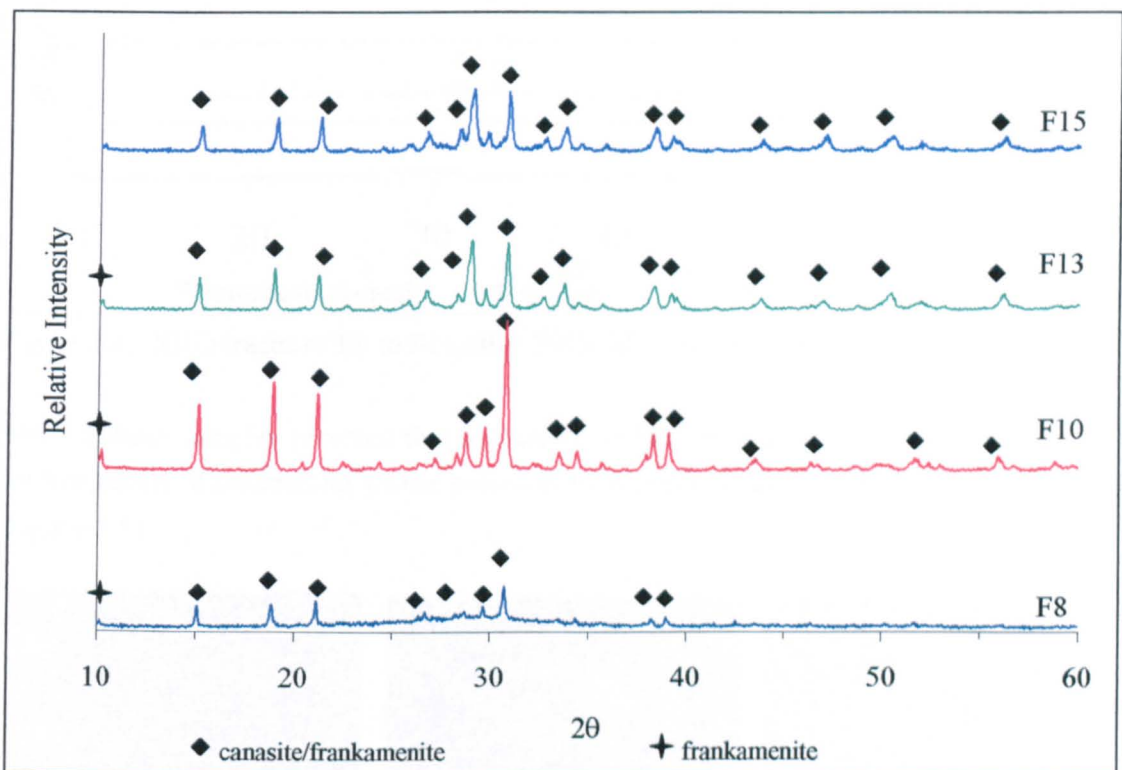


Figure 5.3: XRD traces of F8-F15 heat treated to  $720^\circ\text{C}$  and air quenched.

The phase evolution of this system was better understood by crystalline analysis of the samples which underwent the two stage heat treatment. Shorter nucleation holds of 2hrs at  $620^\circ\text{C}$  showed evidence of  $\text{CaF}_2$  nuclei in F13 and F15 glass ceramics, whereas F8 and F10 were amorphous. Figure 5.4 shows the XRD traces of the F8 to F15 after the 2 hour

nucleation hold and the traces after the subsequent 2 hour crystallisation hold. In addition to canasite/ frankamenite peaks, fluorite peaks are indexed (ICDD 04-0864). The traces of F13 and F15 are most akin to canasite and the predominant phase in F10 seems to be frankamenite. F8 remained largely amorphous after the two stage heat treatment, as in the case of the single stage.

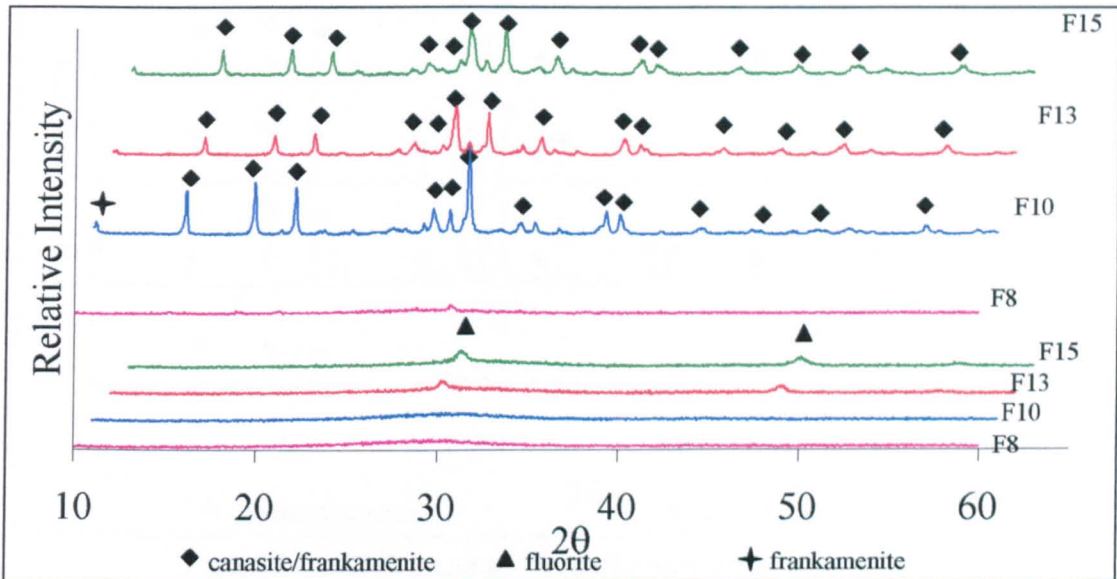


Figure 5.4: XRD traces of F8 to F15 after 2hr hold of 620°C and a two hour hold at 720°C.

SEM of these samples revealed that a decrease in lath sizes accompanied the shift from a predominantly frankamenite phase presence to a predominantly canasite phase presence (Figure 5.5)

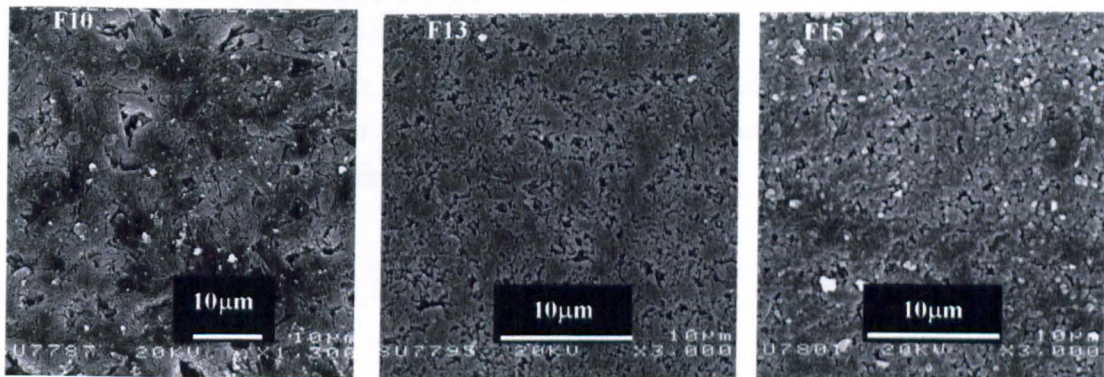


Figure 5.5: SEM images of F10-F15, subjected to a two hour nucleation hold at 620°C and two hour crystallisation hold at 720°C.

Longer nucleation holds of 24 hours at 520°C showed similar results, with F13 and F15 nucleating fluorite crystallites after the nucleation hold, but the 24 hour hold at 620°C resulted in canasite and/or frankamenite crystallisation in all glass ceramics (Figure 5.6).

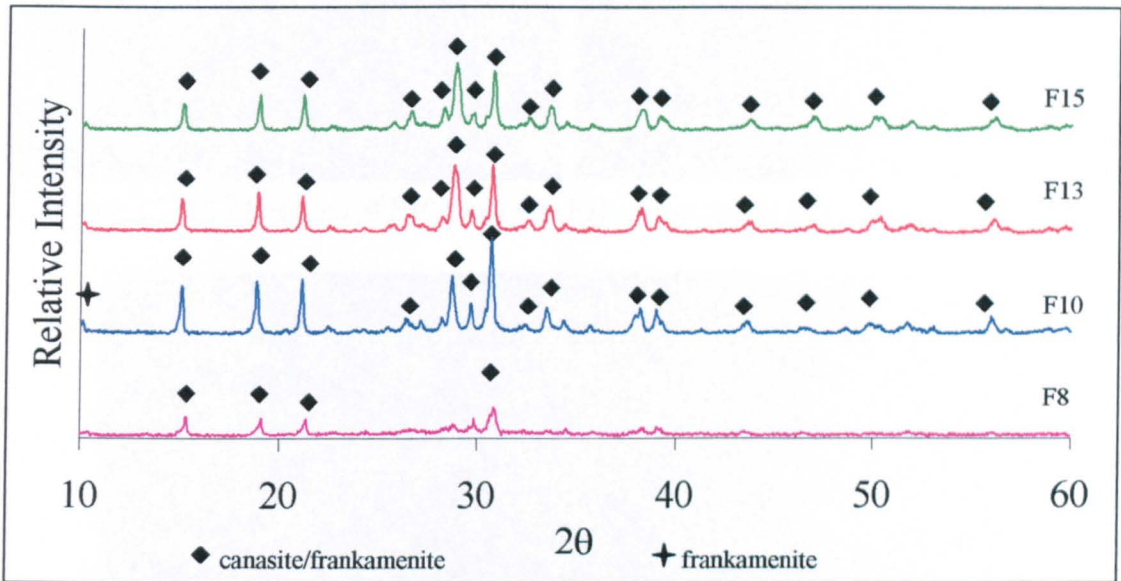


Figure 5.6: XRD traces of F8 to F15 after 24hr hold of 620°C.

In the absence of a nucleation hold, there was uncontrolled spherulitic growth, with lath sizes approximately in the order of  $50\mu\text{m}$  (Figure 5.7). Closer inspection of the XRD traces indicated that in the case of F10 which crystallises to give a predominant frankamenite phase presence a nucleation hold increases the canasite phase presence in the glass ceramic. Although XRD did not record any fluorite after nucleation, there was evidence of  $\text{CaF}_2$  crystals under TEM (Figure 5.8) The two traces in Figure 5.9 are different in that the two stage heat treatment trace has a smaller peak at  $10.1^\circ 2\theta$  and the intensity peak ratio of  $28.6^\circ 2\theta$  to  $30.6^\circ 2\theta$  is larger than that of the single stage heat treated glass ceramic. Both are indicative of greater canasite phase presence.

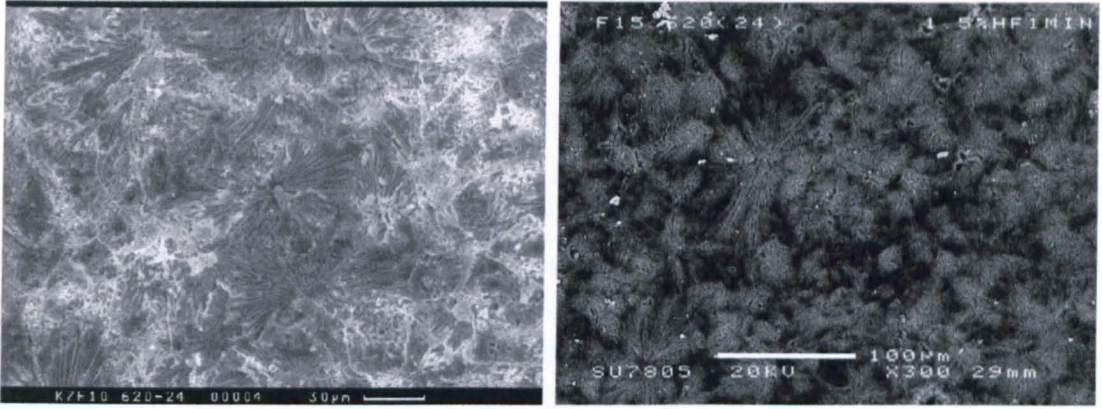


Figure 5.7: SEM images of F10 (left) and F15, subjected to a 24 hour hold at 620°C.

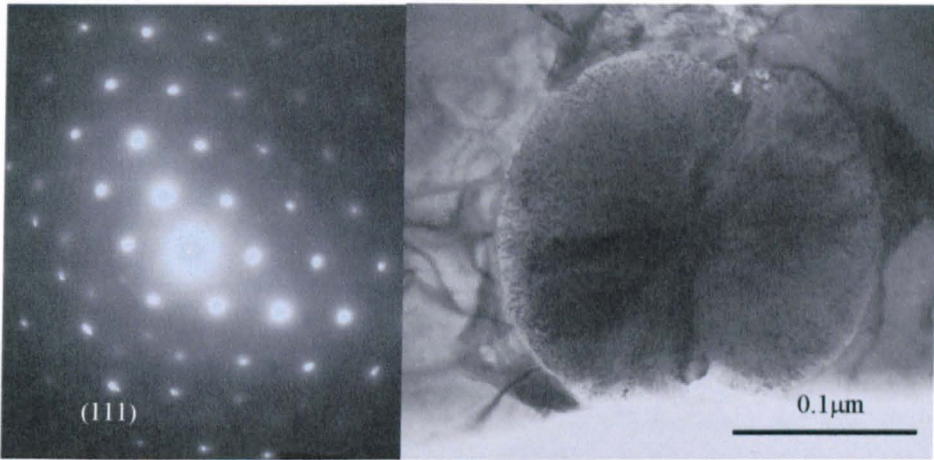


Figure 5.8: TEM image of FCC CaF<sub>2</sub> crystal and corresponding diffraction pattern for F10.

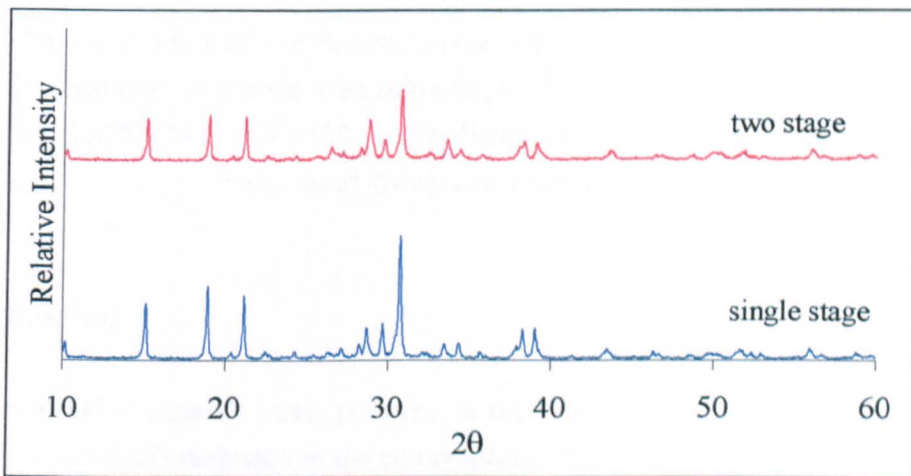


Figure 5.9: XRD traces of single stage heat treatment and two stage heat treatment.

### 5.3.4 Fracture Toughness

The higher fluorine content glass, F15 gave significantly higher fracture toughness values than the glass with stoichiometric fluorine content (Figure 5.10). It was not possible to calculate  $K_{Ic}$  for F8 as after heat treatment the glass ceramics produced were very poorly cerammed and fractured catastrophically upon indentation. This was also true in the case of F10 that had been subjected to the 24 hour nucleation hold at 620°C, prior to the crystallisation hold.

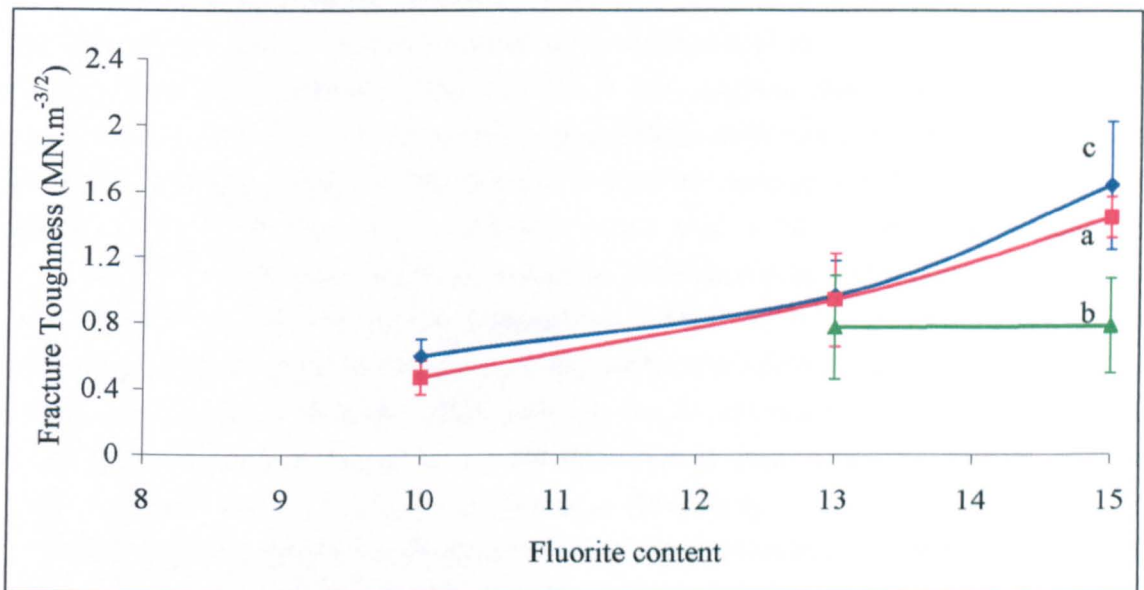


Figure 5.10:  $K_{Ic}$  as a function of fluorite content where a, b and c signify the different heat treatment schedules the glasses were subjected to. a = 540°C(24 hr hold) and 720°C (2 hr hold), b = 620°C (24 hr hold) 720°C (2 hr hold) and c = 620°C (2 hr hold) 720°C (2 hr hold), lines drawn as a guide to the eye.

## 5.4. Discussion

There was a higher canasite phase presence in the F13 and F15 glass-ceramics which had 13 and 15 mol%  $CaF_2$  inclusion in the composition (Figs. 5.2, 5.3 & 5.5). This agrees with the findings of Beall (1983), in that the nucleating phase for canasite is  $CaF_2$ . The

composition of B8 in Chapter 3, which had 18 mol%  $\text{CaF}_2$ , also seemed to contain a greater canasite content than the other compositions. The requirement of the system is highlighted by the need to balance the F content in the parent glass to give an adequate canasite to frankamenite phase ratio to ensure the mechanical strength of the cerammed product. From fracture toughness results so far, frankamenite phase dominance seems to result in a less tough glass-ceramic. Due to the crystallographic similarities between these phases, it has not been possible to achieve or rather, distinguish, a monophase canasite glass-ceramic. Hence, it is difficult to assess if the toughness can be attributed to the canasite phase or to a product that is a result of a both phases 'competing' with each other.

The greater canasite phase presence in F10 after the introduction of a nucleation hold to the heat treatment schedule (Figures 5.8 & 5.9) suggests a heterogeneous nucleation mechanism for canasite, although further crystallographic work needs to be carried out to elucidate this. XRD evidence (Fig 5.2, 5.3 & 5.8) suggests that in the absence of the required amount of  $\text{CaF}_2$ , the crystallising phase which nucleates is frankamenite. Miller *et al* (2004) have suggested that frankamenite crystallises through a different mechanism to that of canasite. The lack of crystallisation in the case of F8 indicates that a minimum amount of fluorine is required for the nucleation of frankamenite which must be lower than the minimum as dictated by the composition. There is no evidence to suggest the crystallisation mechanism of F-canasite. It has not been possible to differentiate between F-canasite and canasite from the XRD traces or the crystal morphology (from the SEM). Considering the similarities in the crystal structures of both, it may necessitate detailed crystallographic work which is outside the remit of this study.

Single stage heat treatments resulted in uncontrolled spherulitic growth with laths of the order of  $50\mu\text{m}$  or more, even in the case of compositions with excess fluorite (Figure 5.6). This could be attributed to fewer nucleation sites being present. The longer, 24 hour, nucleation holds were tried in the hope of a greater dispersion of  $\text{CaF}_2$  nuclei in the glass and hence a finer microstructure being produced. However there was little difference in either the microstructure or the  $K_{Ic}$  of the glass ceramics with nucleation holds of 2 hours at  $620^\circ\text{C}$  and the glass ceramics with nucleation holds of 24 hours at  $540^\circ\text{C}$ . 24 hour holds at  $620^\circ\text{C}$  resulted in canasite crystallisation after the nucleation hold rather than  $\text{CaF}_2$ . The subsequent crystallisation hold at a higher temperature of  $720^\circ\text{C}$  produced a glass-ceramic with inferior mechanical properties (Figure 5.8), most probably due to the larger lath sizes. It has been suggested (Kelly, 1997) that finer crystal sizes of the reinforcing component result in improved mechanical properties by providing a more tortuous route for crack propagation, because  $K_{Ic} = (2E\gamma)^{1/2}$ , where E is the Young's modulus and  $\gamma$  is the surface

energy per unit area. Thus as the crystal sizes decrease and interlocking increases, the crack path travelled increases, hence the surface energy per unit area increases and subsequently the fracture toughness increases. Beall (1986) has identified the two primary mechanisms affecting the fracture toughness of canasite: (1) crack-deflection, which arises from the combined effects of the acicular microstructure and the preferred cleavage fracture, and (2) stress-induced micro-crack toughening, due to the internal stresses caused by the anisotropy in thermal expansion of the individual crystals. Nucleation of  $\text{CaF}_2$ , and the subsequent growth of canasite on these nuclei produces a glass ceramic with a finer microstructure, hence higher fracture toughness. As the crystallisation of either of these phases could not be quantified it is only possible to draw a basic qualitative conclusion that the glass ceramic with the greater canasite phase presence results in the finer microstructure. Finer microstructure also implies smaller defect sizes as grain size limits defect size.

The observed results suggest the crystal structures of canasite and frankamenite influence the indentation fracture toughness of the resulting glass ceramics. Rozhdestvenskaya and Nikishova (1996) report that the structure of canasite is based on tubular  $[\text{Si}_{12}\text{O}_{30}]$  fragments which are linked via closely packed zigzag 'walls'. The octahedral positions associated with the walls are occupied by the Ca and Na cations in an orderly fashion, one of the positions being occupied by either type of cations. Doubled fluorine content in frankamenite results in a different distribution of Ca and Na cations from canasite, increasing the number of isomorphically occupied positions. This leads to a reduction of monoclinic symmetry to P1. The triclinic unit cell of frankamenite represents the minimal fragment of the structure, containing one silicate tube as opposed to the four silicate tubes contained in canasite. Water, which is localised in the tube  $[\text{Si}_{12}\text{O}_{30}]$  together with K atoms, neutralises some valency effects of the anions and alkaline cations, and thereby weakens the strength of the frankamenite structure. The high number of  $(\text{OH})^-$  groups in canasite results in structure stabilisation due to hydrogen bonding between the octahedral walls and the tubular radical. However this is in the case of the minerals.  $(\text{OH})^-$  groups in the canasite structure would be substituted with  $\text{F}^-$  in fluorcanasite thus the reported crystal structures cannot fully explain the fracture toughness results obtained here.

The  $K_{\text{Ic}}$  of F15 ( $1.63 \pm 0.38 \text{ MNm}^{-3/2}$ ) is closer to the fracture toughness values of B8 from chapter 3 ( $2.01 \pm 0.21 \text{ MNm}^{-3/2}$ ), which is a high strength composition and was subjected to the heat treatment schedule as specified by Beall (1983). In addition to this, a value of  $1.63 \pm 0.38 \text{ MPa.m}^{-3/2}$  is a suitable fracture toughness value for a dental restorative material. Seghi *et al* (1995) recorded a fracture toughness value of  $1.29 \pm 0.12 \text{ MNm}^{-3/2}$ , for Empress I (a leucite based commercial dental ceramic) by the indentation technique.

Similarly Gorman *et al* (2000) measured a toughness of  $1.33 \pm 0.08 \text{ MNm}^{-3/2}$ , using the same technique. The fracture toughness of another commercial ceramic, which is prepared via the CAD CAM route is Vita Mark II (crystalline phases of sanidine and nepheline), measured by indentation method was  $1.07 \pm 0.08 \text{ MNm}^{-3/2}$  (Seghi *et al*, 1995) and  $1.26 \pm 0.08 \text{ MNm}^{-3/2}$  (Thompson *et al*, 1996). However the  $K_{Ic}$  values of these glass ceramics are low in comparison to the 'high strength' ceramics which are indicated for use as a posterior restoration. Chapter 4 indicated further compositional variations which could be made to the present formulation, in an effort to improve the mechanical properties and chemical durability of this material. In addition to this it is necessary to note that the heat treatment of this formulation has not been optimised and this in itself would lead to a higher  $K_{Ic}$ .

## 5.5 Conclusions

- $\text{CaF}_2$  is the nucleating phase for canasite, hence canasite seemed to nucleate and crystallise more readily in F13 and F15, resulting in higher fracture toughness values for these glass ceramics.
- Maximum fracture toughness of  $1.63 \pm 0.38 \text{ MNm}^{-3/2}$  was achieved in the case of F15.

## Chapter 6: Effect of Zirconia Additions

### 6.1 Introduction

In agreement with the results of Miller *et al* (2004) the previous chapter identified that  $\text{CaF}_2$  is essential for the crystallisation of canasite. If the glass composition does not have a certain minimum fluorite content, the predominant phase that crystallises is frankamenite, which apparently crystallises homogeneously and which has inferior mechanical properties. An increase in the fluorite content in the parent glass improved the fracture toughness of the material to an acceptable level for a dental restoration. However, increasing fluorite content in the glass composition has been found to decrease the chemical durability of canasite glass ceramic (Stokes, 2003). As canasite crystallisation requires a nucleating agent, it was decided to study zirconia inclusion as an alternative nucleating agent based on the findings of initial compositional variations.

### 6.2 Experimental Procedures

#### 6.2.1 Glass Formulation

Zirconia additions were made to the base glass composition with varying fluorite content and the ratios were re-normalised to 100:

$$\frac{100}{100 + y} \left\{ \frac{100}{90 + x} (60\text{SiO}_2 - 8\text{Na}_2\text{O} - 7\text{K}_2\text{O} - 15\text{CaO} - x\text{CaF}_2) - y\text{ZrO}_2 \right\},$$

$$\text{where } 8 \leq x \leq 15 \text{ and } 0 \leq y \leq 8.$$

The glass compositions used in this study are given in Table 6.1, where F10Z0 is the base glass composition. Glass melting was carried out as described in Chapter 3.

Table 6.1: Glass compositions (as-batched) in mol %.

Composition	K <sub>2</sub> O	CaO	Na <sub>2</sub> O	SiO <sub>2</sub>	CaF <sub>2</sub>	ZrO <sub>2</sub>
<b>F8Z0</b>	7.14	15.31	8.16	61.23	8.16	-
<b>F8Z1</b>	7.07	15.15	8.08	60.61	8.08	0.99
<b>F8Z2</b>	7.00	15.00	8.00	60.02	8.00	1.96
<b>F8Z4</b>	6.86	14.72	7.85	58.87	7.85	3.85
<b>F8Z8</b>	6.61	14.17	7.56	56.69	7.56	7.41
<b>F10Z0</b>	7.00	15.00	8.00	60.00	10.00	-
<b>F10Z1</b>	6.93	14.85	7.92	59.41	9.90	0.99
<b>F10Z2</b>	6.86	14.70	7.84	58.82	9.80	1.96
<b>F10Z4</b>	6.73	14.42	7.69	57.69	9.62	3.85
<b>F10Z8</b>	6.48	13.89	7.41	55.56	9.26	7.41
<b>F15Z0</b>	6.67	14.28	7.62	57.14	14.29	-
<b>F15Z1</b>	6.60	14.14	7.54	56.58	14.14	0.99
<b>F15Z2</b>	6.54	14.01	7.47	56.02	14.01	1.96
<b>F15Z4</b>	6.41	13.74	7.33	54.95	13.74	3.85
<b>F15Z8</b>	6.17	13.23	7.06	52.91	13.23	7.41

### 6.2.2 Differential Thermal Analysis

Differential thermal analysis was used to determine crystallisation temperatures. The samples were crushed using a percussion mortar, and then passed through a 45 $\mu$ m sieve. DTA measurements were carried out on a PerkinElmer PYRIS Diamond analyser as described in section 3.2.1

### 6.2.3 Heat Treatment

All three series of glasses were subjected to single stage heat treatments at 5°C/min up to temperatures varying in 20°C between 600 and 740°C, for phase analysis in Lenton furnaces. These samples were held for two hours at the temperatures and air quenched to retain the phases present at those temperatures. Both XRD and DTA results were used to determine the nucleation and crystallisation temperatures. Two stage heat treatments were used to produce samples for fracture toughness tests. The samples were heated at a rate of

5°C up to the nucleation and growth temperatures and furnace cooled at an approximate rate of 10°C/min. Table 6.2 shows the two stage heat treatment schedules that the glasses were subjected to.

Table 6.2: Two-stage heat treatment schedules used to produce samples for  $K_{Ic}$  measurements

glass	Heating rate (°C /min)	Nucleation temp. (°C)	Hold duration (min)	Heating rate (°C /min)	Crystallisation temp. (°C)	Hold duration (min)
<b>F8Z0</b>	5	550	120	5	720	120
<b>F8Z1</b>	5	550	120	5	720	120
<b>F8Z2</b>	5	550	120	5	740	120
<b>F8Z4</b>	5	550	120	5	760	120
<b>F8Z8</b>	5	550	120	5	780	120
<b>F10Z0</b>	5	550	120	5	720	120
<b>F10Z1</b>	5	550	120	5	750	120
<b>F10Z2</b>	5	550	120	5	750	120
<b>F10Z4</b>	5	550	120	5	750	120
<b>F10Z8</b>	5	550	120	5	800	120
<b>F15Z0</b>	5	550	120	5	700	120
<b>F15Z1</b>	5	550	120	5	720	120
<b>F15Z2</b>	5	550	120	5	800	120
<b>F15Z4</b>	5	550	120	5	800	120
<b>F15Z8</b>	5	550	120	5	800	120

#### 6.2.4 Phase and Microstructural Analysis

X-Ray diffraction was carried out using both the Phillips and the Siemens diffractometers. Fracture surfaces and etched surfaces were examined using the Jeol and the Camscan electron microscopes as detailed in section 3.2.3. TEM was carried out as detailed in section 5.2.5.

### 6.2.5 Mechanical Testing

Fracture toughness was measured using Vickers indentation as described in section 3.3.3. The fracture toughness ( $K_{Ic}$ ) Vickers hardness ( $H_V$ ) and brittleness (B) were calculated using equations 3.1, 3.2 and 3.3.

## 6.3 Results

### 6.3.1 Crystalline Phase Analysis

All compositions melted to form clear homogeneous glass, indicating relatively high zirconia solubility in these glasses.

#### (i) Glasses with 8 mol% fluorite content

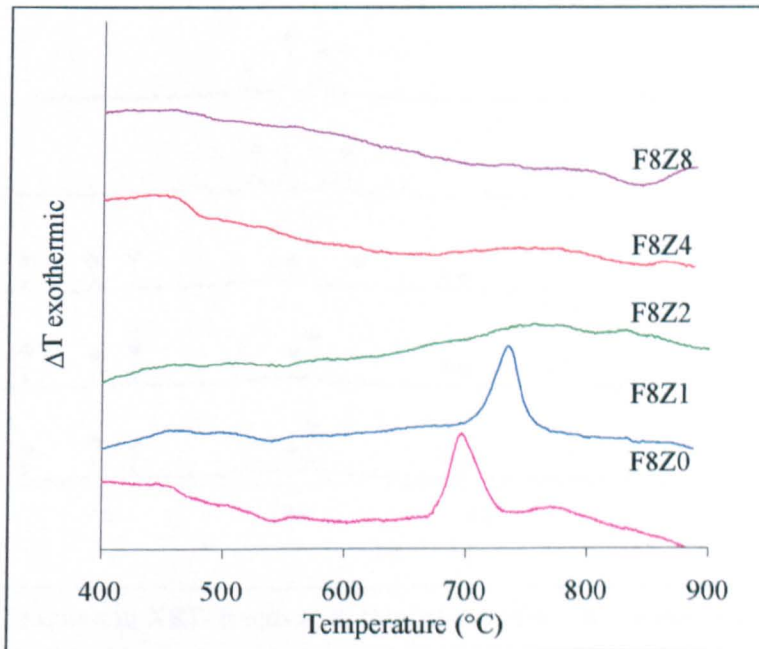


Figure 6.1: DTA traces of F8Z0 to F8Z8

The DTA traces of the F8 glasses including  $ZrO_2$  are given in Figure 6.1.  $T_g$  was observed at temperatures ranging from 530°C to 570°C (Appendix 3), as would be expected with the

addition of an intermediate oxide. Exothermic peaks, corresponding to the crystallisation of canasite/frankamenite from the glass were observed in the composition without any  $ZrO_2$  and the composition containing 1 mol%  $ZrO_2$ . The onset temperature of this exothermic peak increased with the addition of the  $ZrO_2$ . No exothermic crystallisation peaks were observed for the glasses with 2 to 8 mol%  $ZrO_2$  addition.

XRD of the glasses after annealing confirmed an amorphous structure. Single stage heat treatments recorded the phase evolution of canasite (ICDD 13-0553) and/or frankamenite (ICDD 45-1398) in the glasses with up to 2 mol%  $ZrO_2$  addition, with no initial  $CaF_2$  crystallisation as a precursor. There is a shift from a predominantly frankamenite (F8Z0 & F8Z1) to a predominantly canasite glass ceramic (F8Z2). This is noticeable in Figure 6.2 where the traces of the single stage heat treatments which produced maximum crystallinity for the different compositions have been stacked. Longer holds of 2 hours at the temperatures enabled crystal growth despite DTA recording no exothermic peaks for F8Z2, F8Z4 and F8Z8. However due to the poor crystallinity of these glass ceramics it was very difficult to identify and index the phases that crystallised in the case of F8Z4 and F8Z8.

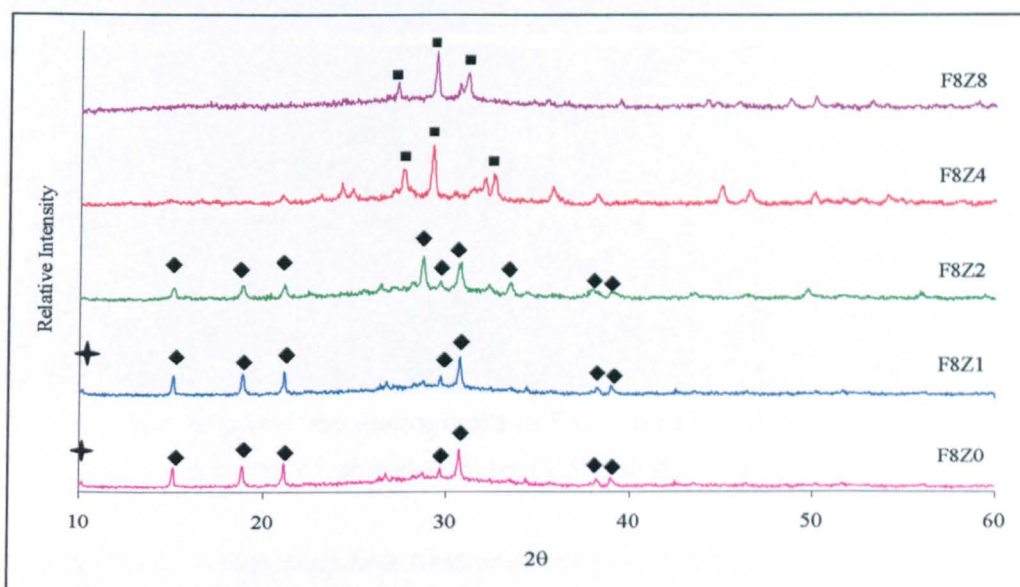


Figure 6.2: Differences in XRD traces at x, fluorite content = 8, subjected to single stage heat treatment to peak DTA temperature. The peaks are indexed  $\blacklozenge$  canasite/frankamenite,  $\blackcross$  frankamenite and  $\blacksquare$  unknown.

Table 6.3: Crystalline phase analysis after two-stage heat treatment

	Crystalline phases
<b>F8Z0</b>	canasite/frankamenite
<b>F8Z1</b>	canasite/frankamenite
<b>F8Z2</b>	canasite/frankamenite
<b>F8Z4</b>	unknown
<b>F8Z8</b>	unknown

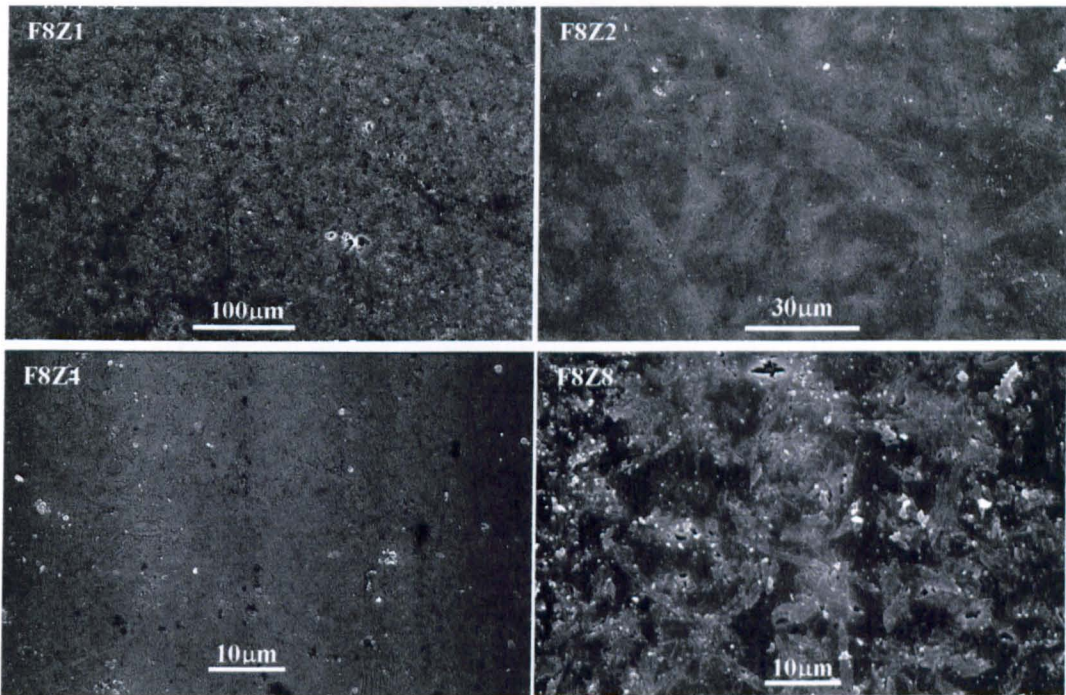


Figure 6.3: Scanning electron micrographs of F8Z1 to F8Z8 subjected to two stage heat treatments, etched samples (1.5%HF for 25 seconds).

When subjected to a two-stage heat treatment, the phases which crystallised were canasite and/or frankamenite for F8Z0, F8Z1 and F8Z2, with the F8Z2 trace being more akin to canasite, as noted for the glasses subjected to single stage heat treatment (Table 6.3). There was no evidence of any crystalline content after the nucleation hold for any of the glass ceramics. The traces for F8Z4 and F8Z8, after the crystallisation hold, remained unidentifiable. XRD recorded the same phase, albeit unknown, in both. Figure 6.3 illustrates the microstructures of F8Z1 to F8Z8. The structure of F8Z0 was very similar to

that of F8Z1 in that it was essentially amorphous with no discernable crystalline content visible after etching. The crystal morphology of the unknown phase in F8Z4 and F8Z8 can be seen more clearly in the micrograph of F8Z8 of Figure 6.3, which shows needle like crystallites of the order of  $10\mu\text{m}$  by  $1\mu\text{m}$  in a largely amorphous matrix.

(ii) Glasses with 10 mol% fluorite content

DTA recorded a shift in the exothermic peak corresponding to canasite and/or frankamenite crystallisation for glasses with 0 to 2 mol%  $\text{ZrO}_2$  inclusion in the composition from  $700^\circ\text{C}$  to  $800^\circ\text{C}$  (Figure 6.4).

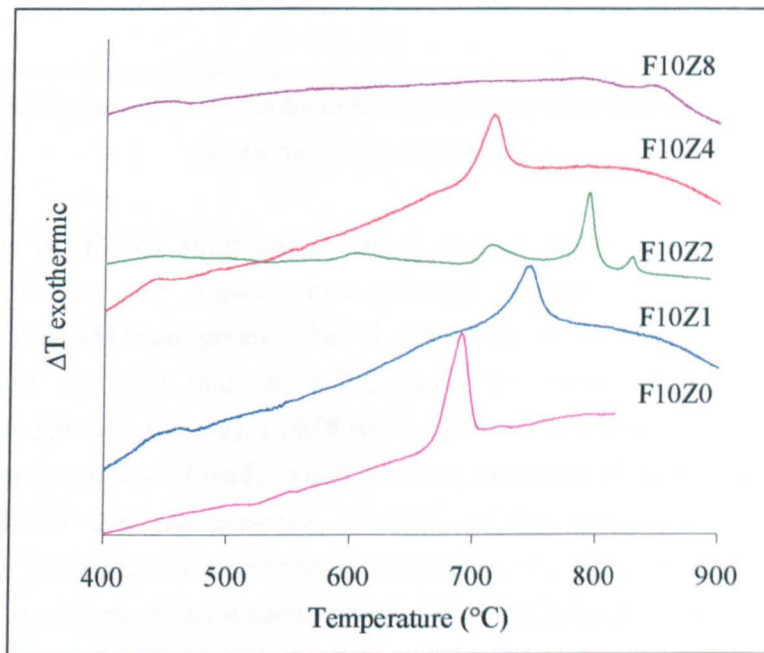


Figure 6.4: DTA traces of F10Z0 to F10Z8

The trace corresponding to F10Z2 indicates 3 phases crystallising out at  $710^\circ\text{C}$ ,  $800^\circ\text{C}$  and  $830^\circ\text{C}$ . XRD evidence demonstrated distinct differences between  $720^\circ\text{C}$  and  $800^\circ\text{C}$  in these glass ceramics (Figure 6.5). However there was insufficient information to identify distinct phases and they were all indexed as canasite/frankamenite phases.

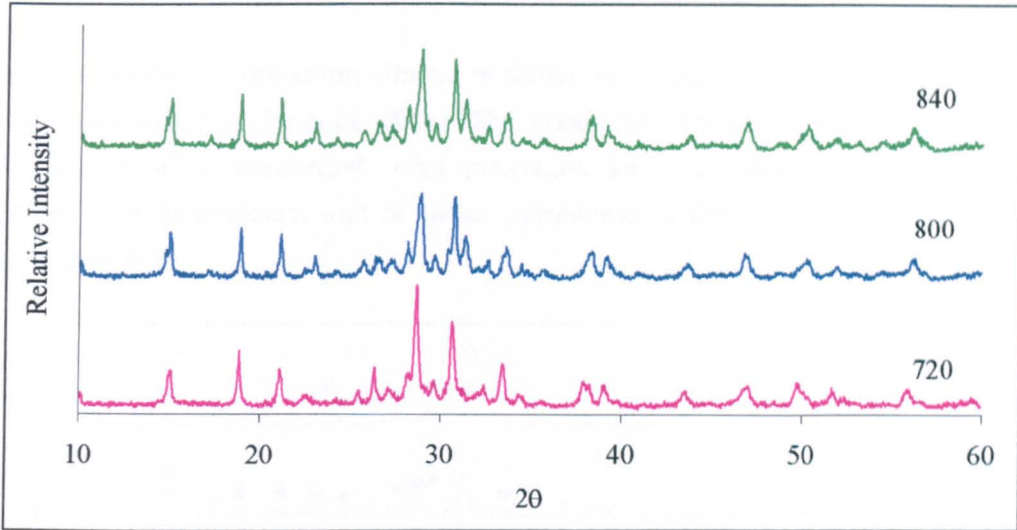


Figure 6.5: XRD traces of F10Z2 subjected to single stage heat treatments and holds at mentioned temperatures ( $^{\circ}\text{C}$ ).

XRD undertaken on F10Z4 subjected to single stage heat treatment indicated a phase distinct from canasite and frankamenite although canasite/frankamenite phases did crystallise. At  $\text{ZrO}_2$  additions greater than 4 mol% the peaks were indexed to wadeite  $\text{K}_2\text{ZrSi}_3\text{O}_9$  (ICDD 43-0231) thus the DTA exothermic peak for F10Z4 (Figure 6.4) corresponds to wadeite (Figure 6.6). F10Z8 when subjected to a single stage heat-treatment, resulted in the crystallisation of wadeite and the same unknown phase seen in the F8 series. The results indicate that the presence of  $\text{CaF}_2$  in the composition encourages the crystallisation of canasite/ frankamenite at zirconia contents up to 4mol% as well as encouraging the evolution of the wadeite phase. However  $\text{ZrO}_2$  is not acting as the hoped for nucleating agent.

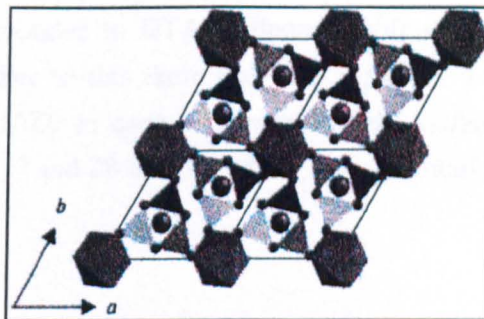


Figure 6.6: Structure of wadeite with  $\text{SiO}_4$  tetrahedras,  $\text{ZrO}_6$  octahedra, large circles depicting  $\text{K}^+$  or  $\text{Na}^+$  and small circles depicting oxygen.

Wadeite, a potassium zirconium silicate is found as a mineral in West Kimberly area in Western Australia (Ferreira *et al*, 2001). The hexagonal structure of wadeite is based on a framework of silica tetrahedral, with potassium and zirconium atoms fitting in the interstices. The fundamental unit of these frameworks is the condensed cyclic trisilicate group (Figure 6.6).

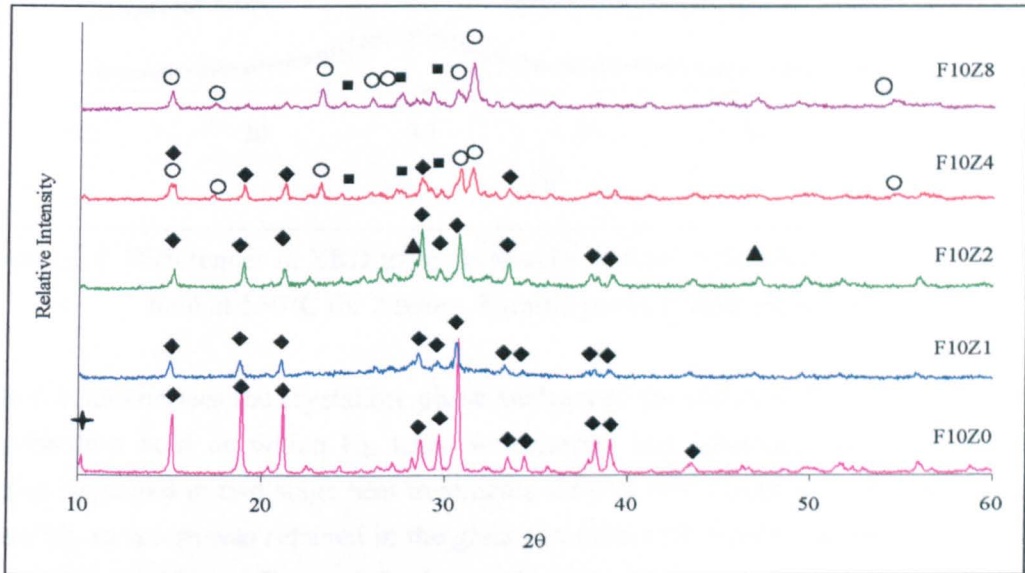


Figure 6.7: Differences in XRD traces at fluorite content = 10, subjected to single stage heat treatment to peak DTA temperature. The peaks are indexed ◆canasite/frankamenite, †frankamenite, ▲ fluorite, ○ wadeite and ■ unknown

Whereas the nucleation holds of the F8 series of glass ceramics resulted in amorphous humps, XRD recorded evidence of  $\text{CaF}_2$  for F10Z2 glass ceramic after the nucleation hold (Figure 6.8). This corresponded to DTA evidence which only records a  $600^\circ\text{C}$  peak for F10Z2 (Figure 6.4). Further to this there was also a shift from a frankamenite dominant crystalline structure in F10Z0 to canasite dominant one, visible in both single stage and double stage analysis ( $10.1^\circ$  and  $28.6^\circ$   $2\theta$  to  $30.6^\circ$   $2\theta$  peak ratio in Figure 6.7)

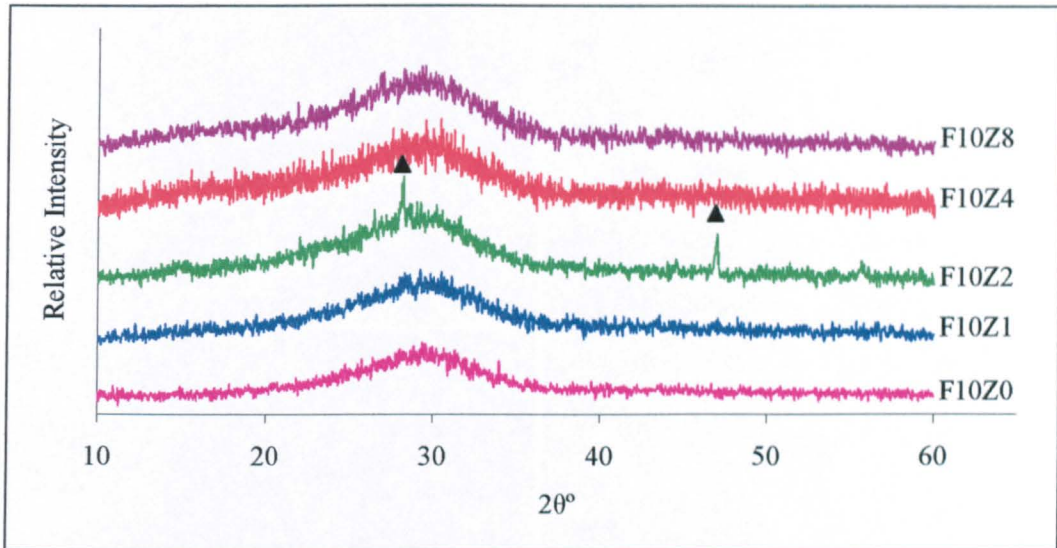


Figure 6.8: Differences in XRD traces at fluorite content = 10, subjected to a nucleation hold at 550°C for 2 hours. Fluorite peaks is indexed as ▲ .

Table 6.4 summarises the crystalline phase analysis of the samples after the nucleation and crystallisation hold on which  $K_{Ic}$  tests were carried out. Microstructural analysis of the samples subjected to two stage heat treatments showed refinement in crystal structure. The spherulitic structure was retained in the glass ceramics with 1 mol% zirconia, but lath sizes decreased from 20  $\mu\text{m}$  (Figure 5.5, chapter 5) to approximately 10  $\mu\text{m}$  (Figure 6.9). The structure of F10Z2 was refined further with the crystal morphology moving away from the uncontrolled spherulitic structure to more interpenetrating laths of the order of 5  $\mu\text{m}$  (Figure 6.9).

Table 6.4: Crystalline phase analysis after two-stage heat treatment

	<b>Crystalline phases</b>
<b>F10Z0</b>	canasite/frankamenite
<b>F10Z1</b>	canasite/frankamenite
<b>F10Z2</b>	canasite/frankamenite, wadeite and unknown
<b>F10Z4</b>	canasite/frankamenite, wadeite and unknown
<b>F10Z8</b>	wadeite and unknown

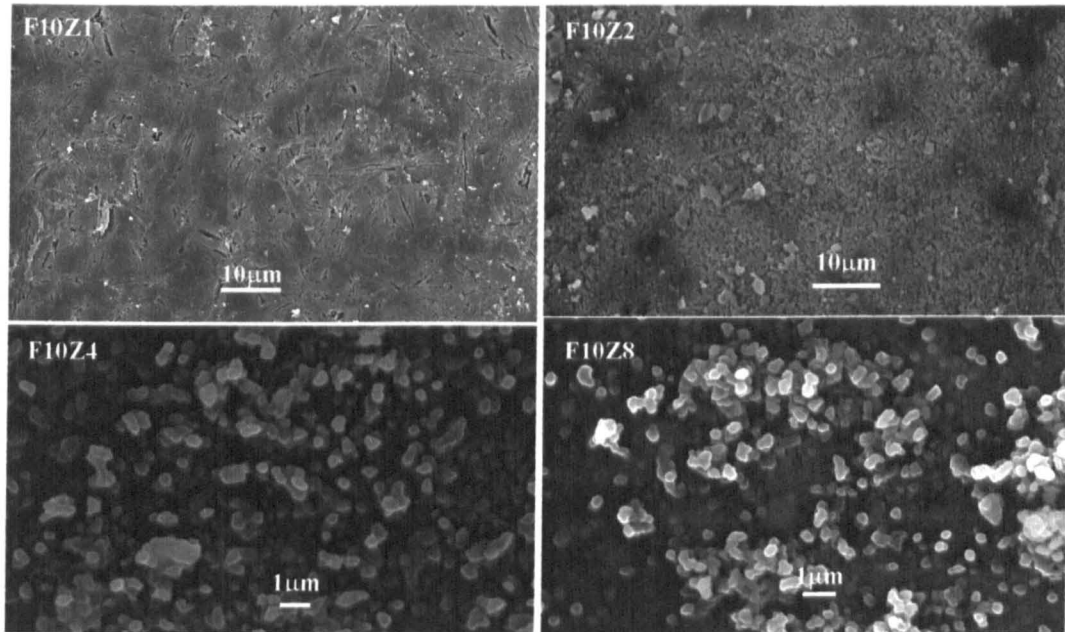


Figure 6.9: Scanning electron micrographs of etched surfaces of F10Z4 to F10Z8 subjected to two stage heat treatments, etched samples (1.5%HF for 1 minute).

Canasite crystal morphology was further altered in F10Z4, which showed mainly crystals of  $< 1 \mu\text{m}$  size, in amorphous regions. It was not possible to distinguish canasite crystals from wadeite, presumably due to the similar morphology as can be seen in F10Z8 (Figure 6.7). No elemental differences could be found under EDS, due to the very fine particle sizes ( $\sim 1 \mu\text{m}$ ). Although XRD evidence indicated the presence of the unknown phase in both F10Z4 and F10Z8, assuming the crystal structure would be similar to that noticeable in F8Z8 (Figure 6.3) it was not possible to distinguish this under microscopy either.

### (iii) Glasses with 15 mol% fluorite content

DTA again recorded a shift in the exothermic peak temperature corresponding to canasite/frankamenite as the  $\text{ZrO}_2$  content was increased (Figure 6.10). A similar peak separation was noticed in the case of F15Z1 as noted previously for F10Z2, and again there was insufficient information from XRD to identify distinct phases and they were all indexed as canasite/frankamenite phases.

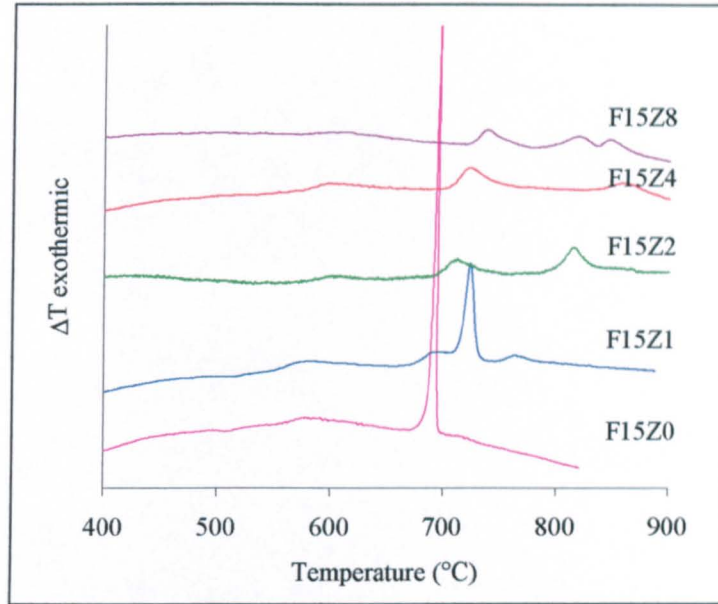


Figure 6.10: DTA traces of F15Z0 to F15Z8

Figure 6.11 shows the XRD patterns obtained from the glass-ceramics subjected to the single stage heat treatments. In addition to canasite/ frankamenite peaks, fluorite peaks were identified in the F15 glass ceramics (ICDD 04-0864).

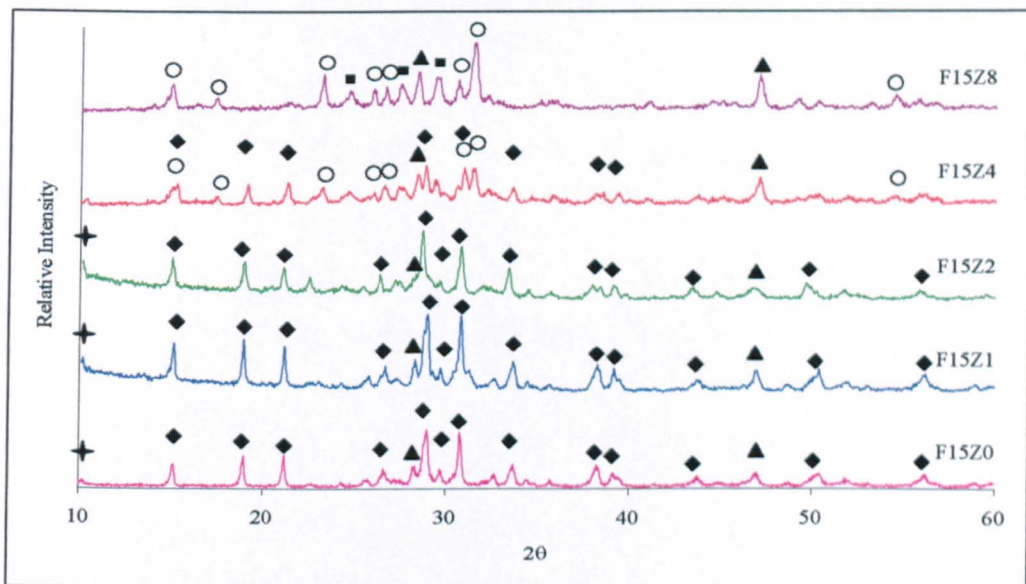


Figure 6.11: Differences in XRD traces at fluorite content = 15, subjected to single stage heat treatment to peak DTA temperature. The peaks are indexed ♦ canasite/frankamenite, † frankamenite, ▲ fluorite, ○ wadeite and ■ unknown

At  $ZrO_2$  additions greater than 4 mol% the peaks were indexed to wadeite and the unknown phase. DTA recorded three crystallisation peaks associated with F15Z8 at 740°C, 820°C and 840°C. From XRD evidence, the phase crystallising out at 740°C is the unknown phase with the latter peak being associated with wadeite crystallisation.

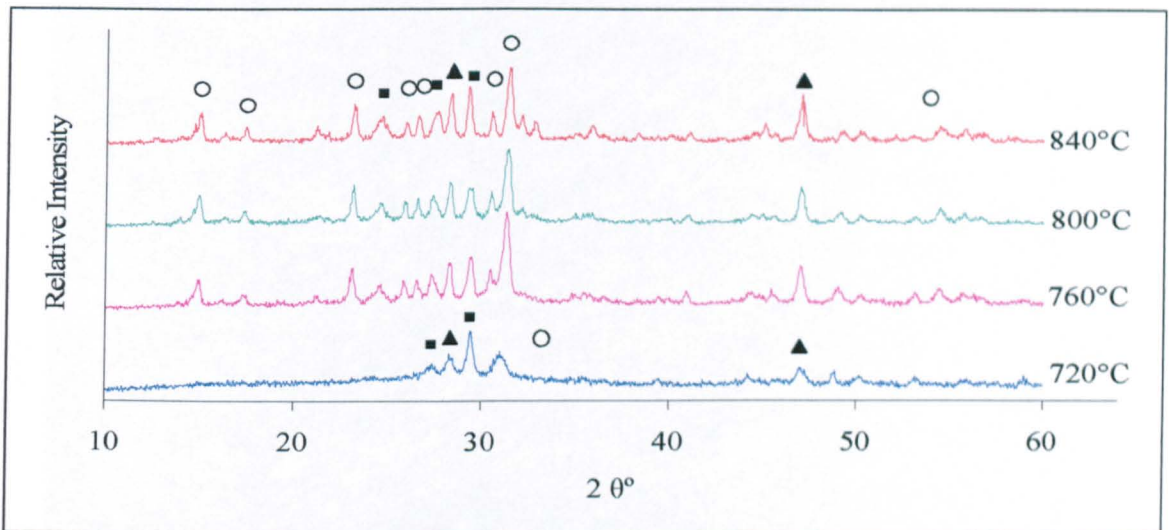


Figure 6.12: XRD traces of F15Z8 subjected to 2 hour holds at stated temperatures. The peaks are indexed ▲ fluorite, ○ wadeite and ■ unknown

The results for the phase analysis on the glass ceramics subjected to two stage heat treatments are summarised in table 6.5 and the corresponding microstructures are shown in Figure 6.13.

Table 6.5: Crystalline phase analysis after two-stage heat treatment

	<b>Crystalline phases</b>
<b>F15Z0</b>	canasite/frankamenite
<b>F15Z1</b>	canasite/frankamenite
<b>F15Z2</b>	canasite/frankamenite
<b>F15Z4</b>	canasite/frankamenite, wadeite and unknown
<b>F15Z8</b>	wadeite and unknown

An interpenetrating ‘house of cards’ structure is demonstrated for the 1 mol% inclusion of zirconia at a fluorite content of 15, distinctly different to the ‘droplet’ type structure of

F15Z0 (Figure 5.5, Chapter 5). The structure becomes more platy with a 2 mol% zirconia inclusion and tends back to the spherulitic structure with larger lath sizes at a 4 mol% zirconia inclusion.

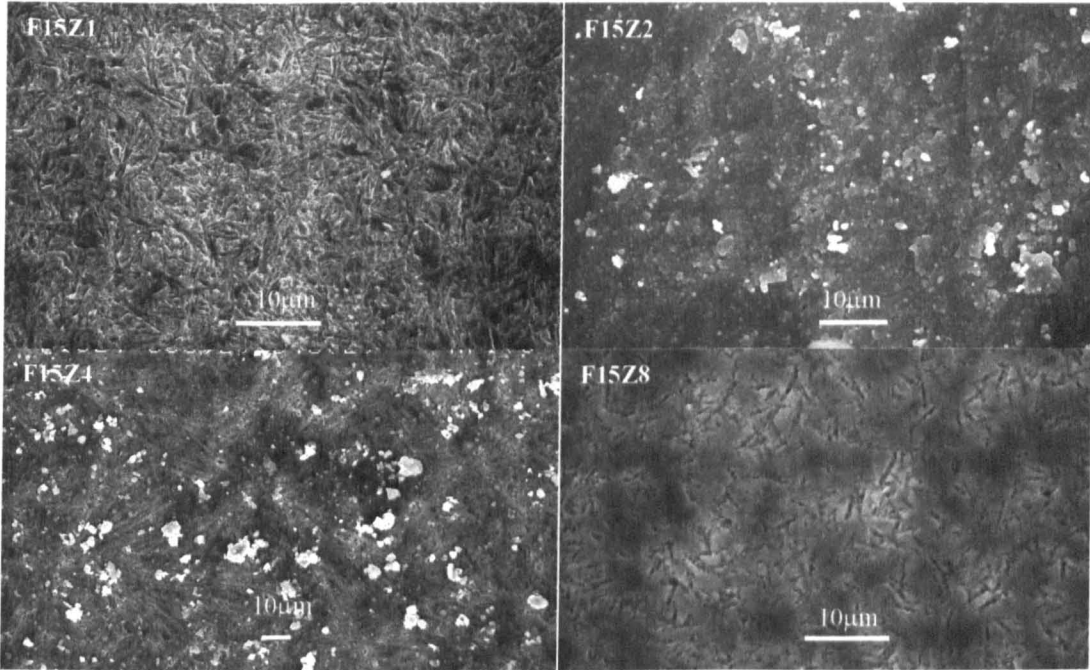


Figure 6.13: Scanning electron micrographs of F15Z4 to F15Z8 subjected to two stage heat treatments, etched samples (5%HF for 25 seconds).

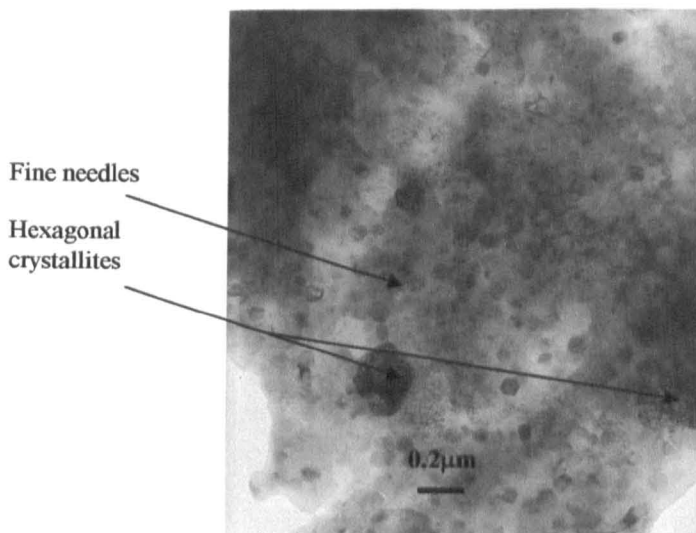


Figure 6.14: Transmission electron micrograph of F15Z8

The needles present in F15Z8 appeared to correspond to only one type of phase from SEM (Figure 6.13). This could be a refinement of the structure of the unknown phase demonstrated in F8Z8 (Figure 6.3). However two distinct phases could be identified under TEM (Figure 6.14), a phase with spherulitic somewhat hexagonal crystallites and distinct regions with very fine needles.

### 6.3.2 Fracture Toughness

The results for the  $K_{Ic}$  of the glass-ceramics and their associated standard deviations are shown in figure 6.15. The circle denotes those values which are not statistically significant (where significance is at  $p < 0.05$ , as calculated by ANOVA, in Microsoft Excel, Windows XP).

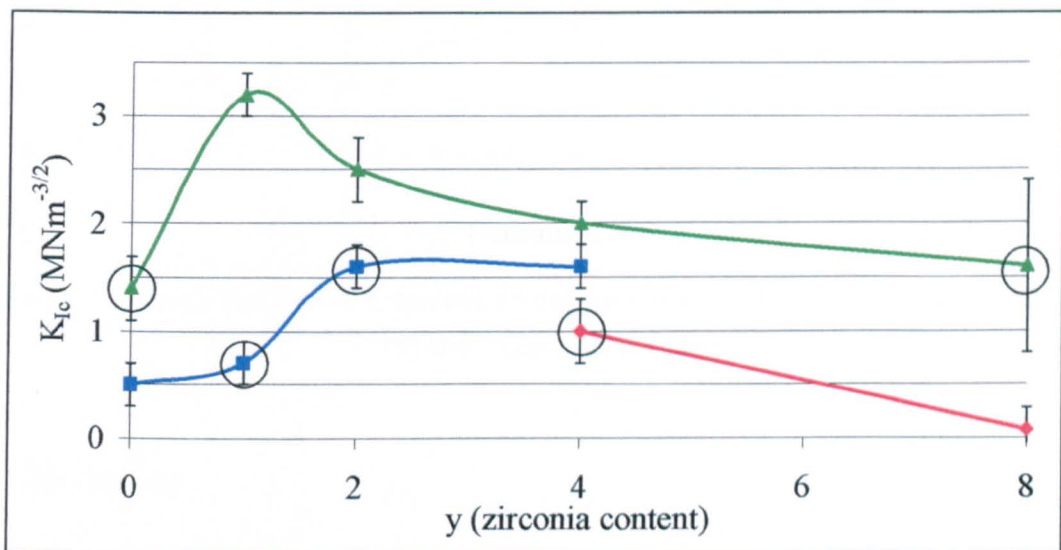


Figure 6.15:  $K_{Ic}$  as a function of  $x$ , fluorite content (red is  $x = 8$ , blue is  $x = 10$  and green is  $x = 15$ ) and  $y$  (zirconia content).

The  $K_{Ic}$  values increase with fluorine content, agreeing with the findings in Chapter 4. Minimum zirconia addition in the case of F15Z1 glass ceramics results in an increase in the fracture toughness from  $1.4 \pm 0.3 \text{ MNm}^{-3/2}$  to  $3.2 \pm 0.2 \text{ MNm}^{-3/2}$ . Subsequent additions of zirconia decrease the  $K_{Ic}$ . In the case of F10 glass ceramics, the maximum  $K_{Ic}$  seems to have shifted to a 2 molar% inclusion of zirconia, with a decrease for subsequent inclusions. In the case of F8 glass ceramics, canasite and/or frankementie crystallisation was poor for

lower zirconia additions, hence  $K_{Ic}$  values were unobtainable. The phases which crystallised at higher zirconia additions were wadiete and an unknown phase, which resulted in lower fracture toughness values.

The hardness values were used to calculate the brittleness index,  $B$  of the glass-ceramics. Figure 6.16 is a plot of the calculated brittleness as a function of the fluorite and zirconia content. The dotted line at  $B = 4.3 \mu\text{m}^{-1/2}$  is the maximum value for the material to be machinable according to Boccaccini (1997).

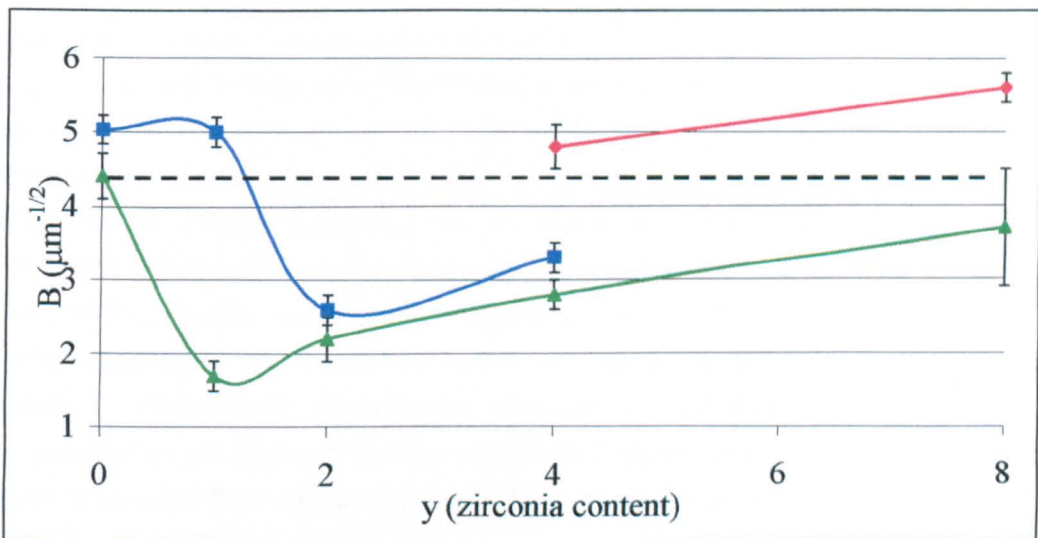


Figure 6.16:  $B$  as a function of  $x$ , fluorite content (red is  $x = 8$ , blue is  $x = 10$  and green is  $x = 15$ ) and  $y$  (zirconia content).

## 6.4 Discussion

The addition of  $\text{ZrO}_2$  significantly changed the fluorcanasite crystallite size, which decreased when the  $\text{ZrO}_2$  concentration increased from 0 wt% to 2 wt% (Figures 6.3, 6.9 and 6.13). The crystals in the F10Z1, F10Z2, F15Z1 and F15Z2 glass-ceramics have an acicular and randomly oriented, interlocked lath like morphology indicative of a greater number of nucleation sites than in the system without zirconia additions where uncontrolled spherulitic growth was observed. It has been suggested that the addition of  $\text{ZrO}_2$  supplements the nucleation role of  $\text{CaF}_2$  thereby allowing the development of fine-grained bodies (Beall, 1983). The findings of this study seem to correlate with this however further work is required to elucidate the exact mechanisms. The increase in the crystallisation onset

temperature of canasite and/or frankamenite phase presence with the addition of  $ZrO_2$  for all fluorite compositions, indicates that  $ZrO_2$  does not act as an effective nucleating agent. Previous studies on  $ZrO_2$  additives in yttria-alumina-silica glasses have found that cubic zirconia crystallises from the parent glass and evidence of yttrium disilicate crystals embedded on zirconia (Vomacka *et al*, 1996). But there has been no evidence of  $ZrO_2$  crystallisation in these glass ceramics. In the case of F10Z2 however, the presence of 2 mol%  $ZrO_2$  (Figure 6.8), increases the  $CaF_2$  crystalline content.  $CaF_2$  is the known nucleating agent for canasite, and under these conditions, it can be stated that  $ZrO_2$  acts as a growth modifier during the crystal growth process.

There is a very definite correlation between the  $K_{Ic}$  results obtained and the crystalline phase and phase morphology of these glass-ceramics. The link between canasite phase dominance and  $K_{Ic}$  has been established in Chapter 5. This study substantiates these findings, as the fracture toughness values related to frankamenite dominant structures (F8Z0, F8Z1 and F10Z0) are lower than the values related to canasite dominant structures (F10Z2, F15Z0, F15Z1 and F15Z2). Further to this the microstructures of these glass ceramics, in particular the crystallite size and the type of interlocking, affected the fracture toughness. The F10Z0 fluorcanasite crystals are spherulites with lath sizes of approximately  $20\mu m$  (Figure 5.5). The crystals that were formed in the F10Z1 and F10Z2 (Figures 6.9) were finer being  $10\mu m$  and  $5\mu m$  respectively and this correlated with an increase in  $K_{Ic}$ , although these toughness values are not statistically different. A better example is the structure of F15Z1 which exhibited a much finer and a randomly oriented interlocked lathlike morphology (Figure 6.13) and hence a high  $K_{Ic}$  of  $3.2 \pm 0.2 MNm^{-3/2}$ . Although F15Z2 has a similar scale of crystallite size, the crystal morphology is less interlocked, and more 'platy' resulting in a decrease in the  $K_{Ic}$  to  $2.5 \pm 0.3 MNm^{-3/2}$ . FZ84, FZ82, FZ108 and FZ158 that contained wadeite and the unknown phase, had microstructures consisting of few very fine needles, approximately  $5\mu m$  in size and large amorphous regions (Figures 6.3, 6.9 and 6.13). F10Z4 and F15Z4 demonstrated higher fracture toughness values than the base composition of F10Z0, although with lower canasite phase content. This was attributed to the fine crystallite size probably obtained due to the competition between different crystal phases.

No fracture toughness data were obtained for the FZ81, FZ82, FZ101 and FZ108 glass ceramics through the indentation method, because of the high porosity found in these samples. As the  $ZrO_2$  content was increased from 2 to 8 mol% the crystalline phase changed from predominantly canasite/frankamenite to wadeite and an as yet unknown phase. The mineral wadeite has the ideal formula  $K_2ZrSi_3O_9$ , the structure of which is

based on a framework of silica tetrahedra the fundamental unit of which being the condensed cyclic trisilicate group with the potassium and zirconium atoms fitting into the interstices (Ferreira *et al*, 2001). Wadeite has been predominantly synthesised by the hydrothermal synthesis route, where the reactants have been heated in water/steam at high pressures and temperatures. No prior nucleation and crystallisation mechanism of wadeite as a glass-ceramic has been identified in previous studies. However increasing  $\text{CaF}_2$  seems to encourage wadeite crystallisation as well as canasite crystallisation. Has and Stelian (1960) have described the use of metallic fluorides to assist crystallisation of glasses. Fluoride crystals are first precipitated and these serve as nucleation sites for the growth of silicate crystals so that the glass is converted to a polycrystalline glass ceramic. The ease with which fluorides can be induced to crystallise out of a glass can be attributed to their weakening effect on the glass network. This means that even if the melt can be cooled to give a clear glass, as in the case of these fluorocanasite compositions, reheating the glass to a temperature within or just above the annealing range permits atomic rearrangement to occur so that crystalline fluoride nuclei may be formed (McMillan, 1979). The results of this study indicate that wadeite may have a similar crystallisation mechanism to that of canasite. The evolution of these phases as the predominant phases in the glass ceramics is associated with a sharp decrease in the  $K_{Ic}$ . Further work on the crystallisation mechanisms of wadeite and to identify the unknown phase at higher zirconia inclusions is necessary, however bearing in mind the lower toughness values associated with these crystalline phases in comparison to canasite, this is not within the scope of the current study.

The maximum  $K_{Ic}$  value achieved with these compositional variations was  $3.2 \pm 0.2 \text{ MNm}^{-3/2}$  which is comparable to the  $K_{Ic}$  values of 'high strength' commercial systems indicated for use as a posterior restorative material ( $3.3 \pm 0.3 \text{ MPa.m}^{1/2}$  for Empress II, reported by Höland *et al*, 2000). There was little variation in the hardness values of these glass ceramics ( $\sim 5 \text{ GPa}$ ) and thus the higher  $K_{Ic}$  values also resulted in brittleness indices of lower than  $4.3 \mu\text{m}^{-1/2}$  (the maximum value for the material to be machinable according to Boccaccini, 1997). A true test of machinability of course, would be a trial of the glass-ceramic material in the CAD-CAM process, which subsequently follows in Chapter 8.

## 6.5 Conclusions

- Increasing  $\text{CaF}_2$  content increased the tendency of the glass ceramics towards canasite formation and thereby increased the fracture toughness.

- **ZrO<sub>2</sub> contents up to 2mol% resulted in a shift from frankamenite to canasite as the dominant phase, for all fluorite content glass-ceramics.**
- **The maximum fracture toughness was obtained for F15Z1 was  $3.2 \pm 0.2 \text{ MNm}^{-3/2}$ , which is comparable to commercial systems.**
- **ZrO<sub>2</sub> contents of 4mol% and greater resulted in wadeite and an unknown phase.**
- **The fracture toughness results indicate wadeite would be not suitable for development as a monophasic dental restorative material.**

## Chapter 7: Effect of silica content

### 7.1 Introduction

The composition of F15Z1 namely  $56.58\text{SiO}_2-7.54\text{Na}_2\text{O}-6.60\text{K}_2\text{O}-14.14\text{CaO}-14.14\text{CaF}_2-0.99\text{ZrO}_2$  has been shown to have a high fracture toughness value comparable to commercial systems for posterior restorations. However, this improvement in the mechanical properties of the glass ceramic occurred when an inclusion of 15 mol%  $\text{CaF}_2$  has been made to the composition. Stokes (2003) has reported a 75% increase in solubility results associated with a 15 mol%  $\text{CaF}_2$  inclusion in the composition. Dissolution in these glass ceramics is known to occur preferentially in the glassy phase. Hence it was decided to increase the silica content in the base glass, in an effort to achieve a high strength, high chemical durability formulation. This chapter deals with the fracture toughness evaluations of silica variation.

### 7.2 Experimental Procedures

#### 7.2.1 Glass Formulation

Table 7.1: Glass compositions (as-batched) in mol%

Composition	$\text{K}_2\text{O}$	$\text{CaO}$	$\text{Na}_2\text{O}$	$\text{SiO}_2$	$\text{CaF}_2$	$\text{ZrO}_2$
S55	6.71	14.37	7.67	55.88	14.37	1.01
S57(=F15Z1)	6.60	14.14	7.54	56.58	14.14	0.99
S65	6.09	13.05	6.96	59.95	13.05	0.91
S70	5.82	12.47	6.65	61.72	12.47	0.87
S80	5.35	11.46	6.11	64.82	11.46	0.80
S90	4.95	10.60	5.65	67.46	10.60	0.74
S110	4.30	9.22	4.92	71.70	9.22	0.65

The glasses, were based on the composition of F15Z1. The  $\text{SiO}_2$  content was varied and the ratios were re-normalised to 100:

$$\frac{100}{43.42 + z} (z\text{SiO}_2 - 7.54\text{Na}_2\text{O} - 6.60\text{K}_2\text{O} - 14.14\text{CaO} - 14.14\text{CaF}_2 - 0.99\text{ZrO}_2),$$

where  $55 \leq z \leq 110$ .

The glass compositions used in this study are given in table 7.1, where S57 is the same composition as F15Z1 from chapter 6.

### 7.2.2 Glass Melting

The glass was melted to produce a plate, approximately 15cm by 7cm and 8mm thick as described in Chapter 3. To produce clear glasses, the annealing schedule needed to be varied according to the silica content in the composition (table 7.2), as with the increase in silica content it was found that  $\text{CaF}_2$  nucleation occurred during annealing at temperatures of 500°C.

Table 7.2 Annealing schedules used

Glass	Temperature (°C)	Hold duration (min)	Cooling Rate (°C/min)
S55	500	60	1
S57	500	60	1
S65	500	120	1
S70	490	120	1
S80	480	180	1
S90	460	240	1
S110	460	240	1

### 7.2.3 Differential Thermal Analysis

Differential thermal analysis was used to determine crystallisation temperatures. Sample preparation and DTA measurements were carried as described in section 3.2.1

### 7.2.4 Heat Treatment

All series of glasses were subjected to single stage heat treatments at 5°C/min up to temperatures varying in 20°C between 600°C and 740°C, for phase analysis. These samples

were held for two hours at the temperatures and air quenched to retain the phases present at those temperatures. Both XRD and DTA results were used to determine the nucleation and crystallisation temperatures and two stage heat treatments were designed for fracture toughness tests. Table 7.3 shows the two stage heat treatment schedules that the glasses were subjected to.

Table 7.3 Two-stage heat treatment schedules used.

<b>Glass</b>	<b>Heating rate</b>	<b>Nucleation temp.</b>	<b>Hold duration</b>	<b>Heating rate</b>	<b>Crystallisation temp.</b>	<b>Hold duration</b>
<b>S55</b>	5	550	120	5	720	120
<b>S57</b>	5	550	120	5	730	120
<b>S65</b>	5	550	120	5	750	120
<b>S70</b>	5	550	120	5	780	120
<b>S80</b>	5	550	120	5	800	120
<b>S90</b>	5	550	120	5	820	120
<b>S110</b>	5	550	120	5	830	120

### 7.2.5 Phase and Microstructural Analysis

X-Ray diffraction was carried out using both the Phillips and the Siemens diffractometers. Fracture surfaces and etched surfaces were examined under the Jeol and the Camscam electron microscopes as detailed in section 3.2.3.

### 7.2.6 Mechanical Testing

Fracture toughness was measured using Vickers indentation as described in section 3.3.3. The radial cracks were optically examined and measured and the fracture toughness ( $K_{Ic}$ ) Vickers hardness ( $H_V$ ) and brittleness (B) were calculated using equations 3.1, 3.2 and 3.3.

## 7.3 Results

### 7.3.1 Crystalline phase analysis

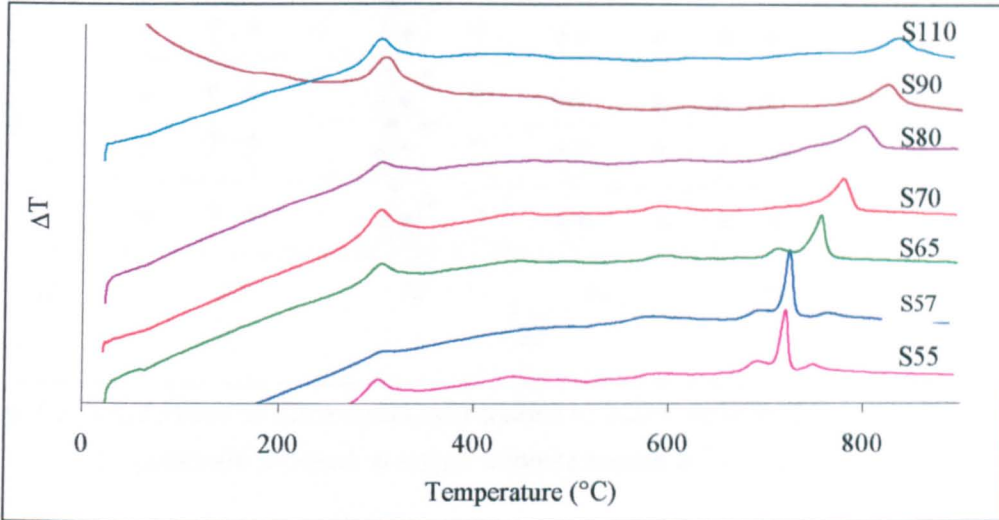


Figure 7.1: DTA traces of Silica series glasses

DTA results indicated an increase in crystallisation onset temperature as the silica content increased.  $\text{SiO}_2$  is of course a major network former in these glasses, hence with the increase in  $\text{SiO}_2$ , the stability of the glass increases. However the peak associated with the crystallisation of  $\text{CaF}_2$  was constant at a temperature of  $600^\circ\text{C}$ , although not clearly seen in Figure 7.1. DTA records a major crystallisation event in the higher silica glasses, but S55, S57 and S65 DTA traces show minor peaks either side of the major phase. XRD did not demonstrate distinguishable differences between crystalline phases at temperatures of  $680^\circ\text{C}$ ,  $700^\circ\text{C}$  and  $720^\circ\text{C}$ . As previously mentioned (see section 6.3.1(ii) and (iii)), these were attributed to either one of the similar phases of frankamenite or f-canasite. The major peak was attributed to canasite for all glass ceramics as the dominant phase discernable from XRD is canasite (see Figures 7.2, 7.3 and 7.4 below). The canasite associated peak becomes broader and flatter as the silica content is increased.

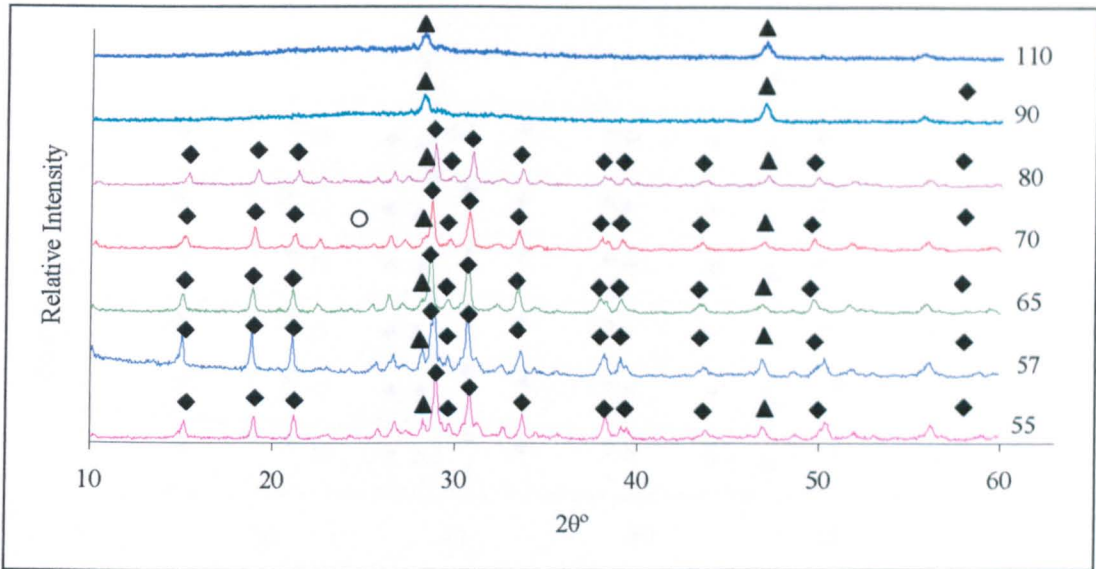


Figure 7.2: XRD traces of silica series heat treated to 720°C held for 2hrs and air quenched. The peaks are indexed ◆ canasite/frankamenite, ▲ fluorite, ○ wadeite

CaF<sub>2</sub> crystallisation occurred in all glass compositions at temperatures ranging between 600°C for S55 and 620°C for S110. Canasite and/or frankamenite crystallisation was evidenced at temperatures ranging between 660°C for S55 and 800°C for S110 (Figures 7.2, 7.3 and 7.4).

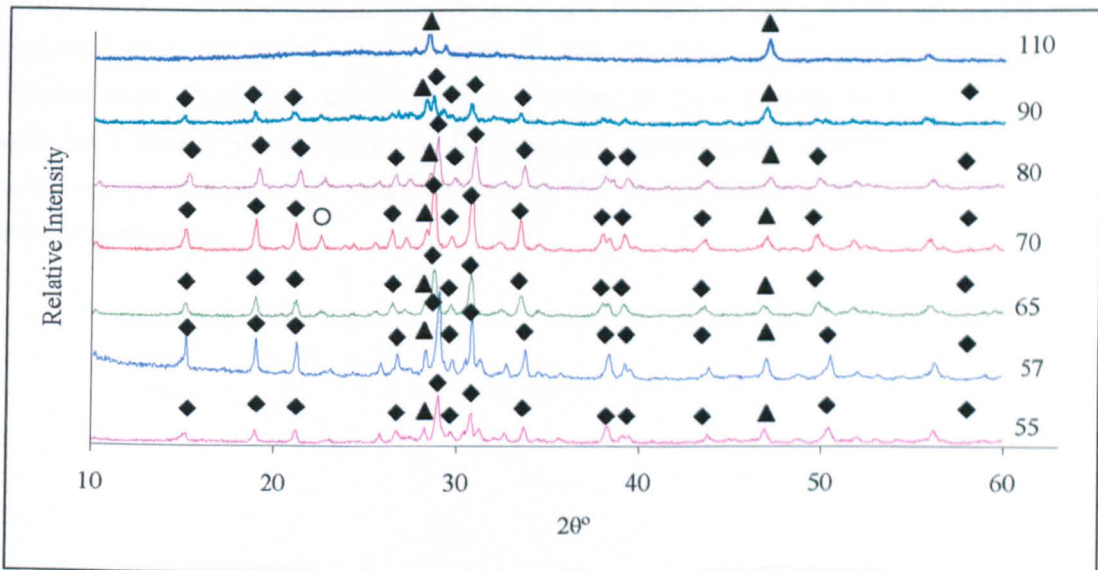


Figure 7.3: XRD traces of silica series heat treated to 760°C held for 2hrs and air quenched. The peaks are indexed ◆ canasite/frankamenite, ▲ fluorite, ○ wadeite

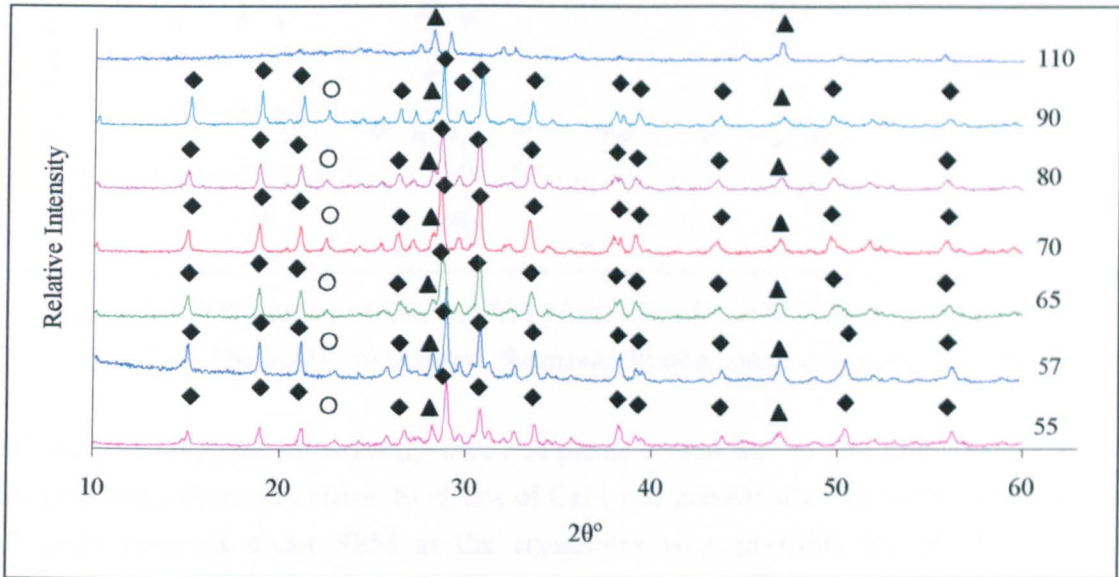


Figure 7.4: XRD traces of silica series heat treated to 800°C held for 2hrs and air quenched. The peaks are indexed ◆ canasite/frankamenite, ▲ fluorite, ○ wadeite

Figure 7.5 shows the crystallisation of canasite in S90 and S110. The  $\text{CaF}_2$ , canasite and frankamenite peaks are indexed according to cards (ICDD 04-0864), (ICDD 13-0553) and (ICDD 45-1398). There was a single peak in all traces which could not be indexed by these cards and it corresponded to  $23^\circ 2\theta$  peak of wadeite (ICDD 43-0231). Beall (1983) suggested that the predominant phases in the fluorcanasite compositions tested were canasite and/or aggrellite and/or fedorite. Further to these phases, xonotlite and miserite have been known to crystallise in fluorcanasite compositions (Miller, 2004). However, there was no evidence of these phases in the compositions studied in either this or preceding chapters.

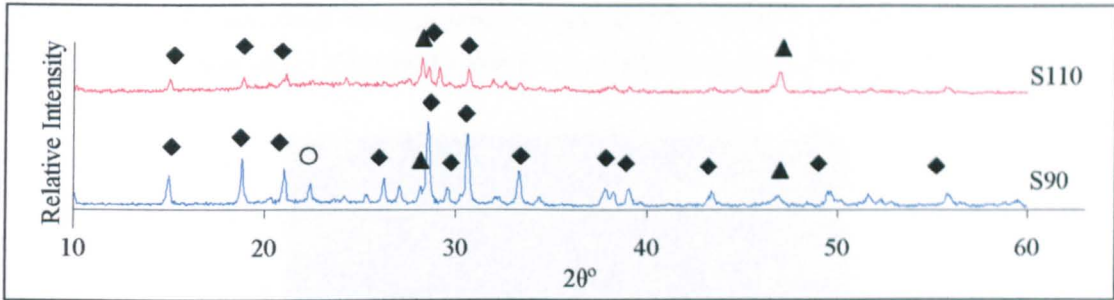


Figure 7.5: XRD traces of S90 and S110 heat treated to 840°C held for 2hrs and air quenched. The peaks are indexed ◆ canasite/frankamenite, ▲ fluorite, ○ wadeite

All samples subjected to two stage heat treatments crystallised to give glass-ceramics with canasite as the dominant phase. Evidence of  $\text{CaF}_2$  was present after the nucleation phase for all glass ceramics under SEM as the crystallites were probably too small for XRD. Subsequent crystallisation holds produced a very fine microstructure (Figures 7.6, 7.7, 7.8, 7.9 and 7.10)

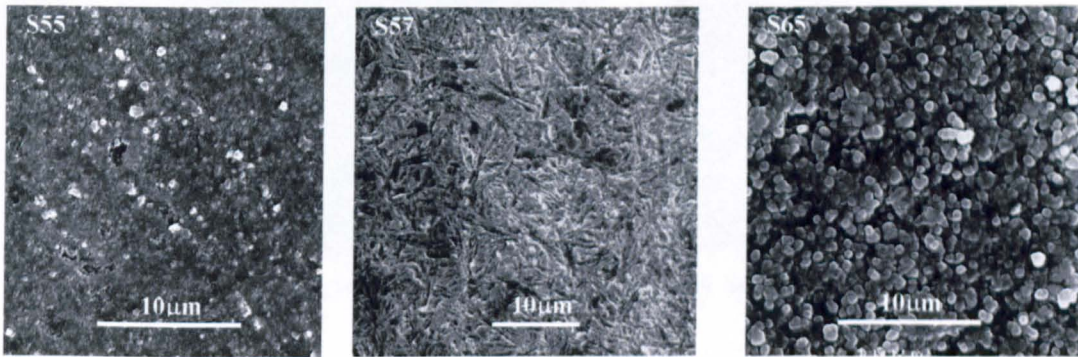


Figure 7.6: Scanning electron micrographs of samples subjected to two stage heat treatments, etched at 5% HF for 25s.

Microstructures of S55-S80 were similar in terms of crystalline size ( $\sim 2 \mu\text{m}$ ) and crystal morphology (globular crystals). The stoichiometric silica content in canasite is 60mol%. The glass compositions of S70, S80, S90 and S110 are in excess of this amount. The reasoning behind choosing to increase silica content in the glass ceramics was that the increased silica in the residual glass would improve the chemical durability. The microstructures of S90 and S110 indicate an influence of increasing silica content on the resulting microstructure. S90 produced a 'platier' structure with longer laths ( $\sim 15 \mu\text{m}$ ). For S110 the bulk of the glass ceramic crystallised to give crystallites of the order of  $2 \mu\text{m}$ .

Interestingly, the scanning electron microscopy revealed spherular regions of the order of  $150\mu\text{m}$  which showed no elemental variation in EDS, to the remainder of the glass ceramic.

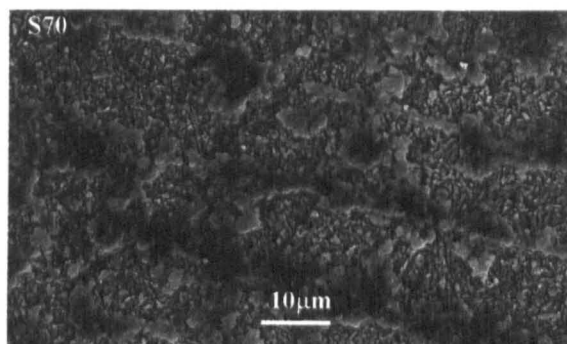


Figure 7.7: S70 subjected to two stage heat treatment, etched at 5% HF for 25s.

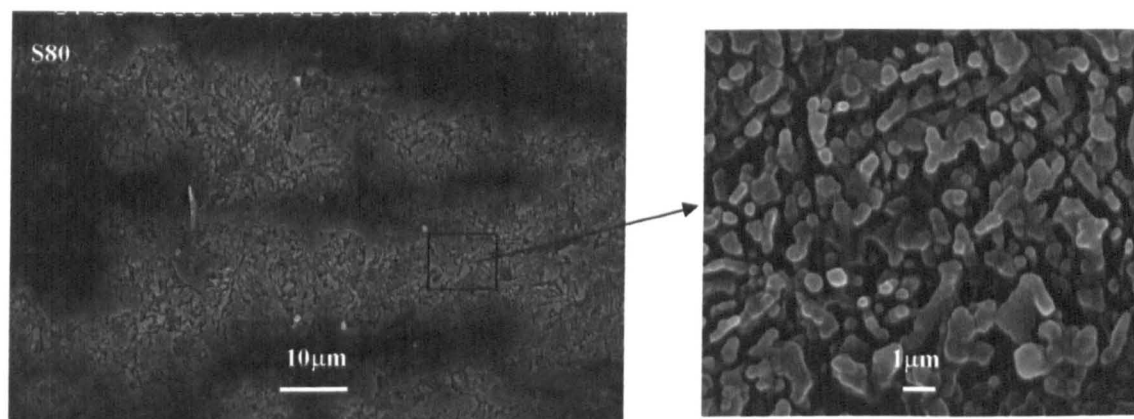


Figure 7.8: S80 subjected to two stage heat treatment, etched at 5% HF for 25s.

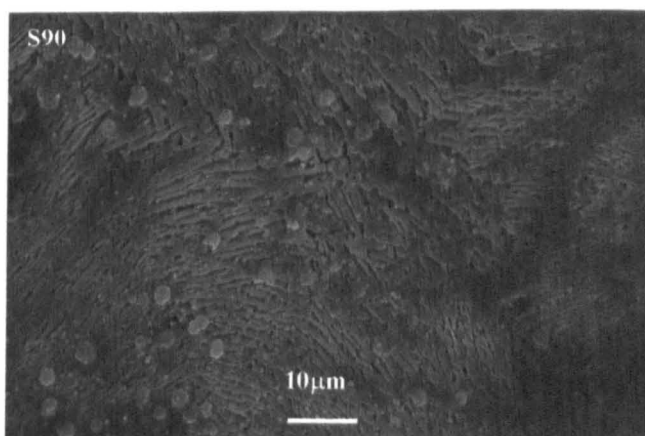


Figure 7.9: S90 subjected to two stage heat treatment, etched at 5% HF for 25s.

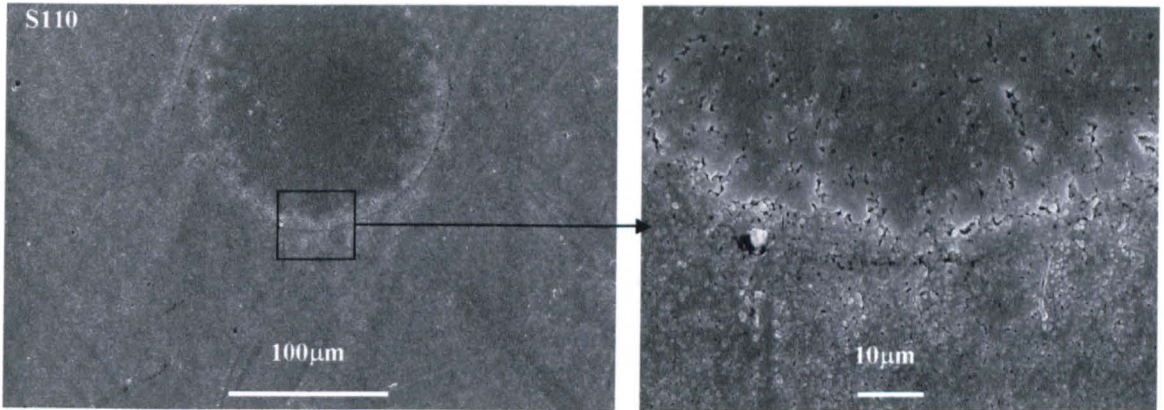


Figure 7.10: S110 subjected to two stage heat treatment, etched at 5% HF for 25s.

### 7.3.2 Fracture toughness

$K_{Ic}$  values of the glass-ceramics and their associated standard deviations are shown in figure 7.11. All values are statistically significant. Figure 7.12 is a plot of the brittleness calculated using the Vicker's hardness values.

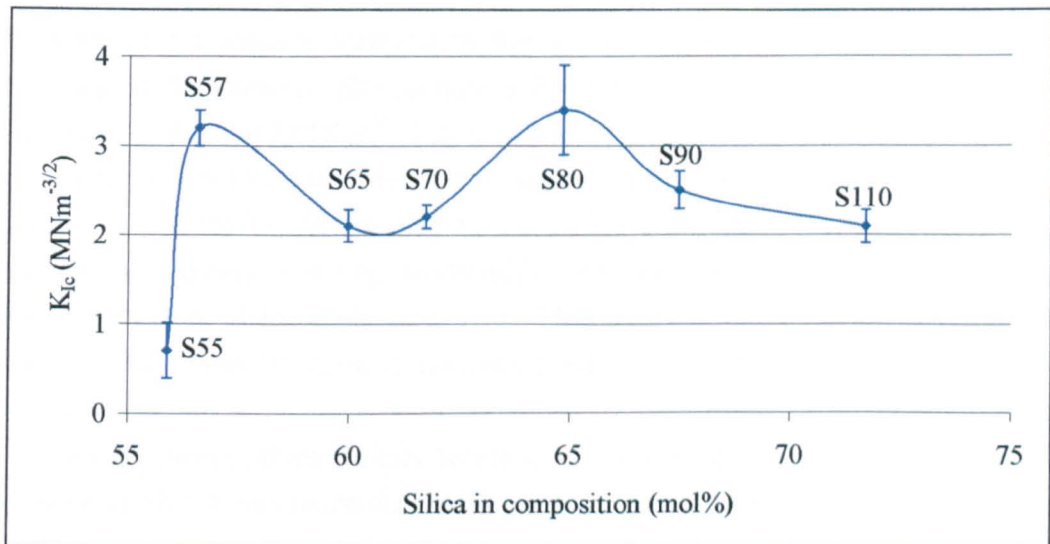


Figure 7.11:  $K_{Ic}$  as a function of silica content

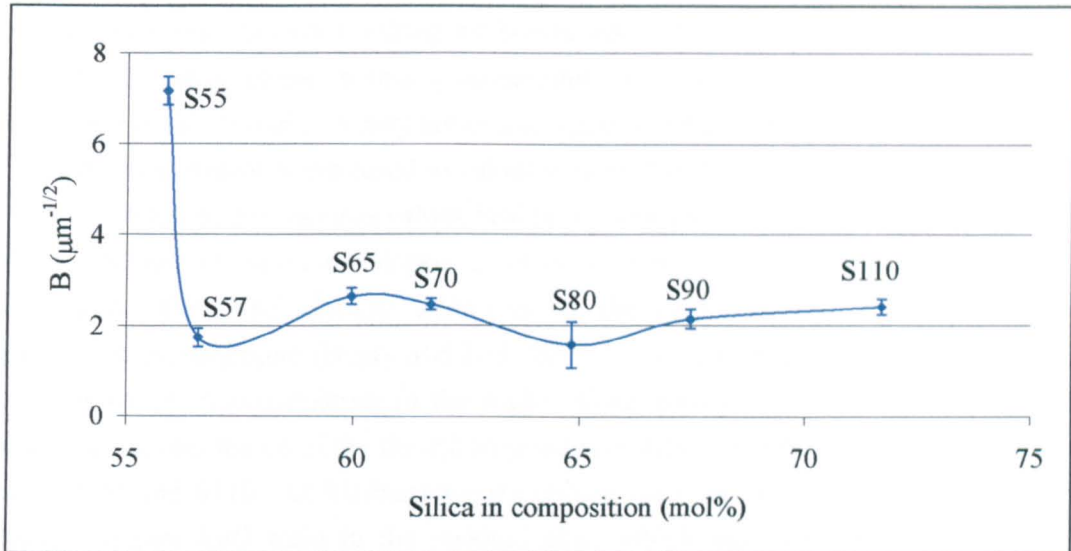


Figure 7.12: B as a function of silica where the dotted line at  $B = 4.3 \mu\text{m}^{-1/2}$  is the maximum value for the material to be machinable according to Boccaccini (1997).

## 7.4 Discussion

A high fracture toughness formulation has been identified which crystallises to give canasite and/or frankamenite glass ceramics. S57 (previously F15Z1 in Chapter 6) resulted in  $K_{Ic}$  values of  $3.2 \pm 0.2 \text{ MNm}^{-3/2}$ . Increase in silica content by about 5 mol% resulted in a reduction of fracture toughness and then subsequent increases resulted in a maximum value for the  $K_{Ic}$  at ~ 65 mol% silica inclusion (S80) of  $3.4 \pm 0.2 \text{ MNm}^{-3/2}$  (Figure 7.11) Results of this study indicate a strong relationship between the fracture toughness and the crystalline structure of these glass ceramics. Microscopy reveals that any move from the ‘house of cards’ type structure is associated with a decrease in the fracture toughness (Figure 7.6).

Fracture toughness values initially decrease with increased silica (S65 and S70) and then an increase at S80. It was found during Vicker’s toughness tests that for S70 and S80 glass ceramics there was no associated catastrophic failure until much greater loads (~ 600 - 700 N in comparison with a maximum of 200 N for previous formulations). The ability of the material to deform (in this case, to produce an indent), under higher loads is usually associated with plastic flow (viscous) flow due to shear. It has been reported that mechanisms that absorb indentation energy in an amorphous material are (a) plastic (viscous) flow due to shear, (b) densification resulting from compression and shear which

in some cases may invoke breaking of bonds, and (c) fracture (Kavouras et al, 2003). Although the major phase in this glass-ceramic is crystalline, if plastic deformation is taking place in this material, it may indicate a higher resistance to impact damage.

As the silica content is increased to values greater than 65 mol% (S90 and S110) there is decline in the fracture toughness values, which is accompanied with the formation of a high volume fraction of under-developed crystals. Similar results were found in a study investigating silica and alumina additions on the crystallinity of trisilicic mica and potassium fluorophlogopite (Henry and Hill, 2003). They attributed a move away from the 'house of cards' microstructure to the higher silica content in the residual glass phase preventing the coarsening of the fluorophlogopite crystals. Despite a decrease in crystalline sizes in S90 and S110, the hardness values remain constant. This may be explained by a relatively higher Si/O ratio in the residual glass which represents a more cross-linked vitreous network (a network with relatively greater Si-O-Si bonds or less non-bridging oxygens). Plastic flow and densification produced from shear stress during the indentation process is less likely to occur in a more cross-linked network, since plastic deformation requires the rupture of a larger number of atomic bonds (Kavouras et al 2003).

The composition of S80 (~65 mol% silica) results in a  $K_{Ic}$  value of  $3.4 \pm 0.2 \text{ MNm}^{-3/2}$ , which is similar to the highest values associated with commercial glass ceramics indicated for use as a restoration in the posterior region of the mouth ( $3.3 \pm 0.3 \text{ MPa.m}^{1/2}$  for Empress II). Further to this the indentation method is known to result in substantially lower fracture toughness results than other methods, in some cases greater than 3-fold (Beall, 1986) which would suggest that this material may be comparable to the high strength Y-TZP ceramics.

## 7.5 Conclusions

- All silica additions resulted in the crystallisation of canasite and frankamenite phases. The addition of silica resulted in significant variations of the microstructure, which affected the fracture toughness of these glass ceramics.
  
- The maximum fracture toughness obtained for S80 was  $3.4 \pm 0.2 \text{ MNm}^{-3/2}$ , which is comparable to commercial systems that are indicated for use as a posterior tooth restoration.

## Chapter 8: Development of fluorcanasite as a dental material

### 8.1 Introduction

The composition of  $60\text{SiO}_2\text{-}8\text{Na}_2\text{O-}7\text{K}_2\text{O-}15\text{CaO-}10\text{CaF}_2$  was shown to offer an increased chemical durability over the original formulations of fluorcanasite (Stokes 2003). This increase in durability came at the expense of fracture toughness. Thus through the course of these studies reformulations have been attempted in order to increase the fracture toughness of the material. Two compositions, S57 and S80 have been identified with fracture toughness values of  $> 3 \text{ MNm}^{-3/2}$ , and hence are comparable to commercial systems. It was therefore necessary to assess the chemical durability of the material to ensure that the reformulation had not adversely affected it. It was decided to conduct a chemical solubility test in accordance with ISO 6872:1995.

Although optimisation of the glass-ceramics in terms of heat treatment is yet to be carried out, it was also decided to assess the biaxial flexural strength of these high  $K_{Ic}$  glass ceramics. Further to this, the practical application of this material is as a dental restoration. Hence it is necessary at this stage to check if there is a viable process route by which this material can be converted into a restoration.

### 8.2 Chemical Solubility

The dental ceramics international standard provides a chemical durability recommendation (ISO 6872:1995 (E)). This test subjects the material to 16 hours in 4% acetic acid solution at  $80^\circ\text{C}$  stipulating that the losses should be  $<100\mu\text{g}/\text{cm}^2$  for a dental veneer or dentine replacement ceramic and  $<2000\mu\text{g}/\text{cm}^2$  for a core ceramic. It was necessary, therefore, to test the solubility of the new fluorcanasite formulations according to the ISO recommendations so that it could be quantitatively compared to existing dental ceramics.

#### 8.2.1 Experimental Method

For chemical solubility analysis, the method used was as described in the ISO 6872:1995

(E) Dental Ceramic Standard. 10 discs 12mm diameter and 1.6mm thick of S57, S80 and B8 were produced by core-drilling from annealed glass plates (melted as described in Chapter 3). These were cerammed using the cycles as described in Table 8.1, where the heating rate used was 5°C/min and the samples were furnace cooled. A separate run of S57 glass discs was carried out to compare the difference between the glassy phase and the cerammed phase.

Table 8.1: Heat treatment schedules glass ceramics were subjected to.

	Nucleation		Crystallisation 1		Crystallisation 2	
	Temp. (°C)	Time (min)	Temp. (°C)	Time (min)	Temp. (°C)	Time (min)
S57	550	120	720	120	-	-
S80	550	120	800	120	-	-
B8	700	120	800	240	900	240

The specimens were ground to the required geometry using diamond and SiC abrasives to a P1200 grade finish and then washed in distilled water. They were subsequently placed into a clean, dry glass beaker and dried at 160 ±5°C for 4 hours. The discs were weighed to the nearest 0.01mg on a balance (Mettler AJ100), with all handling of the specimens by nylon tweezers to avoid introducing any contamination or moisture.



Figure 8.1: S57 glass discs within the extraction apparatus.

The samples were placed into the extraction apparatus and were extracted with 4% acetic acid (HAc) solution by refluxing for 16 hours with a reflux rate of approximately 3 cycles per hour (Figure 8.1). The temperature within the vessel was not allowed to exceed 80°C. Following the extraction procedure, the specimens were washed in distilled water and dried at  $160 \pm 5^\circ\text{C}$  for 4 hours as before and re-weighed to 0.01mg and the results recorded. Chemical solubility was calculated using:  $\text{chemical solubility } (\mu\text{g}/\text{cm}^2) = \text{weight loss } (\mu\text{g}) / \text{surface area } (\text{cm}^2)$

SEM (SEM, CamScan) was used to analyse the discs after the solubility test. The discs were mounted onto stubs and gold coated (Evaporation unit, Edwards, UK) prior to examination.

### 8.2.2 Results

The results of the solubility test are given in Figures 8.2 to 8.5. There was a high standard deviation associated with the results. Although each disc was assessed individually, it was not possible to keep track of which was which once inside the apparatus. This, along with inadequate wetting could be a major factor of the errors.

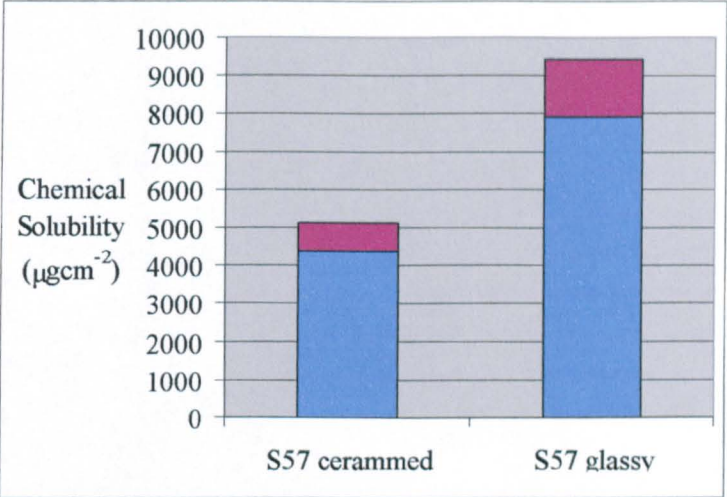


Figure 8.2: Chemical solubility of S57 glass and cerammed samples. The red bar indicates standard deviation.

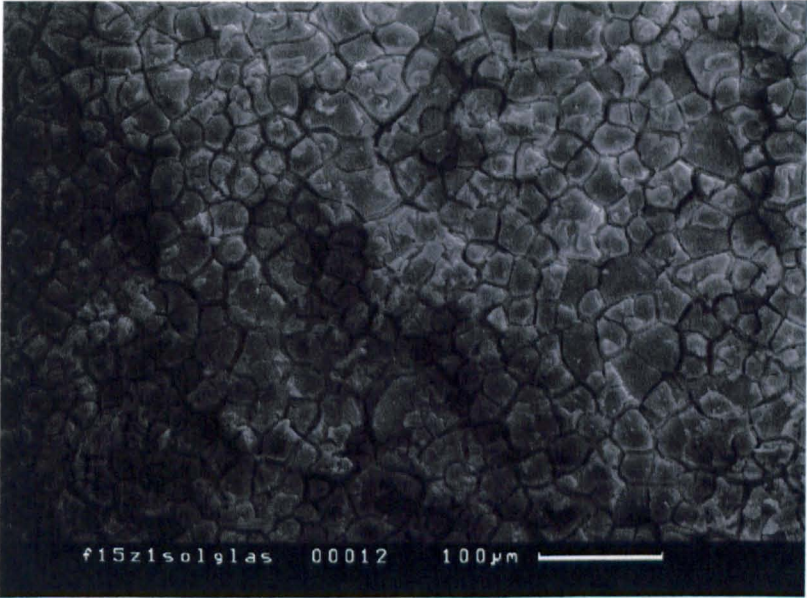


Figure 8.3: Scanning electron micrograph of the surface of the S57 glass disc after 16 hours in 4 % acetic acid at ~ 80°C showing crazing on the surface.

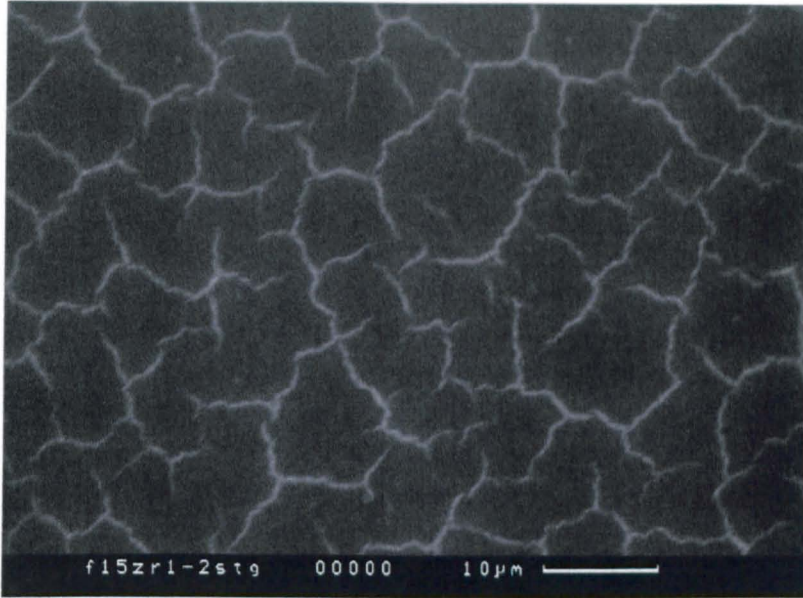


Figure 8.4: Scanning electron micrograph of the surface of the S57 cerraammed disc after 16 hours in 4% acetic acid at  $\sim 80^{\circ}\text{C}$  showing a crazing on the surface.

Crazing patterns were visible to the naked eye for the glass specimens and were evident on the surface of glass ceramic under scanning electron microscopy after solubility testing.

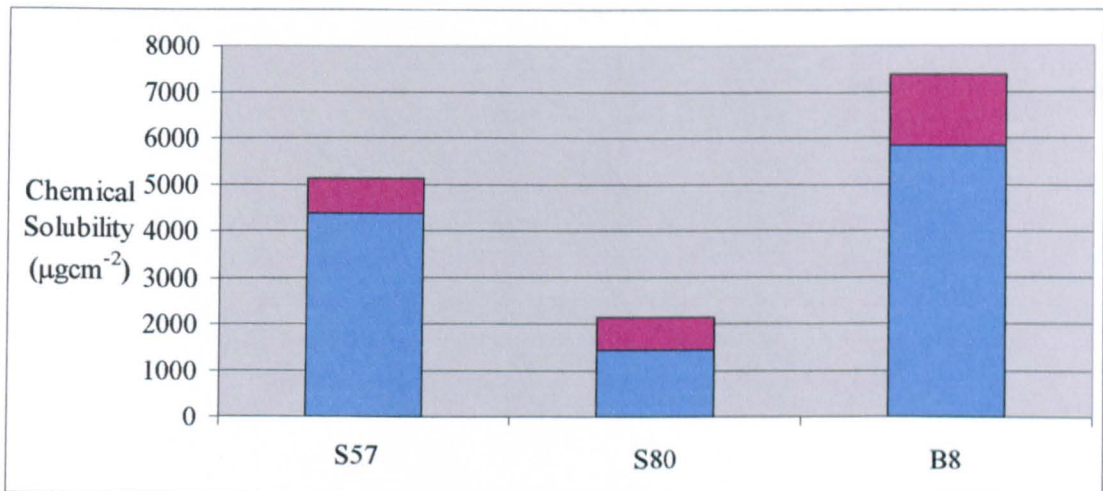


Figure 8.5: Chemical solubility of S57, S80 and B8 cerraammed samples. The red bar indicates standard deviation.

## 8.3 Mechanical Properties

### 8.3.1 Experimental method

Fracture toughness was measured using Vickers indentation as described in section 3.3.3. The radial cracks were optically examined and measured.

Biaxial flexural strength was conducted using a Lloyds LRX tensometer with a 2500N load cell. Ten discs of 12mm diameter and 2mm thickness of S57, S80 and B8 were core-drilled and subsequently cerammed with a two stage heat treatment as specified in Table 8.1. The discs were polished to a 1 $\mu$ m finish using SiC and diamond pastes. Paper shins were placed between the under-side of the disc (compression surface) and the ring to ensure fracture was not initiated due to the sharp edges of the ring. The discs were then fractured using the ball on ring arrangement (Figure 8.6). After fracture the discs were accurately measured to allow computation of the biaxial flexural strength using the formula:

$$\sigma_{\max} = P / h^2 \{0.606 \log_e(a / h) + 1.13\}$$

where  $P$  is the load in Newtons,  $a$  is the radius of the support ring in mm, and  $h$  is the sample thickness in mm. This value represents the maximum stress seen by any portion of the sample. In all cases fracture was observed to have originated at the centre of the disc (Figure 8.7).



Figure 8.6: Ball on ring arrangement in a Lloyds LRX tensometer used for biaxial flexural strength test.

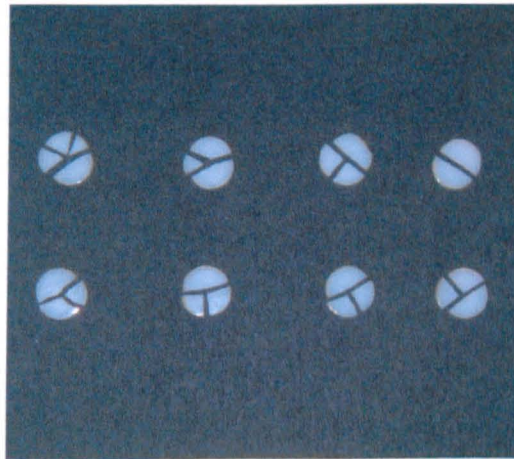


Figure 8.7: Eight S80 glass-ceramic samples exhibiting a failure originating from the centre.

### 8.3.2 Results of Mechanical Testing

The results of the mechanical tests are summarized in Table 8.2.

Table 8.2: Summary of the mechanical testing results.

	$K_{Ic}$ (MNm <sup>-3/2</sup> )	$V_H$ (Nm <sup>-2</sup> )	B (μm <sup>-1/2</sup> )	BFS (MPa)
S57	3.2 ± 0.2	5.6 ± 0.1	1.8 ± 0.2	468 ± 80
S80	3.4 ± 0.2	5.4 ± 0.3	1.6 ± 0.3	374 ± 50
B8	2.0 ± 0.2	3.3 ± 0.1	1.7 ± 1.2	139 ± 32

## 8.4 Dental Restoration Production

Historically, the primary method for forming dental ceramics has been sintering, but this method is time consuming and consequently costly, not to mention difficult due to the large shrinkages on firing. Recent developments have resulted in the hot-pressing of ingots of ceramic materials that allows the lost-wax technique to be used; lost-wax casting being a well established technique for dental alloy casting. Furthermore, the advent of CAD-CAM in dentistry has seen a selection of prefabricated blocks being available that allow milling of digitally designed restorations in a matter of minutes.

### 8.4.1 Experimental procedure

CAD-CAM was carried out on S57, S80 and a VITA Mark II (Vita Zahnfabrik, Bad Sackingen, Germany), a fine-particle feldspathic porcelain with 80 vol% glass matrix as a control. To produce a fluorcanasite restoration using CAD-CAM, blocks were made that were compatible with the milling hardware. The block size required was 15mm x 10mm x 12mm. To produce this, the remainder of the glass plate (after core drilling) was crushed and was re-melted in a platinum crucible for a total of 10 minutes (the time was kept to a minimum so as to minimise any losses due to volatilisation). The molten glass was then poured into a heated steel mould (Figure 8.8).



Figure 8.8: Re-melting of the glass pieces and the mould it was cast in.

This was annealed for 1 hour at 500°C and cooled at 1°C per minute. A block of 15mm x 10mm x 12mm was cut using a diamond coated wheel and these blocks were subjected to heat treatments used in Table 8.1. The completed block is shown in Figure 8.9 with a VITA block for comparison.



Figure 8.9: (a) VITA Mark II blocks. (b) The completed fluorcanasite block prior to milling.

The CAD-CAM unit used was the CEREC-Scan (Sirona, Germany) and is shown in Figure 8.10. A laser scanner scans a model of the preparation. From this impression the CEREC software (version 3.01) was used to generate a milling pattern for a crown using the 'dental database' mode (which uses a collection of information of tooth shapes to develop the biting surface of the crown automatically). A copy of the model used for the cast restoration was trimmed and mounted on a scanning platform. This model was then coated in a titanium dioxide based surface agent to make the surface opaque (CEREC Powder).

The model was then scanned using the CEREC-Scan unit to make a digital impression.



Figure 8.10: The CEREC-Scan hardware with an S80 block inserted.

The blocks were cut to the specific size required on an automatic grinding machine using a carborundum disc and the corners bevelled to match the original VITA Mark II block with SiC paper. A template to mount the aluminium stub that retains the block in the machine was made from hard polyvinylsiloxane (Aquasil Soft Putty, Dentsply, UK). The aluminium mounting stub was then located onto the block using the template and fixed using a two-part epoxy resin adhesive (Araldite Clear) (Figure 8.9b).

#### 8.4.2 Results

S57 blocks produced for milling fractured during the milling process (despite three attempts). S80 block was accepted by the CEREC-Scan milling unit as a valid block and milling took a total of 10 minutes to complete. The milling process was carried out twice on the S80 to ascertain reproducibility. The milling process is shown in Figure 8.11.



Figure 8.11: The fluorcanasite block (S80) being milled.

The completed S80 crown, shown in Figure 8.12, showed good marginal integrity and it was not possible to identify any areas morphologically different to the VITA milled crown optically.

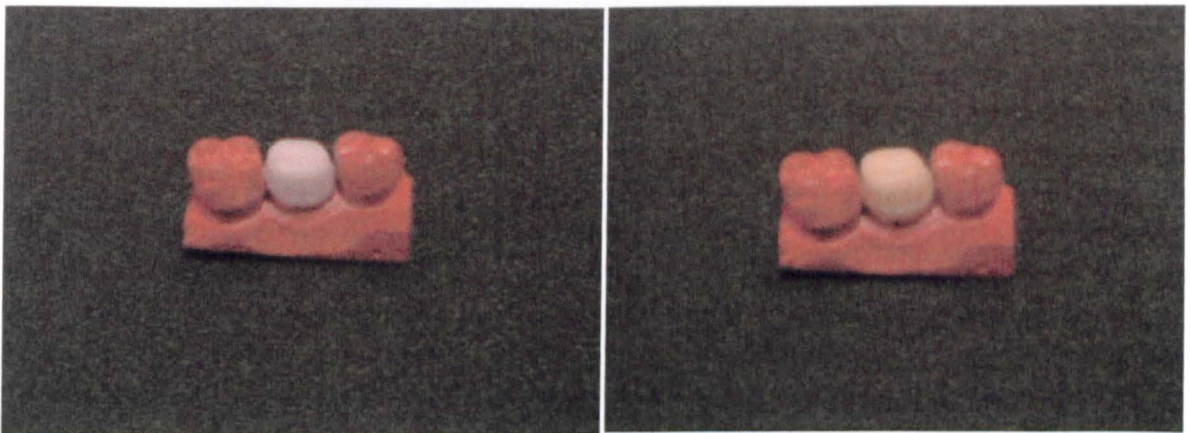


Figure 8.12: A direct comparison of the milled crowns on the mould, the S80 on the left and VITA Mark II crown on the right.

Scanning electron micrographs of the gold coated crowns comparing the occlusal and the interproximal surfaces of both S80 and the Vita block show that the depth of the defects in

the crown caused by machining did not differ from those of the porcelain (Figures 8.13 and 8.14).

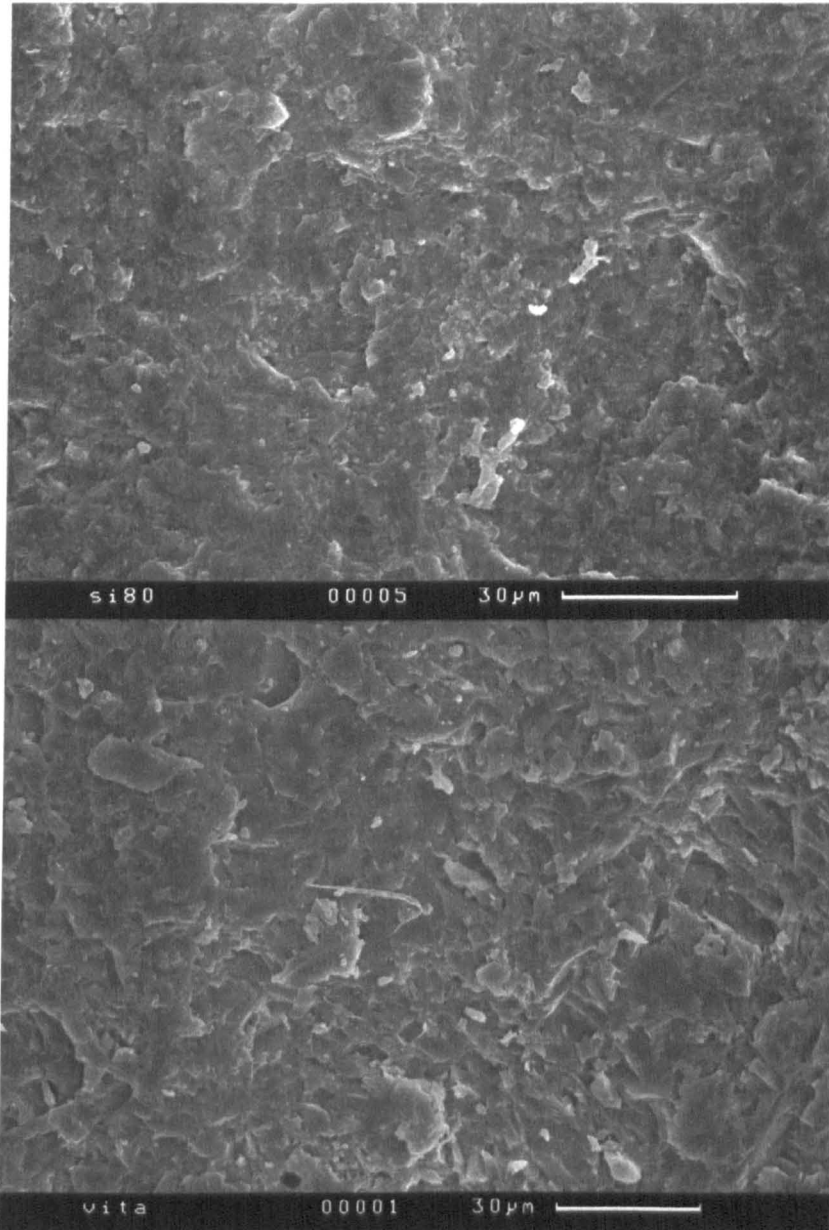


Figure 8.13: Scanning electron micrographs of the occlusal (top of crown) surfaces of the S80 (above) and VITA Mark II (below)

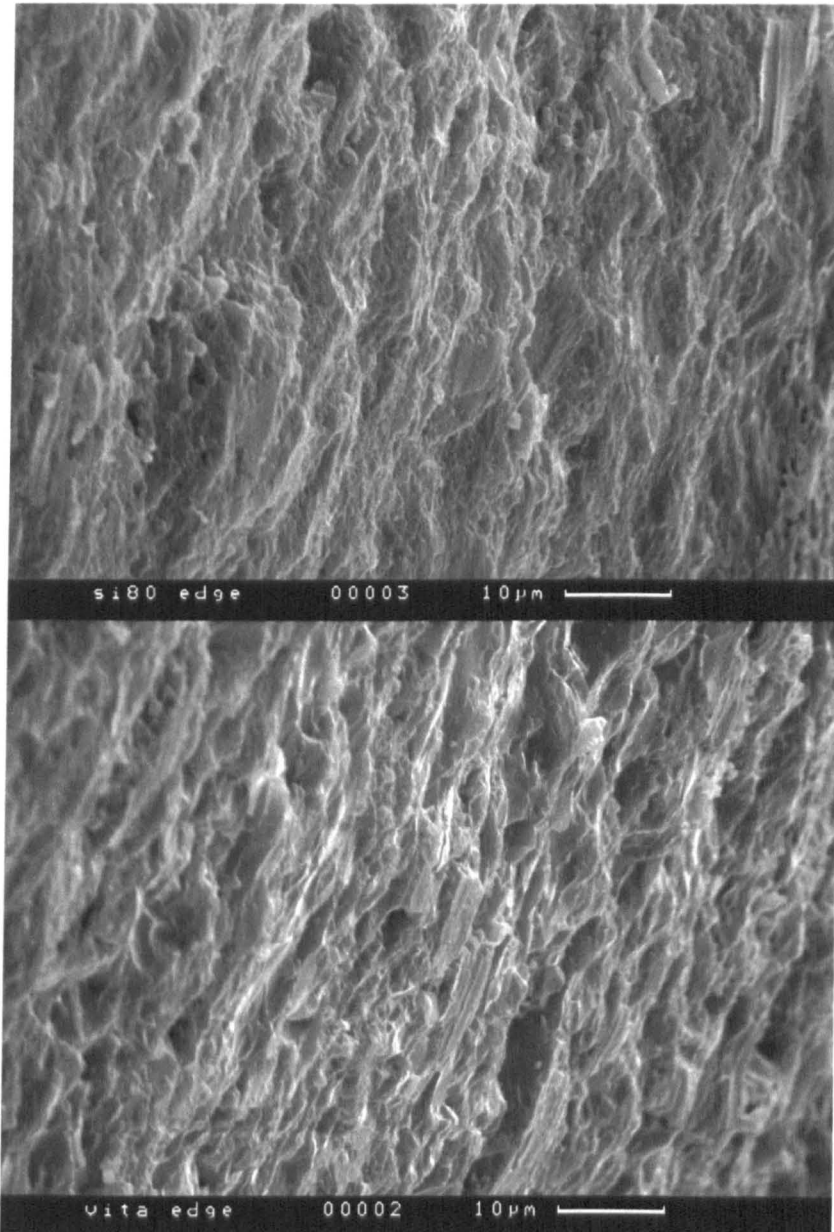


Figure 8.14: Scanning electron micrographs of the interproximal (sides of crown) surfaces of the S80 (above) and VITA Mark II (below)

However the defects associated with the feldspathic porcelain were larger laterally and indicated large chipping defects responsible for material removal (Figure 8.13). In contrast S80 showed small brittle fractures with crack propagation observed to occur by the continual redirection due to the random orientation of the canasite and/or franakamenite crystals (Figure 8.15).

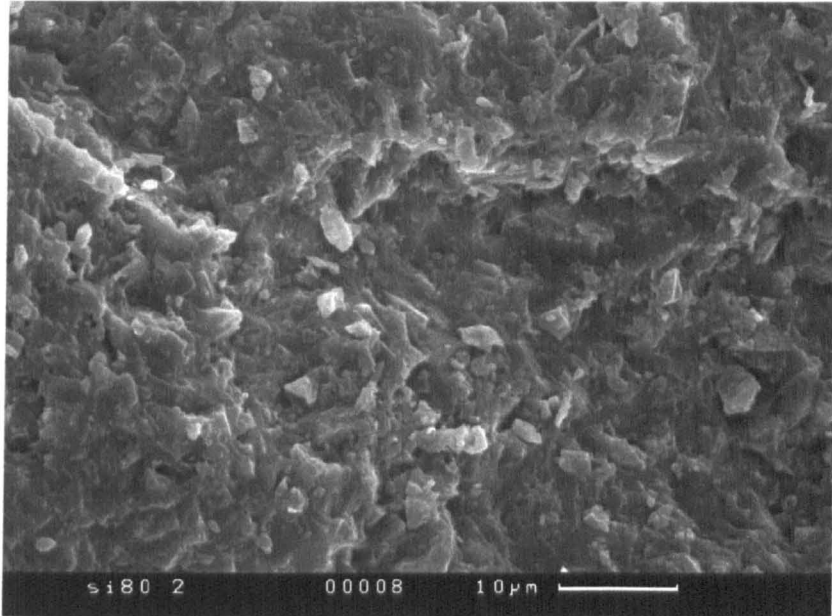


Figure 8.15: Scanning electron micrograph of the ridge on the occlusal surface of the S80, showing fine crystal morphology responsible for the machining crack propagation.

## 8.5 Discussion

This study has identified the S80 composition as having adequate mechanical and chemical properties to be used as a core material in a dental restoration. This formulation produces a glass ceramic which can repeatedly be milled using existing dental laboratory equipment.

The mechanical property tests showed that S57 and S80 formulations produced glass ceramics with  $K_{Ic}$  values of  $3.2 \pm 0.2 \text{ MNm}^{-3/2}$  and  $3.4 \pm 0.2 \text{ MNm}^{-3/2}$  and biaxial flexural strength values of  $468 \pm 80 \text{ MPa}$  and  $374 \pm 50 \text{ MPa}$  respectively which offer a significant improvement in comparison with the base formulation which had a  $K_{Ic}$  of  $0.60 \pm 0.17 \text{ MNm}^{-3/2}$ . The BFS of the base composition was not tested in this study but previous results at Sheffield gave a value of  $139 \pm 32 \text{ MPa}$  for this particular base composition (Stokes, 2003). The  $K_{Ic}$  increased with the increase in silica content, whereas the BFS values decreased. The strength of a brittle material is the stress that is required to ‘break’ that material. Fracture begins from a single location called the fracture origin, which is a discontinuity such as a flaw or a defect that has developed from mechanical, chemical or

thermal processes that will act as a localised stress concentrator. Under a specific critical applied stress, the crack will initiate from these defect-sites and propagate catastrophically, leaving characteristic markings on the fracture surfaces. Similar apparently contradictory results were recorded by Gorman and Hill (2003) in a study on alumino-silicate glass ceramic. The prevention of crack propagation was attributed to microcracking and the reduction of strength was found to be a result of an increase in flaw size. The results found in this study could be due to differing mechanisms, although further evaluation is necessary.

The biaxial flexural strength tests gave results with a high degree of scatter but the differences in values were statistically significant. Morrell *et al* (1999) have assessed some of the issues concerning biaxial flexural strength testing, and identified sources of potential error as the friction at the loading and support positions and the thickness effects. In addition, to this if erroneous results are recorded if the crack originates at the contact edge of the ring and the disc. The use of the paper shin however, ensured the rupture of the samples tested initiated centrally.

The solubility of S57 glass was 7900  $\mu\text{g}/\text{cm}^2$  and ceramic was 4400  $\mu\text{g}/\text{cm}^2$ , indicating the glassy phase may be responsible for the solubility of this glass-ceramic. Although it has to be borne in mind that the crystallisation would alter the glass composition to a certain extent. SEM examination of the surface of both the cerammed and glass specimens after solubility testing showed the presence of crazing on the surface. Sinton and LaCourse (2001) identified the first stage of the reactions of glass with water or other aqueous solution as being the exchange of alkali ions in the glass with hydrogen atoms from the water, i.e.:



The surface of the glass becomes depleted in alkali, and a silica-rich layer may form. This effect would be exaggerated in an acidic environment as was the case of the solubility test where 4% acetic acid was used. The process leads to a dealcalisation of the surface and under static conditions can lead to elevated pH values near the glass. Meanwhile, dissolution of the silica network is greatly encouraged in high pH environments.



Wolters and Verweij (1981) suggested that the water that is inherent within the glass is hydrogen bonded to non-bridging oxygens ( $\text{Si-O}^-$  and  $\text{Si-OH}$ ). When the two non-bridging oxygens are close to each other, they propose that a single water molecule can be bonded to both (like a divalent cation) creating an effective cross-link in the glass structure and blocking a potential channel for alkali diffusion. Such a cross-link could cause the silicate network to contract and thereby contribute to the tensile stresses created by the ion exchange at the surface. These combined tensile stresses are thought to cause the crazing of the surface layer. The presence of the crazing in the cerammed fluorcanasite material may be evidence of high levels of a residual glass, which on leaching forms a hydrosilicate layer. Bunker *et al* (1983) propose that two distinct hydrosilicate phases can form on the glass surface depending on the leaching conditions and glass composition. Under low (room) temperature leaching conditions that are relatively mild, the hydrated surface is brittle. Bunker *et al* (1983) state that this crazed surface is due to tensile stresses generated within this material and not as a result of drying of the surface layer as it is optically observed on the glass surface while the glass is in the leaching solution. However, this cannot be fully substantiated in this study as the surface was not observed in the solution, but under SEM, after the samples had dried.

Solubility of the S57 ceramic at  $4400 \mu\text{g}/\text{cm}^2$  is significantly higher than solubility results quoted for the base compositional glass-ceramic of  $650 \mu\text{g}/\text{cm}^2$  (Stokes, 2003). This can be attributed to the 5mol% increase in  $\text{CaF}_2$  content (to a total value to 15 mol%), which was added to the glass to optimise canasite crystallisation. Fluorine is known to disrupt the glass network, resulting in increased mobility of ionic species; thus aiding dissolution, by the above mentioned mechanisms. This explains the chemical solubility of B8 ( $5900 \mu\text{g}/\text{cm}^2$ ), which had an 18mol% inclusion of fluorite in its composition.

When the silica content was increased (in S80) the chemical solubility of the new formulation decreased by 33%. Bubb *et al* (2004) found that systematic additions of  $\text{SiO}_2$  and  $\text{AlPO}_4$  to a fluorcanasite composition resulted in a reduction of the solubility from 2400 to  $600 \mu\text{g}/\text{cm}^2$  and an increase in associated strength values, consequently larger additions resulted in a reduction in strength. This is in good agreement with the results of this study as, it was noted in Chapter 7 additions of greater than 65 mol% silica resulted in a decrease in the mechanical properties of canasite/ frankamenite glass ceramic. Anusavice and Zhang tested the effect of adding alumina to the frit before casting and results of  $2170 \mu\text{g}/\text{cm}^2$  (2% alumina) and  $790 \mu\text{g}/\text{cm}^2$  (5% alumina) after 16 hours in 4% acetic acid were reported (although the addition of up to 10% alumina significantly reduced the

chemical durability of the material due to phase separation during heat treatment of the glass). Aluminium ions are thought to act similarly in the glass structure as silicon ions, and  $\text{AlO}_4$  groups can replace  $\text{SiO}_4$  tetrahedra in silicate lattices (with the addition of a unit positive charge to ensure electroneutrality). Stability and chemical durability of S80 is due to the increasing connectivity of these silica tetrahedral units. The chemical solubility of the S80 is within the maximum value of  $2000\mu\text{g}/\text{cm}^2$  as stated by the ISO standard for a core ceramic and it would seem that the fluorcanasite glass-ceramic could be used as a high strength core material.

Stokes (2003) varied the alkali content and found a minimum solubility of  $650\mu\text{g}/\text{cm}^2$  with variability between the discs of  $\pm 198\mu\text{g}/\text{cm}^2$  (using the ISO 6872 test) for canasite glass-ceramic. This was achieved with a glass composition of  $60\text{SiO}_2\text{-}8\text{Na}_2\text{O-}7\text{K}_2\text{O-}15\text{CaO-}10\text{CaF}_2$ . Although there was a decrease of 73% over the original formulation (Stokes 2003), it was still not acceptable as a dentine replacement material. A factor of concern is the high standard deviation associated with the ISO 6872 standard chemical solubility test for dental ceramics. Future work may involve solubility testing by the revised bead test proposed by Stokes (2003), which offered reduced variability in the results.

Results from the CAD-CAM trial showed that this is a viable processing route for the canasite and/or frankamenite glass ceramics. Indentation fracture toughness testing indicated that the impact resistance of S80 was much greater than S57 (see Section 7.5, Chapter 7). This ability to deform rather than fracture catastrophically at higher loads is associated with lower hardness values (ref). Hardness value of S80 at  $5.40 \pm 0.31\text{ Nm}^{-2}$  was slightly lower than that of S57 at  $5.57 \pm 0.20\text{ Nm}^{-2}$ , resulting in a slightly lower brittleness index for S80 (Table 8.2). Boccaccini (1997) suggested that brittleness index should be lower than  $4.3\mu\text{m}^{-1/2}$  for a glass ceramic to be easily machinable. The brittleness indices of both S57 and S80 were substantially lower than this value. Verification of this proposed relationship was based on quantitative data gathered from literature specifically on fluorophlogopite mica glass-ceramics of differing compositions. The results of this study indicate that this relationship is not valid for the canasite/ frankamenite glass-ceramic system.

Surface analysis of the CAD-CAM crowns revealed that the depth of the defects in S80 did not differ significantly from the VITA feldspathic porcelain. However the surface morphology of the two crowns indicated differing mechanisms of material removal during machining. Previous studies have attributed material removal in Vita feldspathic porcelains to microcracking and microchipping (Kelly *et al*, 1992 and Sindel *et al*, 1998). Sindel *et al*.

found similar results in a study comparing the machined surfaces of Vita Mark II and Dicor MGC, a tetrasilic fluormica glass ceramic. When observing scanning electron micrographs of machined Vita blocks they found, as in this study, that the removal of material mainly occurred in chipping areas parallel to the surface; compared to the lateral size, the depth of the defects is minor. Interestingly the surface damage due to machining of the Dicor MGC, a glass ceramic with mica crystals of the order  $10\ \mu\text{m}$  was found to be very similar to that of canasite/frankamenite glass ceramics. Sindel *et al.* (1998) attributed this to a combination of both plastically deformed areas and small brittle fractures. Further analysis of machined surfaces of the S80 needs to be carried out to definitively assess if plastic deformation has taken place, but the indents caused during fracture toughness tests are indicative of the material's ability to plastically deform. Henry and Hill (2003) suggest that the machinability of mica materials is a direct result of the of the layered mica crystal structure, where crack propagation takes place preferentially along the cleavage plane of the mica crystal. It is hypothesised that the machinability of canasite and/or frankamenite glass ceramics results from a similarly randomly oriented crystal structure.

## 8.6 Conclusions

- S80 with a  $K_{Ic}$  of  $3.4 \pm 0.2\ \text{MNm}^{-3/2}$  and a BFS of  $374 \pm 50\ \text{MPa}$ , was found to offer improved mechanical properties in comparison with most current commercial systems and equals the mechanical properties of dental restorative materials indicated for posterior use ( $3.3 \pm 0.3\ \text{MPa.m}^{1/2}$  for Empress II, reported by Höland *et al.*, 2000).
- If this material is to be used as a dental restoration with surfaces exposed to the aqueous environment in the mouth, it requires a further development to reduce its solubility, though results indicate the material is within the solubility limits for use as a core material (class 2, ISO 6872:1995 (E)).
- Machining of S80 blocks were successfully carried out on the CEREC-Scan (Sirona, Germany) and showed good correlation with the machining of the commercial VITA Mark II blocks. Thus CAD-CAM offers a viable route for the processing of fluorcanasite into dental restorations.

## Chapter 9: Conclusions

- The base glass composition for the study was the formulation developed to crystallize to a low solubility glass-ceramic of  $8\text{Na}_2\text{O}-7\text{K}_2\text{O}-15\text{CaO}-10\text{CaF}_2-60\text{SiO}_2$ . All compositions studied here were produced by varying one or more components in this formulation. The glass manufacturing procedure for all the glasses in this study was found to ensure a homogeneous glass, with the incorporation of a fritting and re-melting stage into the schedule.
- The glass compositions used have been shown to nucleate both canasite and/or frankamenite phases. Evidence of heterogeneous nucleation with  $\text{CaF}_2$  as a precursor has been found. Further studies are required to evaluate the nucleation mechanism of frankamenite, although it has been established that it is distinct from that of canasite.
- It has not been possible to crystallize a mono-phase canasite or frankamenite glass ceramic, neither has it been possible to quantify the crystallization of these phases in this study. It has been recognized that detailed crystallographic studies are indicated in this respect and as such this was out of the remit of this study.
- It was found that higher  $K_{Ic}$  values were associated with a higher canasite phase dominance. Thus the extent to which differentiation from X-ray diffraction data of the two phases (however limited) was achieved, enabled development of a tougher glass-ceramic material with a bi-phase crystal structure of canasite and frankamenite.
- $\text{ZrO}_2$  additions have been investigated for compositions with differing fluorite contents. It was found that  $\text{ZrO}_2$  inclusions up to 2mol% resulted in a shift from frankamenite to canasite as the dominant phase, for all fluorite content glass-ceramics. A maximum fracture toughness of  $3.2 \pm 0.2 \text{ MNm}^{-3/2}$  achieved for F15Z1 (Chapter 6) is comparable to commercial systems.
- $\text{ZrO}_2$  contents of  $\geq 4 \text{ mol}\%$  resulted in the crystallization of wadeite and an unknown phase. Although values of  $K_{Ic} > 2 \text{ MNm}^{-3/2}$  were found for glass ceramics with the crystalline phases of canasite, frankamenite and wadeite; this was attributed to the

canasite phase or restriction of crystallite size due to phase competition and it was concluded that wadeite would be not suitable for development as a monophasic dental restorative material.

- All silica additions resulted in the crystallization of canasite and frankamenite phases. The change in silica content resulted in significant variations of the microstructure, thereby affecting the fracture toughness of these glass ceramics. Maximum fracture toughness was obtained for S80 was  $3.4 \pm 0.2 \text{ MNm}^{-3/2}$ , which exhibited a 'house of cards' crystal structure consisting of interlocked crystalline laths  $\leq 5\mu\text{m}$ .
- S80, with a specific composition of  $6.11\text{Na}_2\text{O}-5.35\text{K}_2\text{O}-11.46\text{CaO}-11.46\text{CaF}_2-64.82\text{SiO}_2-0.80\text{ZrO}_2$ , was found to have a biaxial strength of  $374 \pm 50 \text{ MPa}$ . This in combination with a  $K_{Ic}$  of  $3.4 \pm 0.2 \text{ MNm}^{-3/2}$  offers improved mechanical properties in comparison with most current commercial systems.
- This formulation has resulted in a solubility of  $1400 \pm 700 \mu\text{gm}^{-2}$  is within the solubility limits for use as a core material (class 2, ISO 6872:1995 (E)).
- Machining of S80 blocks was successfully carried out on the CEREC-Scan (Sirona, Germany) and showed good correlation with the machining of the commercial VITA Mark II blocks. Thus CAD-CAM offers a viable route for the processing of fluorcanasite into dental restorations.
- It was found that the machinability of this glass-ceramic was related to its interlocked structure of very fine randomly orientated laths as machining cracks were deflected by these laths.

## Chapter 10: Further Work

This study has concluded with a fluorcanasite formulation that exhibits a combination of improved mechanical properties and chemical durability. The material has been shown to have adequate machinability in basic runs on the CAD-CAM equipment. However, if the material is to proceed for further development as a dental restorative material, further work is required.

An important aspect is to distinguish and quantify all the crystallising phases, specifically canasite and frankamenite, as this study has indicated how this substantially affects the fracture toughness of the glass-ceramic. TEM work needs to be carried out to elucidate the crystallisation mechanisms associated with the two glass ceramics, to aid specific tailoring of both future compositional variations as well as heat treatment schedules.

It is necessary to emphasize that this study has concentrated on the effect of compositional variation on the fracture toughness of canasite glass-ceramics, and optimisation studies are required to refine the heat treatment schedule and thus the microstructure of the subsequent glass-ceramics. If the material is to be developed as a dentine replacing porcelain, reformulations with zirconia and silica additions with stoichiometric or lower fluoride contents could be attempted in order to achieve a material with higher chemical durability. As it stands, the S80 ( $6.11\text{Na}_2\text{O}-5.35\text{K}_2\text{O}-11.46\text{CaO}-11.46\text{CaF}_2-64.82\text{SiO}_2-0.80\text{ZrO}_2$ ) formulation has acceptable mechanical properties and chemical durability for use as a core porcelain. Further development would require a laminating porcelain that has a thermal expansion matched to the fluorcanasite. Studies would need to evaluate the microstructure, mechanical and chemical properties of the material after the coping has been built up and the material has been subjected to repeated firing at temperatures required for the glazing material.

Although the composition has exhibited adequate fracture toughness, wear tests have not been carried out. Wear tests that simulate oral environments would be beneficial to understand the ability of the material to withstand stress-, solute- and temperature-corrosion.

An aspect of the work that has not been looked at is the aesthetic properties. Stokes (2003) found that the base formulation resulted in a material with adequate translucency and with the possibility of colouration. Translucency tests need to be repeated for S80 and it would

**be necessary to assess the ability of this composition to support shade variations according to the accepted dental standards.**

## Chapter 11: References

Alison J.E. 'Recent advance in ceramic materials and systems for dental restorations' Dental Update 1999; 65-72.

Anstis G.R., Chantikul P., Lawn B.R. and Marshall D.B., Journal of American Ceramic Society, 1981; 64(9): 533-538.

Anusavice K.J. and Zhang N. Z. 'Chemical durability of Dicor and fluorocanaseite-based glass- ceramics.' J Dent Res 1998; 77 (7): 1553-1559.

Anusavice K.J. and Zhang N. Z. 'Effect of alumina content on crystal structure of fluorocanaseite glass-ceramic.' J Dent Res 1998; 77: 16.

Anusavice K.J. and Lee R.B. 'Effect of firing temperature and water exposure on crack propagation in unglazed porcelain', Journal of Dental Research, 1989; 68: 1075-1081.

Anusavice K.J. 'Phillip's Science of Dental Materials'. 10th ed. Philadelphia: Saunders; 1996.

Attar S.G. 'Study of fracture toughness and microstructures of some commercial dental ceramic systems and the experimental canaseite glass-ceramic'. B.Eng. Undergraduate Project., University of Sheffield, 2001.

Baik D.S., No K.S., Chun J.S., Yoon Y.J. and Cho H.Y., Journal of Materials Processing Technology, 1995; 30: 1801.

Beall G.H. 'Design and Properties of Glass-Ceramics', Annual Review of Materials Science, 1992; 22: 91-119.

- Beall G. H. 'Chain Silicate Glass-Ceramics.' *Journal of Non-Crystalline Solids* 1991; 129 (1-3): 163-173.
- Beall G.H. 'Alkali Metal Calcium Fluorosilicate Glass-Ceramic Articles'. US patent 4,386,162. 1983.
- Beall G.H., 'Chain Silicate Glass-Ceramics', *Journal of Non-Crystalline Solids*, 1991; 129: 163-173.
- Beall G.H., Chyung K., Stewart R.L., Donaldson K.Y., Lee H.L. , Baskaran S. and Hasselman D.P.H., 'Effect of Test Method and Crack Size on the Fracture-toughness of a Chain-Silicate Glass-Ceramic', *Journal of Materials Science: Letters*, 1986; 21:2356-2372.
- Bieniek K.W. and Marx R. '[The mechanical loading capacity of new all-ceramic crown and bridge materials].' *Schweiz Manatsschr Zahnmed* 1994; 104 (3): 284-289.
- Blatz M.B., Sadan A. and Kern M. 'Resin Ceramic Bonding: A Review of Litreture', *J Prosthet Dent* 2003; 89: 268-74.
- Boccaccini A.R. 'Machinability and brittleness of glass-ceramics' *Journal of Materials Processing Technology*, 1997; 65: 302-304.
- Bubb N.L., Wood D.J. and Streit P. 'Reduction of the solubility of fluorcanasite based glass ceramics b additions of SiO<sub>2</sub> and AlPO<sub>4</sub>' *Glass Technology*, 2004; 45(2): 91-93.
- Bunker B.C., Arnold G.W. and Beauchamp E.K. 'Mechanisms for alkali leaching in mixed-Na-K silicate glasses.' *Journal of Non-Crystalline Solids* 1983; 58: 295-322.
- Calamia J.R. 'Advances in computer-aided design and computer-aided manufacture technology.' *Curr Op Cosmetic Dent* 1994; 3: 67-73.

- Cannavina G., Johnson A., van Noort R. and Hays M. 'The effect of operator factors on the castability of canasite glass-ceramic.' *Journal of Dental Research* 1998; 77: 1044.
- Cattell M.J., Knowles J.C., Clarke R.L. and Lynch E. 'The biaxial flexural strength of two pressable ceramic systems', *Journal of Dentistry*, 1999; 27: 183-196.
- Chantikul P., Anstis G.R., Lawn B.R. and Marshall D.B. 'A critical evaluation of indentation techniques for measuring toughness: II, strength method', *Journal of American Ceramic Society*, 1981; 64: 539-543.
- Christel P., Meunier A., Heller M., Torre J.P., Peille C.N. 'Mechanical properties and short-term in-vivo evaluation of yttrium-oxide-partially-stablized zirconia', *J Biomed Mater Res* 1989; 23: 45-6.
- Denry *et al.* 'Crystallization kinetics of a low-expansion feldspar glass for dental applications', John Wiley and Sons, Inc., 1998.
- Denry I.L. and Rosenstiel S.F. 'Flexural strength and fracture toughness of Dicor glass-ceramic after embedment modification', *Journal of Dental Research*, 1993; 72: 572-576.
- Dobson R., 'Dental Dangers', *Daily Mail*, 1999:30<sup>th</sup> March, 43.
- Dong J.K., Luthy H., Wohlwend A. and Shärer P. 'Heat pressed ceramics: technology and strength', *The International Journal of Prosthodontics*, 1992; 5: 9-16.
- Doremus R.H. 'Glass Science'. 2nd ed. New York: Wiley-Interscience; 1994.
- Dorfman M.D., Rogachev D.D., Goroshchenko Z.I. and Uspenskaya E.I. 'Canasite, a new mineral.' *Trudy Mineralog Muzeya Akad Nauk SSSR* 1959; 9: 158-166 (In Russian) English abstract in Dorfman *et al.* (1960) *Am. Mineral*, 1945: 1253-1254.

Evans A.G. and Charles E.A. 'Fracture toughness determination by indentation', *Journal of American Ceramic Society*, 1976; 56: 371-372.

Fairhurst C.W., Anusavice K.J., Hashinger D.T. *et al*, 'Thermal Expansion of Dental Alloys and Procelains', *Journal of Biomedical Materials Research*, 1980; 14: 435-446.

Ferracane J.L. and Condon J.R. 'In vito evaluation of the marginal degradation of dental composites under simulated occlusal loading', *Dental Materials*, 1999; 15: 262-267.

Giordano R.A., Pelletier L., Campbell S. and Pober R. 'Flexural strength of an infused ceramic, glass ceramic and feldspathic porcelain', *The Journal of Prosthetic Dentistry*, 1995; 73: 411-418.

Gorman C.M. and Hill R.J. 'Heat-pressed ionomer glass-ceramics. Part II. Mechanical property evaluation'. *Dental Materials*, 2004; 20: 252-261.

Gorman C.M., McDevitt W.E. and Hill R.G. 'Comparison of two heat pressed all-ceramic dental materials', *Dental Materials*, 2000; 16: 389-395.

Graf A., Sindel J., Frankenberger R., Greil P., Petschelt A. 'Fracture strengths and fatigue limits of CAD-CAM machined dental ceramics'. *Proceedings of the Conference Clinically appropriate Alternatives to amalgam Biophysical factors in Restorative Decision Making*, Academy of Dental Materials, 1996 p236.

Henry J. and Hill R.G. 'The influence of Lithia content on the properties of fluorphlogopite glass-ceramics. II. Microstructure hardness and machinability' *Journal of non-crystalline solids*, 2003; 319: 13-30.

Hlavác J. 'The Technology of Glass and Ceramics: An Introduction.' New York, N.Y.: Elsevier Scientific; 1983.

Höland W., Schweiger M., Frank M. and Rheinberger V. 'A comparison of the microstructure and properties of the IPS Empress 2 and the IPS Empress glass-ceramics', *Journal of Biomedical Materials Research*, 2000; 53: 297-303.

International Standards Organisation. 'ISO 6872 (dental ceramics) 1995:E'.

Jambor J.L. and Roberts C 'New Mineral Names' *American Mineralogist*, 2004; 89: 467-471.

James P.F., Iqbal Y., Jais U.S., Jordery S. and Lee W.E. 'Crystallisation of silicate and phosphate glasses' *The Journal of Non-Crystalline Solids*, 1997; 219: 17-29.

Johnson A., Shareef M.Y., van Noort R. and Walsh J.M. 'Effect of furnace type and ceramming heat treatment conditions on the biaxial flexural strength of a canasite glass-ceramic.' *Dent Mater* 2000; 16 (4): 280-284.

Johnson A., Shareef M.Y., Walsh J.M., Hatton P.V. and van Noort R. 'Effect of investment temperature on biaxial flexural strength of castable glass-ceramics.' *J Dent Res* 1998; 77: 1043.

Johnson A., Shareef M.Y., Walsh J.M., Hatton P.V., van Noort R. and Hill R.G. 'The effect of casting conditions on the biaxial flexural strength of glass-ceramic materials.' *Dent Mater* 1998; 14 (6): 412-416.

Jones D.W., *Coatings of ceramics on metals*, Annual New York Academy of Science, 1988; 523: 19-37.

Jones D.W., Jones P.A. and Wilson H.J. 'The relationship between transverse strength and testing methods for dental ceramics', *Journal of Dentistry*, 1972; 1: 85-91.

Kavouras P., Komninou Ph. and Karakostas Th. 'Effect of composition and annealing temperature on the mechanical properties of vitrified waste' *Journal of European Ceramic Society*, 2004; 24:2095-2102.

Kelly J.R. 'Ceramics in restorative and prosthetic dentistry.' *Annual Review of Materials Science* 1997; 27: 443-468.

Koenderink G.H., Brzesowsky R.H. and Balkenende A.R. 'Effect of the initial stages of leaching on the surface of alkaline earth sodium silicate glasses' *The Journal of Non-Crystalline Solids*, 2000; 262: 80-98.

Land C.H. 'Porcelain Dental Art', *Cosmos* 45, 437-444.

Lawn B.R. 'Fracture of brittle solids – second edition', Cambridge University Press, Cambridge, 1993.

Lazebnik K.A. and Lazebnik Yu.D. 'The rare silicates - miserite, canasite, fedorite in the charoite rocks.' *Mineralogy and Geochemistry of the ultrabasic and the basic rocks of Yakutia* 1981: 32-50.

Likitvanichkul S. and Lacourse W. C. 'Effect of fluorine content on crystallization of canasite glass-ceramics.' *J Mater Sci* 1995; 30 (24): 6151-6155.

Luthardt R.G., Holzhuter M., Sandkuhl O., Herold V., Schnapp J.D., Kuhlisch E., Walter M. 'Reliability and Properties of Ground Y-TZP-Zirconia Ceramics', *JDent Res* 2002; 81(7): 487-491.

MacCulloch W.T. 'Advances in dental ceramics.' *British Dental Journal* 1968; 123: 361-356.

Mackert J.R., Butts M.B. and Fairhurst C.W. 'The effect of the leucite transformation on dental porcelain expansion.' *Dent Mater* 1983; 2: 32-36.

Macmillan P.W. 'Glass-Ceramics'. 2nd ed. ed. London: Academic Press; 1979.

Matthias K., Fechtig T. and Strub J.R. 'Influence of water storage and thermal cycling on fracture strength on all-porcelain, resin-bonded fixed partial dentures', *The Journal of Prosthetic Dentistry*, 1994; 71: 251-256.

McLean J.W. and Hughes T.H. 'The reinforcement of dental porcelain with ceramic oxides.' *Brit Dent J* 1965; 119: 251-255.

McLean J.W. 'The Science and Art of Dental Ceramics. Volume 1: The nature of dental ceramics and their clinical use.' Chicago: Quintessence Publishing Co., Inc.; 1979.

Mecholsky J.J., 'Fracture mechanics principles', *Dental Materials*, 1995; 11: 111-112.

Miller C.A., Kokubo T., Reaney I.M., Hatton P.V. and James P.F. 'Formation of apatite layers on modified canasite glass-ceramics in simulated body fluid.' *J Biomed Mater Res* 2002; 59 (3): 473-480.

Miller C.A., Reaney I.M., Hatton P.V. and James P.F. 'Nucleation and crystallisation of canasite-fluorapatite glass ceramics.' *Glastechnische Berichte [Glass Science and Technology]* 2000; 73: 154-161.

Miller C.A. 'Crystallisation of canasite/frankamenite based glass-ceramics for bone tissue repair and augmentation' PhD Thesis, University of Sheffield, 2004 (M008947SH).

Miller C.A., Reaney I.M., Hatton P.V. and James P.F. 'Crystallization of canasite/frankamenite-based glass-ceramics' *Chemical Materials*, 2004; 16: 5736-5743.

- Morena R., Beudreau G.M., Lockwood P.E. *et al*, 'Fatigue of dental ceramics in a simulated oral environment', *Journal of Dental Research*, 1986; **65**: 993-997.
- Morena R., Lockwood P.E. and Fairhurst C.W., 'Fracture toughness of commercial dental porcelains', *Dental Materials*, 1986; **2**: 58-62.
- Morrell R., McCormick N.J., Bevan J., Lodeiro M. and Margeton J. 'Biaxial disc flexure-modulus and strength testing', *British Ceramic Transactions*, 1999; **98(5)**: 234-240.
- Mueller H.J. 'Fracture toughness and fractography of dental ceramics', *Cells and Materials*, 1991; **1(3)**: 265-278.
- Naert I., Van Der Donk A. and Beckers L. 'Precision fit and clinical evaluation of all-ceramic full restorations followed between 0.5 and 5 years'. *Journal of Oral Rehabilitation*, 2005; **32**: 51-57.
- O'Brien W.J. 'Magnesia Ceramic Jacket Crowns', *Dent Clin North Am* 1985; **29**:719-724.
- Omar A. 'Mechanism of fluorocanite formation.' *Second International Ceramics Congress, Vol 1: Traditional Ceramics* 1994: 451-455.
- Piddock V. and Qualtrough A.J.E., 'Dental Ceramics- An Update', *Journal of Dentistry*, 1990; **18**: 227-235
- Piddock V., Marquis P.M. and Wilson H.J. 'Structure-property relationships of dental porcelains used in jacket crowns', *British Dental Journal*, 1984; **156**: 395-398.
- Pinckney L.R., Beall G.H. and Andrus R.L. 'Strong sintered miserite glass-ceramics.' *J Am Ceram Soc* 1999; **82 (9)**: 2523-2528.

- Ponton C.D. and Rawlings R.B. 'Vickers indentation fracture-toughness 1: Review of literature and formulation of standardised indentation toughness equations.' *Mater Sci Technol* 1989; 5 (9): 865-872.
- Poon C.Y. and Bhushan B. 'Surface roughness analysis of glass-ceramic substrates and finished magnetic disks, and Ni-P coated Al-Mg and glass substrates.' *Wear* 1995; 190 (1): 89-109.
- Potiket N., Chiche G. and Finger I.M. 'In vitro fracture strength of teeth restored with different all-ceramic crown systems' *The Journal of Prosthetic Dentistry*, 2004; 92: 491-5.
- Qualtrough A.J.E. 'Techceram Strength in Advanced Technology' *Dental Practice*, 1996; 34 (22): 8
- Qualtrough A.J.E. and Piddock V. 'Recent advances in ceramic materials and systems for dental restorations.' *Dent Update* 1999; 26: 65-72.
- Quinn G.D., Gettings R.J. and Kübler J.J. 'Fracture toughness of ceramics by the surface crack in flexure (SCF) method', *Fracture Mechanics of Ceramics*, Vol. 2, Plenum Press, New York, 1996.
- Quinn J.B. and Quinn G.D. 'Indentation brittleness of ceramics: a fresh approach' *Journal of Materials Science*, 1997; 32: 4331-4346.
- Raigrosdki A.J. 'Contemporary Material and Technologies for All-ceramic Fixed Partial Denture: A Review of Literature', *J Prothet Dent* 2004; 92: 557-62.
- Rastsvetaeva R.K., Rozenberg K.A., Khomyakov A.P. and Rozhdestvenskaya I.V. 'Crystal structure of f-canosite' *Doklady Chemistry*, 2003; 391: 177-180.
- Rosenstiel S.F. and Porter S.S. 'Apparent fracture toughness of all-ceramic crown systems', *The Journal of Prosthetic Dentistry*, 1989; 62: 529-532.

Rozhdestvenskaya I.V. and Nikishova L.V. 'The Crystal Structure of Frankamenite', *Mineralogical Magazine*, 1996; 60: 897-905.

Rozhdestvenskaya I.V., Nikishova L.V. and Lazebnik K.A. 'The crystal structure of frankamenite.' *Minerological Magazine* 1996; 60: 897-905.

Scherrer S.S., Denry I.L. and Wiskott H.W.A, 'Comparison of three fracture toughness testing techniques using a dental glass and dental ceramic', *Dental Materials*, 1998; 14: 246-255.

Seghi R.R., Sorensen J.A., Engleman M.J., Roumanas E. and Torres T.J. 'Flexural trength of New Ceramic Materials', *J Dent Res*, 1990; 69, Abst1521: 299.

Seghi R.R. and Sorensen J.A. 'Relative Flexural Strength of Six New Ceramic Materials', *Int J Prosthodont*, 1995; 8: 239-246.

Seghi R.R., Denry I.L. and Rosenstiel S.F. 'Relative Fracture-Toughness and Hardness of New Dental Ceramics.' *J Prosthet Dent* 1995; 74 (2): 145-150.

Shareef M.Y., Johnson A. and Van Noort R. 'The strength of a canasite glass-ceramic using dental laboratory procedures.' *J Dent Res* 1998; 77: 2467.

Sinton C.W. and LaCourse W.C.'Experimental survey of the chemical durability of soda-lime-silicate glasses' *Materials Research Bulletin*, 2001; 36: 2471-2479.

Stokes C.W., Hand R.J. and Noort R.V., 'Fluorocanasite glass-ceramics for dental applications', *Proc. International Congress of Glass*, 2000; Vol.2. Extended Abstracts.

Stokes, C.W. 'Canasite glass-ceramics for dental restorations' PhD Thesis, University of Sheffield, 2003 (M0090712SH).

Strnad Z. 'Glass-Ceramic Materials', Elsevier, 1986.

Thompson J.Y., Bayne S.C. and Heymann H.O. 'Mechanical properties of a new mica-based machinable class ceramic for CAD/CAM restorations', *The Journal of Prosthetic Dentistry*, 1996; 76: 619-623.

Tian J., Cao X., Zhang, Y. and Wang C. 'Effect of fluorine content on the crystallization of fluorsilicic mica glass' *Journal of Materials Science*, 2002; 37: 1789-1792.

van Noort R., Shareef M.Y., Johnson A. and James P. F. 'Properties of a canasite glass-ceramic.' *J Dent Res* 1997; 76 (21): Abst. 61.

Vomacka P., Ramesh r. and Hampshire S. 'Influence of zirconia addition on the crystallization kinetics of a Y-Si-Al-O-N glass', *Journal of European Ceramic Society*. 1996; 16: 1253-1262.

Weinstein M., Katz S. and Weinstein A.B. 'Fused porcelain to metal teeth', U.S Patent No. 3052 982, 1962.

Wilson H.J. and Whitehead F.I.H. 'Comparison of some physical properties of dental porcelains', *Dental Practice*, 1967; 17: 350-354.

Wolters D.R. and Verweij H. 'Cross-linking and tensile stress during glass hydrolysis.' *Phys Chem Glasses* 1981; 22: 55.

Xu H.H.K., Smith D.T., Jahanmir S., Romberg E., Kelly J.R., Thompson V.P. and Rekow E.D. 'Indentation damage and mechanical properties of human enamel and dentin', *Journal of Dental Research*, 1998; 77(3): 472-480.

Zachariasen W.H. 'The Atomic Arrangement in Glass', *J Am Ceram Soc* 1932; 54: 3841-3851.

Zhang N.Z. and Anusavice K.J. 'Effect of alumina on the strength, fracture toughness, and crystal structure of fluorcanasite glass-ceramics', *J Am Ceram Soc* 1999; 82 (9): 2509-2513.

## **Chapter 12: Apendices**

**Appendix 1 Glass compositions**

**Appendix 2 XRF analysis**

**Appendix 3 Summary of DTA analysis**

<b>Compositions</b>	<b>K<sub>2</sub>O</b>	<b>CaO</b>	<b>Na<sub>2</sub>O</b>	<b>SiO<sub>2</sub></b>	<b>CaF<sub>2</sub></b>	<b>ZrO<sub>2</sub></b>	<b>TiO<sub>2</sub></b>
<b>F10Z2</b>	6.86	14.70	7.84	58.82	9.80	1.96	
<b>F10Z4</b>	6.73	14.42	7.69	57.69	9.62	3.85	
<b>F10Z8</b>	6.48	13.89	7.41	55.56	9.26	7.41	
<b>F15Z0 (=F15)</b>	6.67	14.28	7.62	57.14	14.29	-	
<b>F15Z1</b>	6.60	14.14	7.54	56.58	14.14	0.99	
<b>F15Z2</b>	6.54	14.01	7.47	56.02	14.01	1.96	
<b>F15Z4</b>	6.41	13.74	7.33	54.95	13.74	3.85	
<b>F15Z8</b>	6.17	13.23	7.06	52.91	13.23	7.41	
<b>S55</b>	6.71	14.37	7.67	55.88	14.37	1.01	
<b>S57(=F15Z1)</b>	6.60	14.14	7.54	56.58	14.14	0.99	
<b>S65</b>	6.09	13.05	6.96	59.95	13.05	0.91	
<b>S70</b>	5.82	12.47	6.65	61.72	12.47	0.87	
<b>S80</b>	5.35	11.46	6.11	64.82	11.46	0.80	
<b>S90</b>	4.95	10.60	5.65	67.46	10.60	0.74	
<b>S110</b>	4.30	9.22	4.92	71.70	9.22	0.65	

## Appendix 1

### Glass Compositons in mol%.

Compositions	K <sub>2</sub> O	CaO	Na <sub>2</sub> O	SiO <sub>2</sub>	CaF <sub>2</sub>	ZrO <sub>2</sub>	TiO <sub>2</sub>
<b>B8</b>	7.0	11.8	9.3	54.2	17.9	-	
<b>K7</b>	7.0	15.0	8.0	60.0	10.0	-	
<b>C1</b>	6.8	17.1	7.8	58.5	9.8	0	
<b>C2</b>	6.8	19.4	7.8	58.3	7.8	0	
<b>T2</b>	6.9	14.7	7.8	58.8	9.8	0	1.9
<b>Z2</b>	6.9	14.7	7.8	58.8	9.8	1.4	
<b>F13</b>	6.80	14.56	7.77	58.25	12.62		
<b>F8Z0 (=F8)</b>	7.14	15.31	8.16	61.23	8.16	-	
<b>F8Z1</b>	7.07	15.15	8.08	60.61	8.08	0.99	
<b>F8Z2</b>	7.00	15.00	8.00	60.02	8.00	1.96	
<b>F8Z4</b>	6.86	14.72	7.85	58.87	7.85	3.85	
<b>F8Z8</b>	6.61	14.17	7.56	56.69	7.56	7.41	
<b>F10Z0 (=F10)</b>	7.00	15.00	8.00	60.00	10.00	-	
<b>F10Z1</b>	6.93	14.85	7.92	59.41	9.90	0.99	

**Appendix 2: XRF Analysis**

MW	With normalisation		No. of moles	Corrected		mol%	wt%	wt%
	K7F8 Analysis	Normalised		no. of moles	no. of moles			
F	19.00	5.20	5.09	0.27	-	-	-	-
Na2O	61.98	7.58	7.42	0.12	0.12	7.79	482.82	7.58
MgO	40.30	0.03	0.03	0.00	0.00	0.05	2.02	0.03
Al2O3	101.96	0.05	0.05	0.00	0.00	0.03	3.06	0.05
SiO2	60.08	58.20	56.97	0.95	0.95	61.69	3706.58	58.19
P2O5	141.94	0.02	0.02	0.00	0.00	0.01	1.42	0.02
SO3	80.06	0.02	0.02	0.00	0.00	0.01	0.80	0.01
Cl	35.45	0.01	0.01	0.00	0.00	0.02	0.71	0.01
K2O	94.20	10.54	10.32	0.11	0.11	7.13	671.61	10.54
CaO	56.08	20.46	20.03	0.36	0.22	14.53	814.80	12.79
TiO2	79.88	0.01	0.01	0.00	0.00	0.01	0.80	0.01
Cr2O3	151.99	0.01	0.01	0.00	0.00	0.01	1.52	0.02
Fe2O3	159.69	0.02	0.02	0.00	0.00	0.01	1.60	0.03
SrO	103.62	0.00	0.00	0.00	0.00	0.00	0.00	0.00
ZrO2	123.22	0.01	0.01	0.00	0.00	0.01	1.23	0.02
CaF2	78.07	-	-	-	0.13	8.72	680.81	10.69
Sum		102.16	100.01	1.80	1.54	100.02	6369.76	99.99

MW	With normalisation		No. of moles	Corrected		mol%	wt%	wt%
	K7F15Zr1 Analysis	Normalised		no. of moles	no. of moles			
F	19.00	8.95	8.76	0.46	-	-	-	-
Na2O	61.98	6.42	6.28	0.10	0.10	6.59	408.44	6.41
MgO	40.30	0.03	0.03	0.00	0.00	0.05	2.02	0.03
Al2O3	101.96	0.05	0.05	0.00	0.00	0.03	3.06	0.05
SiO2	60.08	53.46	52.33	0.87	0.87	56.66	3404.36	53.45
P2O5	141.94	0.02	0.02	0.00	0.00	0.01	1.42	0.02
SO3	80.06	0.01	0.01	0.00	0.00	0.01	0.80	0.01
Cl	35.45	0.01	0.01	0.00	0.00	0.02	0.71	0.01
K2O	94.20	9.43	9.23	0.10	0.10	6.38	600.96	9.43
CaO	56.08	23.60	23.10	0.41	0.18	11.80	661.71	10.39
TiO2	79.88	0.01	0.01	0.00	0.00	0.01	0.80	0.01
Cr2O3	151.99	0.00	0.00	0.00	0.00	0.00	0.00	0.00
Fe2O3	159.69	0.03	0.03	0.00	0.00	0.01	1.60	0.03
CuO		0.01	0.01					
ZnO		0.01	0.01					
As2O3								
SeO2								
SrO	103.62	0.00	0.00	0.00	0.00	0.00	0.00	0.00
ZrO2	123.22	1.70	1.66	0.01	0.01	0.88	108.44	1.70
HfO2		0.03						
Au								
PbO								
CaF2	78.07	-	-	-	0.23	15.00	1171.11	18.39
Sum		103.74	101.54	1.96	1.50	97.45	6365.42	99.93

MW	With normalisation			No. of moles	Corrected			wt%
	K7F10		Normalised		no. of moles	mol%		
	Analysis							
F	19.00	6.71	6.53	0.34	-	-	-	-
Na2O	61.98	7.52	7.31	0.12	0.12	7.78	482.20	7.52
MgO	40.30	0.04	0.04	0.00	0.00	0.07	2.82	0.04
Al2O3	101.96	0.08	0.08	0.00	0.00	0.05	5.10	0.08
SiO2	60.08	56.21	54.66	0.91	0.91	60.00	3605.04	56.19
P2O5	141.94	0.03	0.03	0.00	0.00	0.01	1.42	0.02
SO3	80.06	0.01	0.01	0.00	0.00	0.01	0.80	0.01
Cl	35.45	0.01	0.01	0.00	0.00	0.02	0.71	0.01
K2O	94.20	10.29	10.01	0.11	0.11	7.01	660.31	10.29
CaO	56.08	21.88	21.28	0.38	0.21	13.70	768.25	11.97
TiO2	79.88	0.01	0.01	0.00	0.00	0.01	0.80	0.01
Cr2O3	151.99	0.01	0.01	0.00	0.00	0.01	1.52	0.02
Fe2O3	159.69	0.02	0.02	0.00	0.00	0.01	1.60	0.02
SrO	103.62	0.01	0.01	0.00	0.00	0.01	1.04	0.02
ZrO2	123.22	0.00	0.00	0.00	0.00	0.00	0.00	0.00
CaF2	78.07	-	-	-	0.17	11.33	884.58	13.79
Sum		102.83	100.01	1.86	1.52	100.02	6416.18	99.99

MW	With normalisation			No. of moles	Corrected			wt%
	K7F15Zr2		Normalised		no. of moles	mol%		
	Analysis							
F	19.00	8.60	8.36	0.44	-	-	-	-
Na2O	61.98	6.40	6.22	0.10	0.10	6.62	410.30	6.39
MgO	40.30	0.03	0.03	0.00	0.00	0.05	2.02	0.03
Al2O3	101.96	0.69	0.67	0.01	0.01	0.44	44.86	0.70
SiO2	60.08	51.88	50.45	0.84	0.84	55.38	3327.45	51.86
P2O5	141.94	0.05	0.05	0.00	0.00	0.03	4.26	0.07
SO3	80.06	0.01	0.01	0.00	0.00	0.01	0.80	0.01
Cl	35.45	0.00	0.00	0.00	0.00	0.00	0.00	0.00
K2O	94.20	9.23	8.98	0.10	0.10	6.29	592.49	9.23
CaO	56.08	23.11	22.47	0.40	0.18	11.92	668.44	10.42
TiO2	79.88	0.02	0.02	0.00	0.00	0.02	1.60	0.02
Cr2O3	151.99	0.02	0.02	0.00	0.00	0.01	1.52	0.02
Fe2O3	159.69	0.03	0.03	0.00	0.00	0.01	1.60	0.02
CuO		0.01	0.01					
ZnO		0.00	0.00					
As2O3		0.00	0.00					
SeO2		0.00	0.00					
SrO	103.62	0.00	0.00	0.00	0.00	0.00	0.00	0.00
ZrO2	123.22	3.44	3.35	0.03	0.03	1.79	220.57	3.44
HfO2		0.07	0.07					
Au								
PbO								
CaF2	78.07	-	-	-	0.22	14.51	1132.85	17.66
Sum		103.52	100.67	1.91	1.47	97.08	6408.75	99.87

	MW	With normalisation		No. of moles	Corrected		mol%	wt%	
		K7F13			no. of moles	wt%			
		Analysis	Normalised						
F	19.00	8.59	8.29	0.44	-	-	-	-	-
Na2O	61.98	7.03	6.78	0.11	0.11	7.33	454.31	7.02	
MgO	40.30	0.05	0.05	0.00	0.00	0.08	3.22	0.05	
Al2O3	101.96	0.05	0.05	0.00	0.00	0.03	3.06	0.05	
SiO2	60.08	54.67	52.76	0.88	0.88	58.85	3535.94	54.67	
P2O5	141.94	0.03	0.03	0.00	0.00	0.01	1.42	0.02	
SO3	80.06	0.02	0.02	0.00	0.00	0.01	0.80	0.01	
Cl	35.45	0.01	0.01	0.00	0.00	0.02	0.71	0.01	
K2O	94.20	9.82	9.48	0.10	0.10	6.74	634.87	9.82	
CaO	56.08	23.30	22.49	0.40	0.18	12.26	687.50	10.63	
TiO2	79.88	0.01	0.01	0.00	0.00	0.01	0.80	0.01	
Cr2O3	151.99	0.01	0.01	0.00	0.00	0.01	1.52	0.02	
Fe2O3	159.69	0.02	0.02	0.00	0.00	0.01	1.60	0.02	
SrO	103.62	0.01	0.01	0.00	0.00	0.01	1.04	0.02	
ZrO2	123.22	0.00	0.00	0.00	0.00	0.00	0.00	0.00	
CaF2	78.07	-	-	-	-	0.22	14.62	17.65	
Sum		103.62	100.01	1.93	1.49	99.99	6468.23	100.00	

	MW	With normalisation		No. of moles	Corrected		mol%	wt%	
		K7F15Zr4			no. of moles	wt%			
		Analysis	Normalised						
F	19.00	9.14	8.82	0.46	-	-	-	-	-
Na2O	61.98	6.14	5.93	0.10	0.10	6.41	397.29	6.14	
MgO	40.30	0.03	0.03	0.00	0.00	0.05	2.02	0.03	
Al2O3	101.96	0.21	0.20	0.00	0.00	0.13	13.25	0.20	
SiO2	60.08	48.84	47.13	0.78	0.78	52.57	3158.62	48.83	
P2O5	141.94	0.00	0.00	0.00	0.00	0.00	0.00	0.00	
SO3	80.06	0.01	0.01	0.00	0.00	0.01	0.80	0.01	
Cl	35.45	0.02	0.02	0.00	0.00	0.04	1.42	0.02	
K2O	94.20	8.94	8.63	0.09	0.09	6.14	578.36	8.94	
CaO	56.08	23.42	22.60	0.40	0.17	11.45	642.08	9.93	
TiO2	79.88	0.02	0.02	0.00	0.00	0.02	1.60	0.02	
Cr2O3	151.99	0.00	0.00	0.00	0.00	0.00	0.00	0.00	
Fe2O3	159.69	0.03	0.03	0.00	0.00	0.01	1.60	0.02	
CuO		0.01	0.01						
ZnO		0.17	0.16						
As2O3		0.00	0.00						
SeO2		0.01	0.01						
SrO	103.62	0.00	0.00	0.00	0.00	0.00	0.00	0.00	
ZrO2	123.22	6.66	6.43	0.05	0.05	3.50	431.28	6.67	
HfO2		0.13	0.13						
Au		0.00	0.00						
PbO		0.00	0.00						
CaF2	78.07	-	-	-	-	0.23	15.56	18.78	
Sum		103.65	100.03	1.90	1.43	95.89	6443.13	99.59	

MW	K7F15		No. of moles	Corrected		mol%	wt%
	Analysis	Normalised		no. of moles	mol%		
F	19.00	9.67	9.29	0.49	-	-	-
Na2O	61.98	6.75	6.49	0.10	0.10	7.08	438.81
MgO	40.30	0.05	0.05	0.00	0.00	0.08	3.22
Al2O3	101.96	0.05	0.05	0.00	0.00	0.03	3.06
SiO2	60.08	53.01	50.94	0.85	0.85	57.30	3442.81
P2O5	141.94	0.03	0.03	0.00	0.00	0.01	1.42
SO3	80.06	0.01	0.01	0.00	0.00	0.01	0.80
Cl	35.45	0.01	0.01	0.00	0.00	0.02	0.71
K2O	94.20	9.46	9.09	0.10	0.10	6.52	614.15
CaO	56.08	24.97	24.00	0.43	0.18	12.40	695.35
TiO2	79.88	0.01	0.01	0.00	0.00	0.01	0.80
Cr2O3	151.99	0.01	0.01	0.00	0.00	0.01	1.52
Fe2O3	159.69	0.02	0.02	0.00	0.00	0.01	1.60
SrO	103.62	0.01	0.01	0.00	0.00	0.01	1.04
ZrO2	123.22	0.00	0.00	0.00	0.00	0.00	0.00
CaF2	78.07	-	-	-	0.24	16.52	1289.78
Sum		104.06	100.01	1.97	1.48	100.01	6495.08

MW	K7F15Zr8		No. of moles	Corrected		mol%	wt%
	Analysis	Normalised		no. of moles	mol%		
F	19.00	8.89	8.54	0.45	-	-	-
Na2O	61.98	5.48	5.27	0.09	0.09	5.74	355.76
MgO	40.30	0.02	0.02	0.00	0.00	0.03	1.21
Al2O3	101.96	0.03	0.03	0.00	0.00	0.02	2.04
SiO2	60.08	44.63	42.89	0.71	0.71	48.24	2898.45
P2O5	141.94	0.00	0.00	0.00	0.00	0.00	0.00
SO3	80.06	0.00	0.00	0.00	0.00	0.00	0.00
Cl	35.45	0.02	0.02	0.00	0.00	0.04	1.42
K2O	94.20	8.18	7.86	0.08	0.08	5.64	531.26
CaO	56.08	22.09	21.23	0.38	0.15	10.40	583.20
TiO2	79.88	0.03	0.03	0.00	0.00	0.03	2.40
Cr2O3	151.99	0.01	0.01	0.00	0.00	0.01	1.52
Fe2O3	159.69	0.04	0.04	0.00	0.00	0.02	3.19
CuO		0.02	0.02				
ZnO		0.01	0.01				
As2O3		0.08	0.08				
SeO2		0.01	0.01				
SrO	103.62	0.01	0.01	0.00	0.00	0.01	1.04
ZrO2	123.22	11.93	11.46	0.09	0.09	6.29	775.07
HfO2		0.22	0.21				
Au		0.01	0.01				
PbO		0.01	0.01				
CaF2	78.07	-	-	-	0.22	15.19	1185.94
Sum		101.48	97.53	1.81	1.36	91.66	6342.50

	MW	With normalisation		No. of moles	Corrected		mol%	wt%	
		K7F15Zr1Si70 Analysis	Normalised		no. of moles				
F	19.00	8.02	7.85	0.41	-	-	-	-	-
Na2O	61.98	5.75	5.63	0.09	0.09	5.91	366.30	5.75	
MgO	40.30	0.03	0.03	0.00	0.00	0.05	2.02	0.03	
Al2O3	101.96	0.07	0.07	0.00	0.00	0.05	5.10	0.08	
SiO2	60.08	58.41	57.18	0.95	0.95	61.92	3720.40	58.41	
P2O5	141.94	0.03	0.03	0.00	0.00	0.01	1.42	0.02	
SO3	80.06	0.01	0.01	0.00	0.00	0.01	0.80	0.01	
Cl	35.45	0.02	0.02	0.00	0.00	0.04	1.42	0.02	
K2O	94.20	7.79	7.63	0.08	0.08	5.27	496.41	7.79	
CaO	56.08	21.60	21.14	0.38	0.17	11.09	621.89	9.76	
TiO2	79.88	0.01	0.01	0.00	0.00	0.01	0.80	0.01	
Cr2O3	151.99	0.00	0.00	0.00	0.00	0.00	0.00	0.00	
Fe2O3	159.69	0.03	0.03	0.00	0.00	0.01	1.60	0.03	
CuO		0.01	0.01						
ZnO		0.01	0.01						
As2O3		0.02	0.02						
ZrO2	123.22	1.55	1.52	0.01	0.01	0.80	98.58	1.55	
HfO2		0.02							
CaF2	78.07	-	-			0.21	13.44	16.47	
Sum		103.36	101.19	1.93	1.52	98.61	6366.04	99.93	

	MW	With normalisation		No. of moles	Corrected		mol%	wt%
		K7F15Zr1Si90 Analysis	Normalised		no. of moles			
F	19.00	6.67	6.44	0.34	-	-	-	-
Na2O	61.98	5.16	4.98	0.08	0.08	5.38	333.45	5.16
MgO	40.30	0.02	0.02	0.00	0.00	0.03	1.21	0.02
Al2O3	101.96	0.05	0.05	0.00	0.00	0.03	3.06	0.05
SiO2	60.08	63.50	61.28	1.02	1.02	68.36	4107.34	63.50
P2O5	141.94	0.02	0.02	0.00	0.00	0.01	1.42	0.02
SO3	80.06	0.01	0.01	0.00	0.00	0.01	0.80	0.01
Cl	35.45	0.01	0.01	0.00	0.00	0.02	0.71	0.01
K2O	94.20	7.38	7.12	0.08	0.08	5.07	477.57	7.38
CaO	56.08	18.84	18.18	0.32	0.15	10.37	581.52	8.99
TiO2	79.88	0.01	0.01	0.00	0.00	0.01	0.80	0.01
Cr2O3	151.99	0.00	0.00	0.00	0.00	0.00	0.00	0.00
Fe2O3	159.69	0.03	0.03	0.00	0.00	0.01	1.60	0.02
CuO		0.01	0.01					
ZnO		0.00	0.00					
As2O3		0.00	0.00					
ZrO2	123.22	1.37	1.32	0.01	0.01	0.72	88.72	1.37
HfO2		0.03	0.03					
CaF2	78.07	-	-	-	0.17	11.36	886.92	13.71
Sum		103.08	99.48	1.85	1.51	101.38	6485.11	100.25

	MW	K7F15Zr1Si110		No. of moles	Corrected			wt%
		Analysis	Normalised		no. of moles	mol%		
F	19.00	5.80	5.57	0.29	-	-	-	-
Na2O	61.98	4.55	4.37	0.07	0.07	4.76	295.02	4.54
MgO	40.30	0.00	0.00	0.00	0.00	0.00	0.00	0.00
Al2O3	101.96	0.05	0.05	0.00	0.00	0.03	3.06	0.05
SiO2	60.08	68.38	65.71	1.09	1.09	73.91	4440.81	68.37
P2O5	141.94	0.02	0.02	0.00	0.00	0.01	1.42	0.02
SO3	80.06	0.01	0.01	0.00	0.00	0.01	0.80	0.01
Cl	35.45	0.02	0.02	0.00	0.00	0.04	1.42	0.02
K2O	94.20	6.34	6.09	0.06	0.06	4.37	411.63	6.34
CaO	56.08	16.03	15.40	0.27	0.13	8.65	485.07	7.47
TiO2	79.88	0.02	0.02	0.00	0.00	0.02	1.60	0.02
Cr2O3	151.99	0.00	0.00	0.00	0.00	0.00	0.00	0.00
Fe2O3	159.69	0.03	0.03	0.00	0.00	0.01	1.60	0.02
CuO		0.00	0.00					
ZnO		0.00	0.00					
As2O3		0.00	0.00					
ZrO2	123.22	1.17	1.12	0.01	0.01	0.61	75.17	1.16
HfO2		0.02	0.02					
CaF2	78.07	-	-	-	0.15	9.91	773.71	11.91
Sum		102.42	98.41	1.81	1.51	102.33	6491.30	99.93

## Appendix 2: Batch Calculation

### K7Na8F8

	MF	MW		Wt%
K <sub>2</sub> O	0.0714	94.20	6.73	10.59
CaO	0.1531	56.08	8.58	13.51
Na <sub>2</sub> O	0.0816	61.98	5.06	7.96
SiO <sub>2</sub>	0.6123	60.08	36.79	57.90
CaF <sub>2</sub>	0.0816	78.08	6.37	10.03
	<b>1.0001</b>		<b>63.54</b>	<b>100.00</b>

### Batch for 300 gm of glass

	CF	100g Wgt	200g Wgt	300g Wgt
K <sub>2</sub> CO <sub>3</sub>	1.47	15.540	31.079	46.619
CaCO <sub>3</sub>	1.78	24.115	48.230	72.345
Na <sub>2</sub> CO <sub>3</sub>	1.71	13.620	27.239	40.859
SiO <sub>2</sub>	1.00	57.900	115.800	173.701
CaF <sub>2</sub>	1.00	10.033	20.066	30.099
		<b>121.21</b>	<b>242.415</b>	<b>363.622</b>

### K7Na8F10

	MF	MW		Wt%
K <sub>2</sub> O	0.0700	94.20	6.59	10.33
CaO	0.1500	56.08	8.41	13.18
Na <sub>2</sub> O	0.0800	61.98	4.96	7.77
SiO <sub>2</sub>	0.6000	60.08	36.05	56.48
CaF <sub>2</sub>	0.1000	78.08	7.81	12.23
	<b>1.0000</b>		<b>63.82</b>	<b>100.00</b>

### Batch for 300 gm of glass

	CF	100g Wgt	200g Wgt	300g Wgt
K <sub>2</sub> CO <sub>3</sub>	1.47	15.159	30.319	45.478
CaCO <sub>3</sub>	1.78	23.525	47.050	70.575
Na <sub>2</sub> CO <sub>3</sub>	1.71	13.286	26.573	39.859
SiO <sub>2</sub>	1.00	56.484	112.967	169.451
CaF <sub>2</sub>	1.00	12.234	24.469	36.703
		<b>120.69</b>	<b>241.377</b>	<b>362.065</b>

### K7Na8F13

	MF	MW		Wt%
K <sub>2</sub> O	0.0680	94.20	6.41	9.97
CaO	0.1456	56.08	8.17	12.71
Na <sub>2</sub> O	0.0777	61.98	4.82	7.50
SiO <sub>2</sub>	0.5825	60.08	35.00	54.48
CaF <sub>2</sub>	0.1262	78.08	9.85	15.34
	<b>1.0000</b>		<b>64.24</b>	<b>100.00</b>

### Batch for 300 gm of glass

	CF	100g Wgt	200g Wgt	300g Wgt
K <sub>2</sub> CO <sub>3</sub>	1.47	14.631	29.261	43.892
CaCO <sub>3</sub>	1.78	22.687	45.374	68.060
Na <sub>2</sub> CO <sub>3</sub>	1.71	12.821	25.641	38.462
SiO <sub>2</sub>	1.00	54.480	108.961	163.441
CaF <sub>2</sub>	1.00	15.340	30.679	46.019
		<b>119.96</b>	<b>239.916</b>	<b>359.874</b>

### K7Na8F15

	MF	MW		Wt%
K <sub>2</sub> O	0.0667	94.20	6.28	9.74
CaO	0.1429	56.08	8.01	12.42
Na <sub>2</sub> O	0.0762	61.98	4.72	7.32
SiO <sub>2</sub>	0.5714	60.08	34.33	53.22
CaF <sub>2</sub>	0.1429	78.08	11.16	17.30
	<b>1.0001</b>		<b>64.51</b>	<b>100.00</b>

### Batch for 300 gm of glass

	CF	100g Wgt	200g Wgt	300g Wgt
K <sub>2</sub> CO <sub>3</sub>	1.47	14.291	28.582	42.873
CaCO <sub>3</sub>	1.78	22.173	44.346	66.519
Na <sub>2</sub> CO <sub>3</sub>	1.71	12.520	25.041	37.561
SiO <sub>2</sub>	1.00	53.218	106.437	159.655
CaF <sub>2</sub>	1.00	17.297	34.593	51.890
		<b>119.50</b>	<b>238.999</b>	<b>358.498</b>

**K7Na8F15Zr1**

	MF	MW	Wt%	
K <sub>2</sub> O	0.0660	94.20	6.22	9.55
CaO	0.1414	56.08	7.93	12.19
Na <sub>2</sub> O	0.0754	61.98	4.67	7.18
SiO <sub>2</sub>	0.5658	60.08	33.99	52.24
CaF <sub>2</sub>	0.1414	78.08	11.04	16.97
ZrO <sub>2</sub>	0.0099	123.22	1.22	1.87
	<b>0.9999</b>		<b>65.07</b>	<b>100.00</b>

**Batch for 300 gm of glass**

	CF	100g Wgt	200g Wgt	300g Wgt
K <sub>2</sub> CO <sub>3</sub>	1.47	14.018	28.035	42.053
CaCO <sub>3</sub>	1.78	21.749	43.498	65.247
Na <sub>2</sub> CO <sub>3</sub>	1.71	12.281	24.562	36.843
SiO <sub>2</sub>	1.00	52.238	104.476	156.714
CaF <sub>2</sub>	1.00	16.966	33.932	50.898
ZrO <sub>2</sub>	1.00	1.875	3.749	5.624
		<b>119.127</b>	<b>238.253</b>	<b>357.380</b>

**K7Na8F15Zr2**

	MF	MW	Wt%	
K <sub>2</sub> O	0.0654	94.20	6.16	9.38
CaO	0.1401	56.08	7.86	11.97
Na <sub>2</sub> O	0.0747	61.98	4.63	7.05
SiO <sub>2</sub>	0.5602	60.08	33.66	51.26
CaF <sub>2</sub>	0.1401	78.08	10.94	16.66
ZrO <sub>2</sub>	0.0196	123.22	2.42	3.68
	<b>1.0001</b>		<b>65.66</b>	<b>100.00</b>

**Batch for 300 gm of glass**

	CF	100g Wgt	200g Wgt	300g Wgt
K <sub>2</sub> CO <sub>3</sub>	1.47	13.767	27.533	41.300
CaCO <sub>3</sub>	1.78	21.357	42.715	64.072
Na <sub>2</sub> CO <sub>3</sub>	1.71	12.059	24.118	36.176
SiO <sub>2</sub>	1.00	51.261	102.521	153.782
CaF <sub>2</sub>	1.00	16.660	33.321	49.981
ZrO <sub>2</sub>	1.00	3.678	7.357	11.035
		<b>118.782</b>	<b>237.564</b>	<b>356.346</b>

**K7Na8F15Zr4**

	MF	MW	Wt%	
K <sub>2</sub> O	0.0641	94.20	6.04	9.04
CaO	0.1374	56.08	7.71	11.54
Na <sub>2</sub> O	0.0733	61.98	4.54	6.80
SiO <sub>2</sub>	0.5495	60.08	33.01	49.44
CaF <sub>2</sub>	0.1374	78.08	10.73	16.07
ZrO <sub>2</sub>	0.0385	123.22	4.74	7.10
	<b>1.0002</b>		<b>66.77</b>	<b>100.00</b>

**Batch for 300 gm of glass**

	CF	100g Wgt	200g Wgt	300g Wgt
K <sub>2</sub> CO <sub>3</sub>	1.47	13.268	26.536	39.803
CaCO <sub>3</sub>	1.78	20.596	41.192	61.788
Na <sub>2</sub> CO <sub>3</sub>	1.71	11.635	23.271	34.906
SiO <sub>2</sub>	1.00	49.442	98.884	148.326
CaF <sub>2</sub>	1.00	16.067	32.133	48.200
ZrO <sub>2</sub>	1.00	7.105	14.209	21.314
		<b>118.113</b>	<b>236.225</b>	<b>354.338</b>

**K7Na8F15Zr8**

	MF	MW	Wt%	
K <sub>2</sub> O	0.0617	94.20	5.81	8.44
CaO	0.1323	56.08	7.42	10.78
Na <sub>2</sub> O	0.0706	61.98	4.38	6.35
SiO <sub>2</sub>	0.5291	60.08	31.79	46.17
CaF <sub>2</sub>	0.1323	78.08	10.33	15.00
ZrO <sub>2</sub>	0.0741	123.22	9.13	13.26
	<b>1.0001</b>		<b>68.86</b>	<b>100.00</b>

**Batch for 300 gm of glass**

	CF	100g Wgt	200g Wgt	300g Wgt
K <sub>2</sub> CO <sub>3</sub>	1.47	12.385	24.769	37.154
CaCO <sub>3</sub>	1.78	19.232	38.463	57.695
Na <sub>2</sub> CO <sub>3</sub>	1.71	10.868	21.735	32.603
SiO <sub>2</sub>	1.00	46.166	92.332	138.498
CaF <sub>2</sub>	1.00	15.002	30.004	45.007
ZrO <sub>2</sub>	1.00	13.261	26.521	39.782
		<b>116.913</b>	<b>233.825</b>	<b>350.738</b>

K7Na8F15Zr1Si70

	MF	MW		Wt%
K <sub>2</sub> O	0.06	94.20	5.48	8.51
CaO	0.12	56.08	6.99	10.86
Na <sub>2</sub> O	0.07	61.98	4.03	6.26
SiO <sub>2</sub>	0.62	60.08	37.08	57.58
CaF <sub>2</sub>	0.12	78.08	9.74	15.12
ZrO <sub>2</sub>	0.01	123.22	1.07	1.66
	<b>0.9985</b>		<b>64.39</b>	<b>100.00</b>

Batch for 300 gm of glass

	CF	100g Wgt	200g Wgt	300g Wgt
K <sub>2</sub> CO <sub>3</sub>	1.47	12.492	24.983	37.475
CaCO <sub>3</sub>	1.78	19.383	38.766	58.148
Na <sub>2</sub> CO <sub>3</sub>	1.71	10.699	21.398	32.097
SiO <sub>2</sub>	1.00	57.585	115.170	172.755
CaF <sub>2</sub>	1.00	15.120	30.240	45.361
ZrO <sub>2</sub>	1.00	1.665	3.330	4.994
		<b>116.943</b>	<b>233.886</b>	<b>350.829</b>

K7Na8F15Zr1Si90

	MF	MW		Wt%
K <sub>2</sub> O	0.05	94.20	4.66	7.31
CaO	0.11	56.08	5.94	9.31
Na <sub>2</sub> O	0.06	61.98	3.50	5.49
SiO <sub>2</sub>	0.67	60.08	40.53	63.50
CaF <sub>2</sub>	0.11	78.08	8.28	12.97
ZrO <sub>2</sub>	0.01	123.22	0.91	1.43
	<b>1.0000</b>		<b>63.83</b>	<b>100.00</b>

Batch for 300 gm of glass

	CF	100g Wgt	200g Wgt	300g Wgt
K <sub>2</sub> CO <sub>3</sub>	1.47	10.719	21.437	32.156
CaCO <sub>3</sub>	1.78	16.622	33.245	49.867
Na <sub>2</sub> CO <sub>3</sub>	1.71	9.382	18.765	28.147
SiO <sub>2</sub>	1.00	63.499	126.998	190.498
CaF <sub>2</sub>	1.00	12.967	25.934	38.901
ZrO <sub>2</sub>	1.00	1.429	2.857	4.286
		<b>114.618</b>	<b>229.236</b>	<b>343.854</b>

K7Na8F15Zr1Si110

	MF	MW		Wt%
K <sub>2</sub> O	0.04	94.20	4.05	6.39
CaO	0.09	56.08	5.17	8.16
Na <sub>2</sub> O	0.05	61.98	3.05	4.81
SiO <sub>2</sub>	0.72	60.08	43.08	68.00
CaF <sub>2</sub>	0.09	78.08	7.20	11.36
ZrO <sub>2</sub>	0.01	123.22	0.80	1.26
	<b>1.0001</b>		<b>63.35</b>	<b>100.00</b>

Batch for 300 gm of glass

	CF	100g Wgt	200g Wgt	300g Wgt
K <sub>2</sub> CO <sub>3</sub>	1.47	9.382	18.763	28.145
CaCO <sub>3</sub>	1.78	14.568	29.136	43.704
Na <sub>2</sub> CO <sub>3</sub>	1.71	8.232	16.464	24.696
SiO <sub>2</sub>	1.00	68.001	136.003	204.004
CaF <sub>2</sub>	1.00	11.364	22.728	34.093
ZrO <sub>2</sub>	1.00	1.264	2.529	3.793
		<b>112.811</b>	<b>225.623</b>	<b>338.434</b>

## Appendix 2: Wt% lost = wt% in batch - wt% in glass (from XRF)

	CaF2 in batch	F in batch	F in glass	F lost	CaO in batch	CaO in glass	CaO lost	SiO2 in batch	SiO2 in glass	SiO2 lost
<b>F8</b>	10.03	4.88	5.20	-0.32	13.51	12.79	0.72	57.90	58.20	-0.30
<b>F10</b>	12.23	5.95	6.71	-0.76	13.18	11.97	1.21	56.48	56.21	0.27
<b>F13</b>	15.34	7.47	8.59	-1.12	12.71	10.63	2.08	54.48	54.67	-0.19
<b>F15</b>	17.30	8.42	9.67	-1.25	12.42	10.71	1.71	53.22	53.01	0.21
<b>Z1</b>	16.97	8.26	8.95	-0.69	12.19	10.39	1.80	52.24	53.46	-1.22
<b>Z2</b>	16.66	8.11	8.60	-0.49	11.97	10.42	1.55	51.26	51.88	-0.62
<b>Z4</b>	16.07	7.82	9.13	-1.31	11.54	9.93	1.61	41.44	48.84	-7.40
<b>Z8</b>	15.00	7.30	9.06	-1.76	10.78	9.98	0.80	46.17	44.63	1.54
<b>S70</b>	15.12	7.36	8.01	-0.65	10.86	9.76	1.10	57.58	58.41	-0.83
<b>S90</b>	12.97	6.31	6.65	-0.34	9.31	8.99	0.32	63.50	63.50	0.00
<b>S110</b>	11.36	5.53	5.80	-0.27	8.16	7.47	0.69	68.00	68.38	-0.38

	Na2O in batch	Na2O in glass	Na2O lost	K2O in batch	K2O in glass	K2O lost	ZrO2 in batch	ZrO2 in glass	ZrO2 lost
<b>F8</b>	7.96	7.58	0.38	10.59	10.54	0.05	0.00	0.00	0.00
<b>F10</b>	7.77	7.52	0.25	10.33	10.29	0.04	0.00	0.00	0.00
<b>F13</b>	7.50	7.03	0.47	9.97	9.82	0.15	0.00	0.00	0.00
<b>F15</b>	7.32	6.75	0.57	9.74	9.46	0.28	0.00	0.00	0.00
<b>Z1</b>	7.18	6.42	0.76	9.55	9.43	0.12	1.87	1.70	0.17
<b>Z2</b>	7.05	6.40	0.65	9.38	9.23	0.15	3.68	3.44	0.24
<b>Z4</b>	6.80	6.14	0.66	9.04	8.94	0.10	7.10	6.66	0.44
<b>Z8</b>	6.35	5.48	0.87	8.44	8.18	0.26	13.26	11.93	1.33
<b>S70</b>	6.26	5.75	0.51	8.51	7.79	0.72	1.66	1.55	0.11
<b>S90</b>	5.49	5.16	0.33	7.31	7.38	-0.07	1.43	1.37	0.06
<b>S110</b>	4.81	4.55	0.26	6.39	6.34	0.05	1.26	1.17	0.09

### Appendix 3

Tg's and Tc's calculated from DTA traces

<b>Compositions</b>	<b>Tg (°C)</b>	<b>Tc (°C)</b>
<b>B8</b>	500	680
<b>K81</b>	528	722
<b>K82</b>	528	711
<b>K83</b>	532	700
<b>K84</b>	532	700
<b>K85</b>	530	695
<b>K86</b>	530	700
<b>K7</b>	530	700
<b>C1</b>	540	705
<b>C2</b>	545	710
<b>T2</b>	545	720
<b>Z2</b>	540	710
<b>F13</b>	515	703

<b>F8Z0 (=F8)</b>	535	698
<b>F8Z1</b>	535	720
<b>F8Z2</b>	545	-
<b>F8Z4</b>	555	-
<b>F8Z8</b>	571	-
<b>F10Z0 (=F10)</b>	525	695
<b>F10Z1</b>	532	750
<b>F10Z2</b>	535	718; 795; 831
<b>F10Z4</b>	560	718
<b>F10Z8</b>	565	754
<b>F15Z0 (=F15)</b>	505	696
<b>F15Z1</b>	510	691; 727; 767
<b>F15Z2</b>	517	715; 818
<b>F15Z4</b>	540	725; 865
<b>F15Z8</b>	560	742; 823; 850
<b>S55</b>	507	695; 721; 753
<b>S57(=F15Z1)</b>	510	691; 727; 767

<b>S65</b>	517	716; 757
<b>S70</b>	525	781
<b>S80</b>	530	803
<b>S90</b>	539	828
<b>S110</b>	544	840